DISSERTATION

INFLUENCE OF *FADS2* EXPRESSION ON CARDIOVASCULAR RISK: ROLE OF MITOCHONDRIAL ARACHIDONIC ACID

Submitted by

Lance Christopher Li Puma

Department of Biomedical Sciences

In partial fulfillment of the requirements

For the Degree of Doctorate of Philosophy

Colorado State University

Fort Collins, Colorado

Fall 2020

Doctoral Committee:

Advisor: Adam J. Chicco

Gerrit J. Bouma
Gregory C. Amberg
Christopher L. Gentile
Marie E. Legare

ABSTRACT

INFLUENCE OF *FADS2* EXPRESSION ON CARDIOVASCULAR RISK: ROLE OF MITOCHONDRIAL ARACHIDONIC ACID

Long-chain polyunsaturated fatty acids (LC-PUFA) are widely believed to influence cardiovascular health and disease in humans and can be supplied through the diet or endogenously synthesized from the essential PUFAs linoleic acid (LA; *n*6) and alpha-linolenic acid (ALA; *n*3). Redistribution of PUFAs in serum and tissue phospholipids has been associated with various pathologies, manifesting primarily as a proportional loss of the essential PUFA LA paralleled by reciprocal increases in its long-chain product arachidonic acid (AA; *n*6). Epidemiological studies have linked greater AA/LA ratios in serum phospholipids to multiple parameters of cardiometabolic disease (CMD), such as obesity, insulin resistance, hypertension, atherosclerosis, and coronary artery disease. Single nucleotide polymorphisms in the *FADS2* gene are associated with haplotypes of greater expression of *FADS2*, which may increase the production of AA from LA and increase serum AA/LA ratios. *FADS2* encodes delta-6 desaturase, the rate-limiting enzyme in endogenous LC-PUFA biosynthesis, which is believed to participate in the development of CMD by interacting with the high dietary LA content found in the modern Western diet to disproportionally produce AA over other LC-PUFAs.

The overarching hypothesis of this dissertation is that greater expression of *FADS2* promotes the development of cardiovascular risk parameters. To investigate this, we generated mice with global (CMV promoter) transgenic overexpression of *Fads2* (*Fads2*^{TG}); these mice exhibit classic serum shifts in PUFA distribution characteristic of human *FADS2* polymorphisms.

A series of three projects were undertaken: 1) Investigate the interaction between dietary essential fatty acid intakes and *Fads2* expression on cardiovascular risk; 2) Establish methodology for simultaneous measurement of mitochondrial respiration and ROS release *in vitro*; 3) Investigate effects of *Fads2* expression on cardiac mitochondrial responses to Ca^{++}-overload.

These studies discovered that greater *Fads2* expression is sufficient to increase several aspects of cardiovascular risk that were independent of the dietary ratio of *n*6:*n*3 essential PUFAs. Further investigation demonstrated that cardiac cardiolipin AA content predicted ischemia-reperfusion (IR) injury, suggesting a mechanistic role of mitochondria in this phenotype. Gain- and loss-of-function approaches in mice established that greater *Fads2* expression lowers mitochondrial tolerance to Ca^{++}-overload demonstrated by loss of OXPHOS-linked respiration, greater mitochondrial ROS release, and increased mitochondrial permeability transition. Furthermore, mitochondrial permeability transition by Ca^{++}-overload could be attenuated by inhibition of AA release or metabolism. Collectively, the significance of these studies establish the influence of *Fads2* on serum and tissue PUFA composition and the pathogeneis of IR injury through moduation of mitochondria membrane composition, thereby demonstrating *Fads2* expression as an independent factor for cardiovarscular risk.

ACKNOWLEDGEMENTS

I would like to express my appreciation and gratitude for my advisor Dr. Adam Chicco, who has been a mentor in and outside of the lab the last five years. You have continuously supported me in all areas of my graduate career; from benchtop research, experimental design, teaching, and mentoring junior lab members, your guidance has been essential. I greatly appreciate the opportunities you allotted me to develop my own research questions and build my own methods within the lab. This freedom to pursue my own interests afforded me the opportunity to develop as a researcher and further my skills as a principal investigator. You constantly pushed me to grow and sharpen my skills all the way to the very end; thank you for always encouraging me to produce my best work. I would also like to thank you for the discussions we have had about career planning and life; I believe this mentoring will influence who I am for the rest of my life.

I am also grateful to the other members of my committee: Dr. Gerrit Bouma, Dr. Gregory Amberg, and Dr. Christopher Gentile, for providing valuable guidance throughout my graduate career. “It takes a village to raise a child”, and you all were my village. In addition, I would like to individually thank Dr. Marie Legare for joining my committee this past year and for all the time and effort she has put in to understand my research projects so she could provide me with support. I greatly value your willingness to tell me the hard truths without any “sugar”.

My introduction to research was made my Dr. Connor B. Whitaker and (soon to be Dr.) Amanda J. Evans. I would like to express my appreciation for your patience when I first joined the lab. In addition, I want to thank the junior lab members that worked alongside me in the lab and made my time both easier and sometimes more difficult: AO, LAW, KF, KSS, JMH, MRE, ABB, CSI, and PTZ.

DEDICATION

I dedicate this dissertation to my parents, Mary Lou and Jerry Li Puma, and my wife, Dr. Maggie Li Puma. To my parents: you have always pushed me to excel in academia and earn a doctorate. You taught me how to always go "all in" in whatever pursuit I was attempting to accomplish. This dissertation was only possible because you each love me, and I thank you for that. To my wife Maggie: we started dating when we both entered our doctorate programs and would have "date-nights" where we sat quietly and studied for tests or prepared manuscripts. As miserable as that sounds to most people, I wouldn't trade those nights for anything else. Thank you for being my partner and building a life with me. I also want to give a shout out to my dog Fox, who has been a great companion during the writing process. Each of you have supported me beyond belief during this process and I would not be crossing this finish line without your support.

I would also like to include my friends who became my family through the years: NLB, SRG, JDS, ECM, DM, ME, NH, MG, ERA, KFC, and VSG. You all have supported me during this doctorate and I am forever grateful.

Finally, I would like to dedicate this dissertation to my friend Bill Hanneman, who treated me as an "adopted son" in his lab. I often stop and ask myself, "what would Bill do?" when faced with adversity. I am fortunate to have had your friendship and mentoring in my life; see you in the next one.

TABLE OF CONTENTS

LIST OF TABLES

LIST OF FIGURES

APPENDIX

CHAPTER 1: HYPOTHESES AND EXPERIMENTAL AIMS

1. Overarching Hypothesis

The studies in this dissertation test the overarching hypothesis that greater expression of the *FADS2* gene encoding delta-6 desaturase (D6D), the rate-limiting enzyme in long-chain polyunsaturated fatty acid biosynthesis, promotes the development of cardiovascular disease (CVD). This hypothesis is based in part on evidence from genome wide association studies demonstrating single nucleotide polymorphisms (SNPs) located within or near binding sites for transcriptional regulation of *FADS2* that predict development of CVD in humans. The idea is further supported by correlations between serum D6D product/precursor ratios and CVD risk across diverse human populations, and cardiovascular benefits of pharmacological D6D inhibition in rodent models of heart failure and aging. To address this hypothesis, I completed three research projects comprised of experimental aims that integrated *in vivo* and *in vitro* approaches with new method and model development to investigate the physiological and biochemical effects of *Fads2* expression on CVD risk outcomes in mice.

2. Projects

2.1 Investigate the interaction between dietary essential fatty acid intakes and Fads2 expression on cardiovascular risk.

Polyunsaturated fatty acids (PUFAs) have been intensively studied over the last several decades due to their putative role in biological membrane dynamics, cell signaling, and influence upon cardiovascular health and disease. Dietary *n*6:*n*3 essential PUFAs, linoleic acid (LA; *n*6) and α-linolenic acid (ALA; *n*3) have been theorized to have existed in near balance in the ancestral

human diet; whereas today these PUFAs are consumed in a 20:1 or greater ratio. Evolutionarily, greater desaturase activity was selected for in regions where dietary PUFAs were scarce. However, greater desaturase activity in the background of an overabundance of dietary *n*6 PUFAs may lead to the overproduction of the potent pro-inflammatory lipid arachidonic acid (AA; *n*6). Epidemiological studies have correlated higher serum ratios of AA/LA, suggestive of greater endogenous AA production, with multiple CVD risk parameters, but experimental evidence supporting these links is lacking. Therefore, I sought to investigate these links by testing the hypothesis below with the following experimental aims.

Hypothesis: *Fads2* expression promotes a pathogenic effect of dietary LA on cardiovascular risk by modulating serum and/or cardiac arachidonic acid content.

Specific Aim 1: Determine the individual and interactive effects of *Fads2* expression and the dietary LA:ALA ratio on cardiovascular risk parameters in mice.

Specific Aim 2: Determine if variations in cardiovascular risk parameters influenced by *Fads2* expression and dietary LA:ALA intake correlate with changes in serum and/or myocardial phospholipid composition.

To accomplish these aims, I used a novel *Fads2*^{TG} mouse generated by our lab to model the phenotype of human *FADS2* SNPs associated with a greater serum AA/LA ratio and cardiovascular risk profile compared to other haplotypes. *Fads2*^{TG} and FVB controls were fed engineered diets containing three LA:ALA ratios devoid of long-chain PUFAs for 12-weeks and evaluated for multiple parameters of cardiometabolic risk. Results show a main effect of *Fads2* on

glucose intolerance, aortic stiffening and left ventricular hypertrophy, and a *Fads2* x Diet interactive effect of ischemia-reperfusion (IR) injury. *Fads2* overexpression increased serum AA/LA in mice fed a high *n*6:*n*3 diet, consistent with *FADS2* SNPs in humans consuming a modern diet, but none of our CVD outcomes paralleled serum AA/LA ratio across groups. Variations in IR injury closely paralleled the AA content of the mitochondrial specific phospholipid cardiolipin, but not total myocardial or serum PUFA composition.

Taken together, these studies support the hypothesized influence of *FADS2* expression on cardiovascular risk in humans, and reveal a novel interaction between dietary essential PUFA composition and *FADS2* genotype on myocardial IR tolerance. The latter finding may involve changes in mitochondrial membrane composition, which may lead to functional changes in mitochondria that exacerbate cardiomyocyte death during IR.

2.2 Establish methodology for simultaneous measurement of mitochondrial respiration and ROS release in vitro

Altered mitochondrial function in the myocardium has been identified as a primary component of cardiac pathology in multiple conditions, including IR injury. Results from Project 1 demonstrated a close correlation between IR injury and AA accumulation in mitochondrial phospholipids, which may impact mitochondrial responses to stress in this context. Therefore, we next wanted to explore the effect of *Fads2* expression on mitochondrial responses to simulated IR stress, modeled by progressive mitochondrial Ca^{++}-overload *in vitro*.

Mitochondrial function can be extensively studied by high resolution fluorespirometry using the Oroboros Oxygraph-2k system (Oroboros Instruments), which enables simultaneous monitoring of oxygen consumption (JO_2) and reactive oxygen species release (JH_2O_2) by mitochondria in response to multiple assay titrations and conditions. This relatively new

instrumentation provides an ideal approach for evaluating the effects of progressive Ca^{++}-overload on cardiac mitochondrial function *in vitro*. However, dynamic changes in chamber oxygen concentration and accumulation of H_2O_2 (resorufin) fluorescence present cofounding problems for monitoring authentic mitochondrial JO_2 and JH_2O_2 during an extended experiment, which have not been thoroughly characterized. Therefore, it is of critical importance to define the methodological limitations of this approach so that strategies can be developed to avoid or correct for interferences that could lead to erroneous results and conclusions. Accordingly, I sought to characterize these limitations using the Oroboros system in our lab to address the following hypothesis and experimental aims.

Hypothesis: Chamber oxygen concentration and background conditions influence assayed rates of mitochondrial oxygen consumption and mtROS release in vitro, requiring specific calibrations and methodology to enable valid data collection.

Specific Aim 1: Characterize the effect of chamber oxygen concentration on rates of respiration and ROS release from cardiac mitochondrial preparations.

Specific Aim 2: Develop strategies for avoiding or correcting for variations in fluorespirometry signals during prolonged experimental protocols.

To address these aims, I utilized high-resolution fluorespirometry to investigate JO_2 and JH_2O_2 from cardiac mitochondrial preparations across a range of oxygen concentrations commonly encountered during multi-substrate experimental protocols. Chemical background and chamber oxygen concentration were found to impose significant limitations on valid monitoring

of cardiac mitochondrial respiration (JO_2) and mtROS release (JH_2O_2), including a 10-15% decrease in JO_2 and a 75% decrease in JH_2O_2 as chamber [O_2] decreased from 400 to 50 μM. Accumulation of the H_2O_2 fluorophore product resorufin above 3 μM also significantly decreased assayed rates of H_2O_2 release, further complicating valid measurement of mitochondrial JH_2O_2 over time. However, I found that these limitations could be overcome by designing protocols that limit data collection to narrow [O_2] ranges, maintaining [O_2] above threshold levels to avoid diffusion limitations of JO_2, and avoid threshold levels of chemical background fluorescence. In addition to contributing important methodological insights to scientists in the field, the strategies I developed can be applied for valid measurement of cardiac mitochondrial JO_2 and JH_2O_2 in response to progressive Ca^{++}-overload, thus enabling the development of the next project in my dissertation.

2.3 Investigate effects of Fads2 expression on cardiac mitochondrial responses to calcium overload

The extent of myocardial infarction due to IR stress correlates with future complications and death, therefore research is centered on investigating factors that contribute to or predispose myocardium to greater IR injury. Both ischemia and reperfusion contribute to damage and impairments in mitochondrial function; however, mitochondrial matrix accumulation of Ca^{++} has been recognized as the primary factor for opening of the mitochondrial permeability transition pore (mPTP) leading to cell death. During IR, Ca^{++} accumulation activates phospholipases leading to the release and metabolism of AA, generating lipid second messengers (eicosanoids) that increase the susceptibility of mPTP opening. Both pharmacological and genetic inhibition of the release and/or metabolism of AA has been shown to reduce damage from IR injury. Previously we

have shown *Fads2* dependent accumulation of AA in mitochondrial membranes correlates with IR injury.

Hypothesis: *Fads2* expression alters cardiac mitochondrial responses to Ca^{++}-overload by regulating mitochondrial content and metabolism of arachidonic acid.

Specific Aim 1: Determine if *Fads2* expression regulates cardiac mitochondrial responses to Ca^{++}-overload that are consistent with effects on myocardial IR injury.

Specific Aim 2: Determine if mitochondrial arachidonic acid content, release, and metabolism modulates functional responses to Ca^{++}-overload.

These aims were completed by isolating cardiac mitochondria from mice with transgenic overexpression ($Fads2^{TG}$) or heterozygous knockdown ($Fads2^{KD}$) of the murine *Fads2* gene, compared to their respective wild-type controls. Mitochondrial phospholipid fatty acids profiles were generated by gas chromatography, and AA content was found to correlate positively with *Fads2* expression. Mitochondrial responses to Ca^{++}-overload were investigated by monitoring JO_2 and JH_2O_2 by high-resolution fluorespirometry and mitochondrial swelling/mPTP opening using kinetic spectrophotometry on a plate-reader. Results demonstrated that higher *Fads2* expression impair mitochondrial response to Ca^{++}-overload (lower JO_2, higher JH_2O_2, and greater mitochondrial swelling), and pharmacological inhibition of AA release and/or metabolism attenuates these effects. Therefore, as I hypothesized, *Fads2* expression regulates cardiac mitochondrial AA content and functional responses to Ca^{++}-overload, which may explain my previously demonstrated effects of *Fads2* expression on myocardial IR tolerance.

CHAPTER II: *FADS2* POTENTIATES EFFECTS OF DIETARY ESSENTIAL FATTY ACIDS ON CARDIOVASCULAR RISK [1,2]

1. Introduction

Substantial effort has been devoted to determining the influence of polyunsaturated fatty acids (PUFA) on cardiovascular health and disease. Prevailing evidence supports a moderate benefit of long-chain *n*3-PUFA such as docosahexaenoic acid (22:6*n*3; DHA) on cardiovascular disease (CVD) risk factors in some populations [1, 2], but the influence of *n*6-PUFAs has been more controversial [3]. The essential *n*6-PUFA linoleic acid (18:2*n*6; LA) accounts for greater than 90% of dietary PUFAs in the modern Western diet, but was in near balance with or lower than the essential *n*3-PUFA alpha-linolenic acid (18:3*n*3; ALA) in the human ancestral diet [4]. This disproportionate intake of *n*6:*n*3 PUFA may contribute to the modern prevalence of CVD in Western societies by favoring greater production of long-chain *n*6-arachidonic acid (20:4*n*6; AA) over *n*3-DHA and eicosapentaenoic acid (20:5*n*3; EPA) [5, 6]. However, lower serum LA levels have predicted higher cardiovascular morbidity and mortality in multiple large-cohort studies [7, 8], fueling controversy over its role in dietary recommendations for CVD risk reduction.

Accumulating evidence suggests that endogenous metabolism of essential PUFAs varies across individuals, and may be a critical determinant of CVD risk in the context of the modern Western diet. LA and ALA are converted to their long-chain PUFA products (AA and DHA, respectively) by a desaturation-elongation pathway catalyzed by the *FADS2* gene product delta-6-

---

[1]This chapter has been prepared for submission to Cardiovascular Research

[2]Authors List: Li Puma LC, Whitaker CM, Evans AJ, Battson ML, Izon CS, Zilhaver PT, Olson AW, Le CH, Gentile CL, Chicco AJ

desaturase (D6D) as the first rate-limiting reaction. The primary *n*6 product (AA) and substrate (LA) of this pathway are the most abundant PUFAs found in human serum, so are commonly reported together (AA/LA) as an index of systemic (largely hepatic) D6D pathway activity. A higher serum AA/LA ratio predicts obesity [9], diabetes/insulin resistance [10], cardiovascular morbidity [11], and mortality [12] in humans, suggesting that high D6D activity increases cardiometabolic risk. Variations in the serum AA/LA ratio have been linked to single nucleotide polymorphisms (SNPs) of the *FADS2* gene located within or near binding sites of transcriptional regulators [13], which distinguish functional *FADS2* haplotypes that also influence CVD risk across diverse human populations [14-16]. However, no experimental studies have investigated whether higher *FADS2* expression independently affects cardiovascular function or interacts with dietary PUFA composition to modulate cardiovascular responses to pathogenic stress (e.g., ischemia).

The aim of the present study was to test the hypothesis that *FADS2* expression potentiates the effect of a higher dietary LA:ALA intake on CVD risk outcomes. To address this, we examined the impact of three dietary LA:ALA ratios on selected cardiovascular parameters of mice with moderate transgenic over-expression of *Fads2* compared to wild-type controls. Results demonstrate independent and diet-interactive effects of *Fads2* on systemic glucose tolerance, aortic stiffness, and myocardial ischemic tolerance that are consistent with an important contribution of *FADS2* genotype on CVD risk in humans consuming an *n*6 PUFA-rich diet.

2. Material and Methods

2.1 Animal Models

Transgenic mice with global over-expression of murine *Fads2* (*Fads2*^{TG}) were generated using the cytomegalovirus (CMV) promoter to direct moderate overexpression of the transgene globally. Once the *Fads2* plasmid DNA was transformed into E. coli, isolated plasmid was cut with MfeI and BstBI to excise the 4.3kb transgene fragment, which was then purified for pronuclear injection at the University of Colorado Transgenic Mouse Core. *Fads2*^{TG} founder mice were genotyped and bred through at least eight backcrossed generations in a colony maintained at Colorado State University to produce mice used in these studies. A parallel colony of FVB wild-type mice in the fourth generation maintained at Colorado State University served as the control (FVB) mice for these studies. Mice were randomly assigned into experimental groups 14 days after weaning and maintained on one of three diets for 12 weeks prior to sacrifice. Animals were housed in a temperature and humidity controlled facility on a 12:12 hour light:dark cycle and provided water and diets *ad libitum* until sacrifice by midline thoracotomy and removal of the heart following confirmation of deep anesthesia by sodium pentobarbital injection (100 mg/kg i.p.). All procedures were approved by the Colorado State University Care and Use Committee and conform to the Guide for the Care and Use of Laboratory Animals published by the U.S. National Institutes of Health (NIH Publication No. 85-23, revised 1996).

2.2 Experimental Diets

Fads2^{TG} and FVB mice were fed custom LC-PUFA-free AIN93G diets containing 17% kcal fat supplied from corn oil (57:1 LA:ALA; high *n*6), flaxseed oil (~1:4 LA:ALA; high *n*3), or a mixture of each to provide 1:1 LA:ALA (mix) for 12 weeks. See Table 1 for a description of experimental diet compositions. To reduced animal ingestion of peroxidized lipids, diets were supplemented with tert-Butylhydroquinone as a preservative, stored at -20C in vacuum sealed bags under N_2 gas, and were changed every three days in cages.

2.3 Serum and Tissue Phospholipid Fatty Acid Composition

Analysis of the fatty acids (FA) present in serum and tissue phospholipids was performed by gas chromatography (GC) as previously described [17]. Briefly, serum (50 µl), left ventricle (LV) tissue (~20 mg), and liver tissue (~20 mg) were homogenized in ice-cold methanol (1:10 w/v) and centrifuged to pellet the non-lipid material. Lipids in the methanol supernatant were transferred to a glass tube containing sodium methoxide solution to generate fatty acid methyl esters (FAMEs) from phospholipid FAs. Hexane was then added to FAMEs, dried under nitrogen flow, and resuspended in hexane prior to analysis. GC analysis was performed using an Agilent Technologies DB-225 30 m × 0.250 mm × 0.25 µm column (model 122-2232, J&W Scientific) on an Agilent 6890 Series gas Chromatographer with a flame ionization detector, with a flow rate of 1.7 mL/min and split ratio of 15:1 in 25 minutes. For separation of individual phospholipid species, lipids from LV were extracted in 2:1 choloroform:methanol and dried under nitrogen flow and

Table 1: Nutrient and lipid composition of the three experimental diets. Custom diets were manufactured from Harlan Laboratories with varying ratios of flaxseed and corn oil per experimental design; however, the percent-kcal from protein, carbohydrate, and fat were maintained across diets.

	n6 Diet	mix Diet	n3 Diet
Protein % weight (% kcal)	18.3 (19.4)	18.3 (19.4)	18.3 (19.4)
Carbohydrate % weight (% kcal)	60.1 (63.8)	60.1 (63.8)	60.1 (63.8)
Fat % weight (% kcal)	7.0 (16.7)	7.0 (16.7)	7.0 (16.7)
Corn Oil (g/Kg)	70.0	29.0	0.0
Flaxseed Oil (g/Kg)	0.0	41.0	70.0
Saturated Fatty Acid (% Total)			
Palmitic Acid (16:0)	12	9	6
Stearic Acid (18:0)	2	3	4
Unsaturated Fatty Acid (% Total)			
Oleic Acid (18:1)	28	24	20
Linoleic Acid (18:2n6)	57	32	15
Alpha Linolenic Acid (18:3n3)	1	32	55
LC PUFAs (% Total)	0	0	0
n6:n3 PUFA Ratio	57:1	1:1	1:4

resuspended in hexane prior to analysis by a normal phase liquid chromatographer (Agilent Zorbax Rx-Sil column, 4.6 X 250 mm, 5 um). Phospholipid species were collected by elution time of known standards and prepared for GC as described above.

2.4 Echocardiography

Analysis of LV structure and function was performed as previously described [18]. Briefly, transthoracic echocardiography was performed under light (1.5%) isoflurane anesthesia immediately prior to and following the 12-week experimental period using a 15 MHz transducer connected to a Philips HD11 Ultrasound. Short-axis 2D images of LV end-diastolic and end-systolic areas (EDA and ESA, respectively) were obtained for assessment of LV chamber morphology and fractional shortening ((EDA − ESA)/ EDA) × 100). Data were averaged from five consecutive high-resolution cycles by the same experienced technician.

2.5 Glucose Tolerance Test

Eight hours prior to glucose tolerance test (GTT), mice were placed into fresh cages with no food and free access to water. After the eight-hour fast, a small incision at the base of the tail vein to obtain 2-5 μL of blood for baseline (fasting) glucose readings using an AlphaTRAK 2 glucometer (Zoetis, NJ, USA). Following the baseline reading, a glucose bolus of 2 mg/kg body weight was given via intraperitoneal (IP) injection. Blood glucose readings were taken from the initial tail vein incision 30, 60, 90, and 120 minutes after bolus injection. A gauze pad was applied with pressure 30 seconds after each reading to minimize blood loss in between tests.

2.6 Aortic pulse wave velocity

Arterial stiffness was determined by aortic pulse wave velocity (aPWV) as previously described by our laboratory [19, 20]. Briefly, mice were anaesthetized with 2% isoflurane and oxygen at 2L per minute, placed supine on a heating board with legs secured to ECG electrodes,

and maintained at a target heart rate of ~450 bpm by adjusting isoflurane concentration. Doppler probes (20 MHz) (Mouse Doppler data acquisition system; Indus Instruments, Houston, TX) were placed on the transverse aortic arch and abdominal aorta and the distance between the probes was determined simultaneously with precision calipers. Five consecutive 2-second recordings were obtained for each mouse and used to determine the time between the R-wave of the ECG and the foot of the Doppler signal for each probe site (Δtime). aPWV (in cm/s) was calculated as aPWV = (distance between the two probes) / ($\Delta time_{abdominal}$ - $\Delta time_{transverse}$). All data was measured by the same experienced technician.

2.7 Myocardial Ischemia-Reperfusion Injury

Myocardial tolerance to ischemia-reperfusion (IR) stress was accessed by use of an *ex vivo* isolated perfused heart system with global, no-flow ischemia as previously described [20]. Briefly, mice were placed under deep anesthesia with intraperitoneal injection of a heparinized pentobarbital 50 mg/kg solution prior to sacrifice by midline thoracotomy and rapid heart excision by cutting the pulmonary trunk, pulmonary arteries, the aortic arch distal to the brachiocephalic trunk, and the superior/inferior vena cava. Hearts were immediately placed in ice-cold Krebs-Henseleit buffer (in mM: 117.4 NaCl, 4.7 KCl, 1.9 $CaCl_2$, 1.2 $MgSO_4$, 1.2 KH_2PO_4, 5 pyruvate, 11 glucose, 0.5 EDTA, 25 $NaHCO_3$, and pH to 7.4 with 95/5% O_2/CO_2) to remove any excess lung or adipose tissue. Hearts were then cannulated via the ascending aorta and retrogradely perfused in Langendorff mode generating a constant perfusion pressure of ~80 mmHg. All hearts underwent 20 minutes of stabilization prior to 45 minutes of global, no-flow ischemia, then reperfused for 120 minutes prior to infarct size assessment by Triphenyltetrazolium Chloride (TTC) staining described below. Coronary effluent was collected directly from perfused hearts immediately prior to ischemia and 5, 10, 15, 30, 60, 90, and 120 minutes after reperfusion. To quantitate the extent

of myocardial infarction following the IR protocol, hearts were removed from the cannula and dissected to isolate the left ventricle and septum. The left ventricle was then weighed prior to placing into a matrix and sliced transversely into five, 1mm transverse slices. Each slice was weighed prior to incubation in 0.1% TTC solution for 10 minutes in a shaking incubator at 37C. Slices were then fixed in 10% Formalin for one hour prior to imaging using a camera attached to a dissecting scope (Ken-A-Vision). TTC stains active tissue brick-red, while infarcted tissue appears white/yellow. NIH ImageJ software was used to calculate the ratio of active to dead tissue. Infarct size (percent of total LV) was calculated by averaging the ratio of white/red on each side of the slice and then weighting that average by the percent that slice made up of the total LV: (((%Infarct Side A) + (%Infarct Side B))/2) * ((Mass of Slice/Total LV Mass) *100) and then each slice added together to get percent infarct of the LV. All procedures were performed by the same experienced technician.

2.8 Immunoblotting

Total soluble protein was extracted from whole liver and aorta by homogenization with Mammalian Protein Extraction Reagent (Thermo Fisher Scientific, MA, USA). Protein (40 μg) from each sample was separated by SDS-PAGE, Bolt™ 4-12%, Bis-Tris (Invitrogen, CA, USA), and transferred onto PVDF membrane (Bio Rad, CA, USA). The membrane was blocked with 5% milk in TBST and incubated overnight with 1:1000 dilution of each of the respective antibodies: *FADS2* H-40 (Santa Cruz Biotechnology, TX, USA), anti-AGE (Abcam, MA, USA), and anti-beta actin (Abcam, MA, USA). The membrane was washed and incubated with HRP-conjugated secondary antibodies (1:3000 dilution) for 1 hour. Membranes were incubated with amido black (Bio Rad, CA, USA) to quantify total protein as a loading control. The blots were developed using

the chemiluminescent system ChemiDoc XRX imaging system (Bio Rad, CA, USA), and pixel density quantified using ImageJ software (NIH).

2.9 Statistics

Statistical analysis was performed using Graphpad Prism 8 (Graphpad Software, CA, USA). Groups were compared by a 2 (genotype) X 3 (diet) ANOVA to resolve main and interactive effects of *Fads2* expression and dietary LA:ALA ratio on all parameters. Pairwise comparisons between individual groups were made by Tukey post-hoc analyses following a significant ANOVA, or students *t*-test when only two groups were compared. Statistical significance was set at $P < 0.05$ for all analyses.

3. Results

3.1 Fads2 overexpression increases the serum AA/LA ratio in mice fed a high n6 diet

To validate our model, we evaluated the hepatic protein expression of D6D, which was significantly greater in all *Fads2*^{TG} compared to FVB mice irrespective of dietary PUFA composition (Figure 1B). These data, along with evidence for a greater serum AA/LA ratio in the *Fads2*^{TG} versus FVB fed the high *n*6 diet (Figure 1C), aligns with previous studies linking *FADS2* SNPs to higher serum AA/LA ratios in humans [21, 22]. Since the serum phospholipid FA profile reflects both dietary consumption and metabolism of endogenous FA, we performed a comprehensive analysis of serum FAs from FVB and *Fads2*^{TG} mice fed each of the three custom diets (Table 2). Saturated (palmitic and stearic acid) and monounsaturated (palmitoleic, oleic, and vaccenic acid) FAs were similar across groups. There was a significant main effect of diet on serum *n*6 PUFA levels, whereby a lower dietary LA:ALA ratio decreased serum LA, gamma-linoleic acid (18:3*n*6; GLA), AA, and adrenic acid (22:4*n*6; AdA), while dihomo-gamma-linoleic

acid (20:3*n*6; DGLA) increased. Conversely, a lower dietary LA:ALA ratio increased serum proportions of all *n*3 PUFAs: ALA, eicosatrienoic acid (20:3*n*3; ETE), EPA, docosapentaenoic acid (22:5*n*3; DPA), and DHA. A significant main effect of *Fads2* genotype was found only on serum LA and AA, where *Fads2*^{TG} mice fed the high-*n*6 diet had lower serum LA compared to FVB and both genotypes fed the balanced *n*6:*n*3 diet, and higher serum AA compared to all groups.

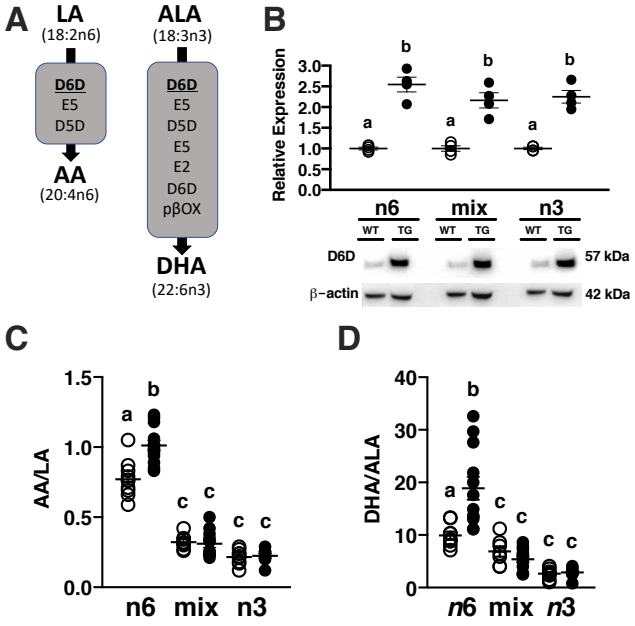

Figure 1: The interaction of dietary polyunsaturated fatty acid ratios and *Fads2* expression produce distinct serum fatty acid indices associated with pathology. A) Polyunsaturated fatty acid (PUFA) desaturation pathway. **B)** Densitometric analysis of immunoblots for the fold change of delta-6 desaturase/β-actin between groups (n=4/group) and representative immunoblots taken from animals in *Table 1*. 2 x 3 ANOVA; *Fads2*: $p < 0.05$. **C)** Product/precursor ratio of the *n*6-PUFA linoleic acid and its long-chain PUFA product arachidonic acid from *Table 1*; n=8-12/group. 2 x 3 ANOVA; Diet: $p < 0.05$, *Fads2*: $p < 0.05$, Int: $p < 0.05$. **D)** Product/precursor ratio of the n3-PUFA alpha-linolenic acid and its long-chain PUFA product docosahexaenoic acid from *Table 1*; n=8-12/group. 2 x 3 ANOVA; Diet: $p < 0.05$, *Fads2*: $p < 0.05$, Int: $p < 0.05$. Data presented as mean ± SEM. Tukey HSD was used to investigate pairwise comparisons between groups; p-value < 0.05 denoted by difference in letter.

Consequently, the serum AA/LA ratio was significantly greater in *Fads2*^{TG} mice fed the high *n*6 diet compared to FVB mice, but also decreased with lower dietary LA:ALA intake in both genotypes. Interestingly, a similar trend was found for the serum *n*3 D6D pathway

product/precursor ratio, DHA/ALA, which was also greater in the *Fads2*^{TG} fed a high *n*6 diet compared to all other groups (Figure 1D). As a result of these changes, *Fads2* overexpression decreased the total serum *n*6:*n*3 ratio and increased the fatty acid peroxidizability index (greater double bond content) in mice fed the high *n*6 diet, reflecting a global shift in serum PUFA composition (Table 2).

Table 2: Dietary polyunsaturated fatty acid ratios and *Fads2* expression produce varied serum phospholipid fatty acid profiles. Serum phospholipid fatty acid ratios (expressed as % of total fatty acids) from FVB and *Fads2*^{TG} animals after 12 weeks on one of three custom diets; n=8-12/group. Data presented as mean ± SEM. Tukey *post-hoc* was used to investigate pairwise comparisons; p-value < 0.05 denoted by difference in letter.

	n6		**mix**		**n3**		**2 x 3 ANOVA**		
	FVB	*Fads2*^{TG}	FVB	*Fads2*^{TG}	FVB	*Fads2*^{TG}	Diet	*Fads2*	Int
16:0, Palmitic	22.94±0.35	21.74±0.46	23.21±0.38	22.33±0.63	21.58±0.64	21.48±0.44	0.0738	0.0937	0.5586
16:1, Palmitoleic	0.91±0.08	0.91±0.03	0.82±0.08	1.15±0.20	1.21±0.09	1.19±0.11	0.0575	0.3289	0.2949
18:0, Stearic	16.21±1.13	18.13±1.19	18.14±1.60	19.48±1.55	19.39±1.87	20.00±1.82	0.2461	0.3080	0.9134
18:1n9, Oleic	10.91±0.75	9.74±0.72	9.65±0.98	9.40±0.57	12.10±1.50	10.63±0.98	0.1606	0.2050	0.7966
18:1n7, Vaccenic	0.30±0.06	0.50±0.08	0.45±0.10	0.60±0.15	0.59±0.14	0.60±0.14	0.3829	0.3216	0.7786
18:2n6, LA	23.14±0.77**a**	20.35±0.67**b**	24.27±0.63**a**	22.95±1.00**a**	20.02±0.89**b**	21.60±0.88**b**	**0.0073**	0.2282	**0.0401**
18:3n6, GLA	0.47±0.06**a**	0.43±0.05**a**	0.38±0.07**ab**	0.33±0.05**ab**	0.27±0.06**b**	0.23±0.04**b**	**0.0026**	0.4031	0.9918
18:3n3, ALA	0.34±0.01**a**	0.28±0.02**a**	1.35±0.19**b**	1.86±0.22**b**	3.56±0.57**c**	3.20±0.64**c**	**<0.0001**	0.9194	0.4409
20:3n6, DGLA	0.92±0.11**a**	0.97±0.11**a**	1.26±0.10**b**	1.33±0.24**b**	1.15±0.11**b**	1.33±0.11**b**	**0.0483**	0.4248	0.9178
20:4n6, AA	18.01±0.64**a**	20.80±0.55**b**	7.79±0.43**c**	6.89±0.33**c**	4.28±0.39**d**	4.79±0.33**d**	**<0.0001**	**0.0495**	**0.0021**
20:3n3, ETE	0±0**a**	0±0**a**	0±0**a**	0±0**a**	0.19±0.04**b**	0.11±0.02**b**	**<0.0001**	0.7235	0.8073
20:5n3, EPA	0±0**a**	0±0**a**	2.34±0.32**b**	2.52±0.39**b**	5.38±0.57**c**	5.00±0.61**c**	**<0.0001**	0.8255	0.7574
22:4n6, AdA	1.64±0.25**a**	1.38±0.08**a**	0±0**b**	0±0**b**	0±0**b**	0±0**b**	**<0.0001**	0.3400	0.3906
22:5n3, DPA	0±0**a**	0±0**a**	1.40±0.43**b**	1.81±0.38**b**	2.13±0.50**b**	2.18±0.49**b**	**<0.0001**	0.6253	0.4086
22:6n3, DHA	3.65±0.33**a**	4.44±0.22**a**	8.81±0.40**b**	8.64±0.31**b**	8.16±0.32**b**	7.84±0.38**b**	**<0.0001**	0.6965	0.1683
GLA/LA	0.021±0.003**a**	0.021±0.003**a**	0.015±0.003**b**	0.014±0.002**b**	0.013±0.003**b**	0.011±0.002**b**	**0.0016**	0.6539	0.8350
AA/DHA	5.26±0.42**a**	4.8±0.24**a**	0.89±0.05**b**	0.82±0.06**b**	0.52±0.043**b**	0.63±0.062**b**	**<0.0001**	0.2169	0.2749
n6/n3	12.23±0.87**a**	9.55±0.55**b**	2.43±0.09**c**	2.14±0.08**c**	1.38±0.16**c**	1.56±0.10**c**	**<0.0001**	**0.0139**	**0.0043**
PI	131.8±3.1**a**	147.6±2.8**b**	154.5±3.1**b**	152.9±3.5**b**	157.9±2.9**b**	156.5±4.5**b**	**<0.0001**	0.1357	**0.0172**

3.2 Fads2 overexpression increases body weight and LV mass

Obesity is associated with LV hypertrophy and a greater risk of cardiovascular morbidity and mortality [23]. Therefore, we hypothesized that both may be increased by *Fads2* expression and/or dietary PUFA composition. Indeed, body mass was significantly greater in *Fads2*^{TG}

compared to FVB mice, but was not affected by dietary LA:ALA (Table 3). Whole heart/ body mass did not change between groups, but LV mass expressed as percent of whole heart was significantly greater in *Fads2*^{TG} compared to FVB across all diets. These results demonstrate that greater *Fads2* expression, primarily independent of dietary LA:ALA, increases body mass and LV mass.

Table 3: Animal Characteristics. Body and tissue weights were collected at sacrifice after 12 weeks on one of three custom diets; Body mass: n=10/group; Heart: n=5/group; Left Ventricle (LV): 6-7/group. Data presented as mean ± SEM. Tukey HSD was used to investigate pairwise comparisons between groups; p-value < 0.05 denoted by difference in letter.

	n6		**mix**		**n3**		**2 x 3 ANOVA**		
	FVB	*Fads2*^{TG}	FVB	*Fads2*^{TG}	FVB	*Fads2*^{TG}	Diet	*Fads2*	Int
Body Mass, g	24.1±0.9**a**	28.1±1.0**b**	25.0±1.3**a**	28.7±1.9**b**	24.1±1.0**a**	27.6±1.3**b**	0.7085	**0.0005**	0.9777
Heart, mg	131±11	123±9	136±18	139±11	133±1	131±4	0.6295	0.7777	0.8701
LV, mg	46.0±1.9**a**	53.3±2.8**bc**	51.2±1.6**c**	63.7±2.2**d**	44.2±0.7**a**	50.9±1.0**b**	**<0.0001**	**<0.0001**	0.1971
LV, % Heart mass	35±1**a**	41±2**bc**	39±1**c**	49±2**d**	34±1**a**	39±1**b**	**<0.0001**	**<0.0001**	0.2647

3.3 Fads2 overexpression promotes glucose intolerance regardless of diet

Impairments in serum glucose disposal are a hallmark of Type 2 diabetes and insulin resistance, which have been linked to *FADS2* SNPs [10, 24] and dietary PUFA intake [25, 26], and are primary risk factors of CVD [27]. Therefore, we predicted that *Fads2* overexpression would reduce whole-body glucose tolerance, which might be modified by the dietary LA:ALA intake. Indeed, blood glucose levels recorded for 120 minutes following an IP glucose injection in fasted mice revealed a greater area under the curve (AUC) in *Fads2*^{TG} mice compared to FVB mice across all diets (Figure 2A and B), indicating a significant impairment of glucose tolerance irrespective of dietary LA:ALA content. Similarly, peak blood glucose levels recorded 30 minutes after a glucose injection were greater in *Fads2*^{TG} mice compared to FVB regardless of diet (Figure 2C). Notably, the high *n*6 diet reduced fasting blood levels in FVB mice compared to all other groups (Figure 2D), with no other significant variations between diets in either genotype.

3.4 Fads2 overexpression promotes aortic stiffening and LV hypertrophy

Aortic stiffness expressed as aortic pulse wave velocity (aPWV) is a strong predictor of future cardiovascular events and all-cause mortality in humans [28]. Therefore, aPWV was measured by Doppler ultrasound in all cohorts. There was a significant main effect of diet, whereby decreasing dietary LA:ALA tended to decrease aPWV in both *Fads2*^{TG} and FVB mice

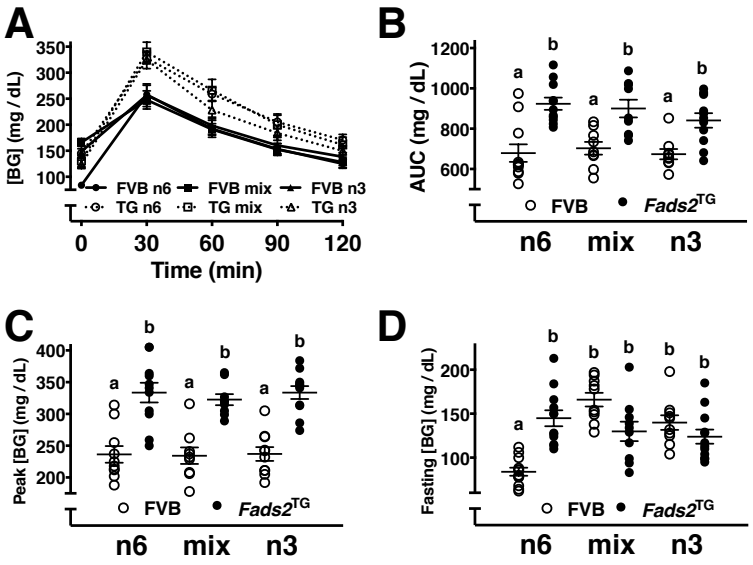

Figure 2: Impact of *Fads2* expression and diet on systemic glucose tolerance. A) Blood glucose levels of FVB and *Fads2*^{TG} animals after 12-weeks on one of three custom diets after an eight-hour fast and intraperitoneal (IP) injection of dextrose (2mg/kg); n=10/group. **B)** Area under the curve (AUC) calculated from *Panel A*. 2 x 3 ANOVA; *Fads2*: $p < 0.05$. **C)** Peak blood glucose levels, 30 minutes post IP injection from *Panel A*. 2 x 3 ANOVA; *Fads2*: $p < 0.05$. **D)** Fasting blood glucose levels after an 8 hour fast from *Panel A*. 2 x 3 ANOVA; Diet: $p < 0.05$, Int: $p < 0.05$. Data presented as mean ± SEM. Tukey HSD was used to investigate pairwise comparisons between groups; p-value < 0.05 denoted by difference in letter.

(Figure 3A). However, similar to the glucose tolerance AUC results (Figure 2B), aPWV was greater in *Fads2*^{TG} compared to FVB across all diets, indicating a strong main effect of *Fads2* genotype.

Based on these results, we hypothesized that the greater aortic stiffness in *Fads2*^{TG} mice might result in part from a vascular accumulation of advanced glycation end products (AGEs), a

primary mechanism of vascular stiffening in diabetes [29]. Indeed, aortic levels of AGEs were greater in *Fads2*^{TG} compared to FVB across all diets, which was attenuated by lower dietary LA:ALA in *Fads2*^{TG} without any effect on FVB groups (Figure 3B), indicating that *Fads2* expression potentiates the effect of diet on aortic protein glycation.

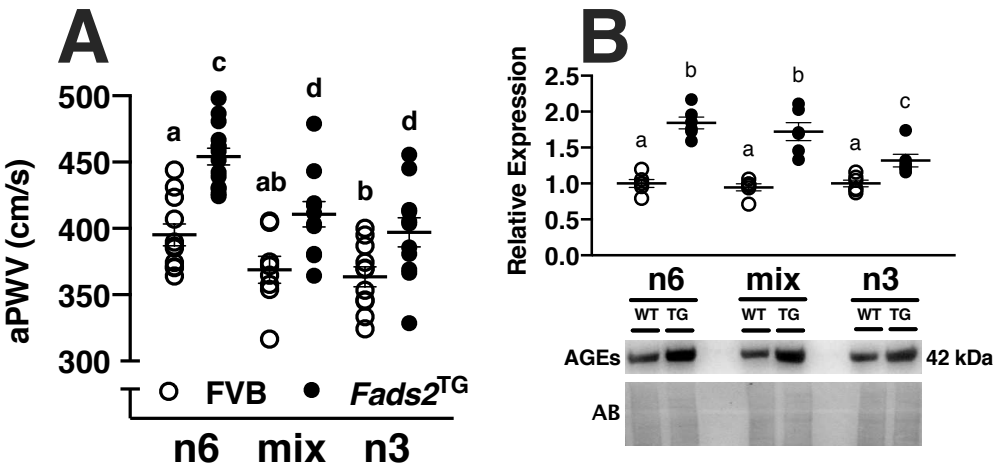

Figure 3: *Fads2* expression and linoleic acid intake modulate aPWV and AGEs expression. A) Aortic pulse wave velocity (aPWV) was measured *in vivo* from animals after 12-weeks on one of three custom diets; n=8-14/group. 2 x 3 ANOVA; Diet: $p < 0.05$, *Fads2*: $p < 0.05$. **B)** Densitometric analysis of immunoblots for the fold change of advanced glycation end-products (AGEs)/amido black from aortas taken from *Panel A*; n=6/group. Representative immunoblots for AGEs and amido black. 2 x 3 ANOVA; Diet: $p < 0.05$, *Fads2*: $p < 0.05$, Int: $p < 0.05$. Data presented as mean ± SEM. Tukey HSD was used to investigate pairwise comparisons between groups; p-value < 0.05 denoted by difference in letter.

A stiffer aorta is less able to buffer pulsatile pressure by the LV during systole, leading to greater LV afterload and ultimately maladaptive LV remodeling [30-32]. Consistent with an increase in aortic stiffness (Figure 3A) and greater LV mass (Table 3), *Fads2*^{TG} mice exhibited greater end diastolic area (Figure 4A) and end systolic area (Figure 4B) compared to FVB mice across all diets. These changes occurred without any differences in basal LV fractional shortening across groups (Figure 4C), indicating a preservation of systolic function. Taken together, these

results suggest that greater *Fads2* expression increases cardiovascular risk in part by linking glucose intolerance to LV remodeling through aortic stiffening and accumulation of AGEs.

3.5 Fads2 potentiates effects of dietary PUFAs on myocardial ischemic tolerance

To determine effects of *Fads2* expression and dietary PUFA composition on cardiac responses to pathogenic stress, myocardial tolerance to ischemia-reperfusion was evaluated in

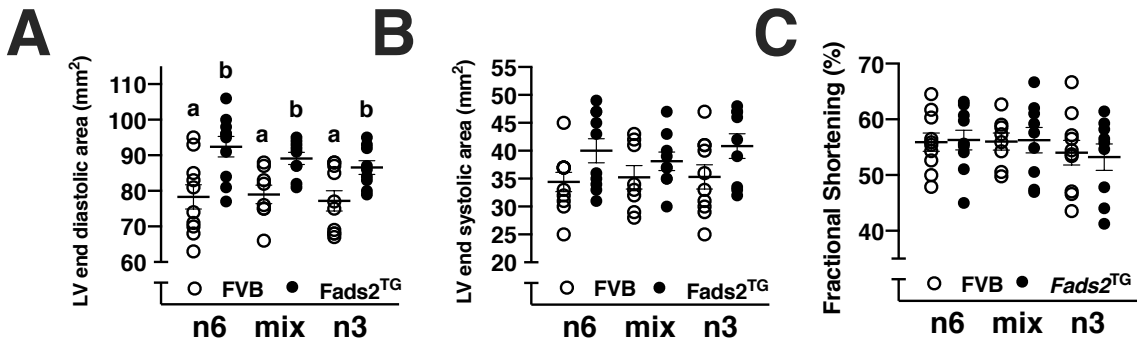

Figure 4: *Fads2* overexpression favors left ventricle dilation with preserved contractile function. Transthoracic echocardiography of WT and TG animals after being fed one of three custom diets for 12-weeks: **A)** Left ventricle (LV) end diastolic area (2 x 3 ANOVA; *Fads2*: $p < 0.05$), **B)** LV end systolic area (2 x 3 ANOVA; *Fads2*: $p < 0.05$), and **C)** LV fractional shortening; n=8-10/group. Data presented as mean ± SEM. Tukey HSD was used to investigate pairwise comparisons between groups; p-value < 0.05 denoted by difference in letter.

hearts from *Fads2*^{TG} and FVB mice following 12 weeks on the experimental diets. Based on evidence that *FADS2* SNPs associated with elevated D6D activity predict greater cardiovascular mortality in humans [12], we hypothesized that greater *Fads2* expression would reduce myocardial tolerance to IR stress. Indeed, myocardial infarct size was significantly greater in *Fads2*^{TG} compared to FVB mice, but only when the *Fads2*^{TG} mice were fed the high n6 and mix diets (Figure 5A and 5B). There were no effects of dietary LA:ALA on infarct size in FVB mice, indicating that *Fads2* overexpression potentiated the effects of dietary LA:ALA on cardiac ischemic tolerance.

Reperfusion of the myocardium after ischemia is essential to limit myocyte cell death and organ failure. Accordingly, the extent of coronary flow following reperfusion predicts myocardial recovery and prognosis after acute myocardial infarction [33-35]. Consistent with the infarct size data, post-ischemic coronary flow rates were significantly higher in FVB compared to *Fads2*^{TG}

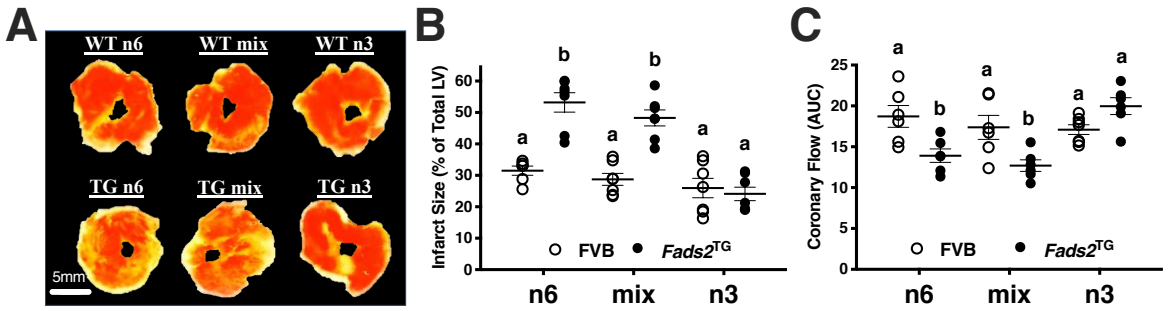

Figure 5: *Fads2* aggravates cardiac ischemia-reperfusion injury when dietary n6 ≥ n3 polyunsaturated fatty acid. A) Representative images of triphenyltetrazolium chloride stained heart sections showing myocardial infarct size in FVB and *Fads2*^{TG} animals after being fed one of three custom diets for 12-weeks. **B)** Myocardial infarct size; n=6-7/group. 2 x 3 ANOVA; Diet: $p < 0.05$, *Fads2*: $p < 0.05$, Int: $p < 0.05$. **C)** Coronary flow (ml min^{-1} LV mass^{-1}) during the reperfusion period expressed as area under the curve (AUC) of hearts from *Panel B*; n=6-7/group. 2 x 3 ANOVA; Diet: $p < 0.05$, *Fads2*: $p < 0.05$, Int: $p < 0.05$. Data presented as mean ± SEM. Tukey HSD was used to investigate pairwise comparisons between groups; p-value < 0.05 denoted by difference in letter.

mice fed the high *n*6 and mix diets, but not different between *Fads2*^{TG} and FVB mice fed the high *n*3 diet (Figure 5C). These findings indicate that *Fads2* overexpression exacerbates myocardial IR injury only when the dietary LA:ALA ratio is ≥ 1, consistent with reports of greater cardiovascular morbidity and mortality associated with *FADS2* SNPs in humans consuming a modern diet [11, 12, 21].

3.6 Effects of Fads2 expression and diet on myocardial phospholipid PUFA composition

Changes in myocardial membrane PUFA distribution have been linked to multiple cardiac pathologies, including LV hypertrophy, heart failure, and ischemic heart disease [17, 36, 37]. In particular, previous studies have linked D6D activity and dietary PUFA intake to compositional

changes in the mitochondria-specific phospholipid, cardiolipin, which may influence cardiac responses to hypertension, diabetes, and ischemia [17, 18, 38-40]. Therefore, we evaluated the effects of *Fads2* expression and diet on the distribution of major PUFAs present in myocardial total phospholipids (TPL) and cardiolipin (Table 4) from a cohort of mice in the present study (full

Table 4: Myocardial total phospholipid fatty acid profile contrasts fatty acid profile of myocardial cardiolipin. Select polyunsaturated fatty acids from total phospholipid (n=4-5/group) and cardiolipin (n=4-6/group) fatty acid ratios (expressed as % of total fatty acids) from FVB and *Fads2*^{TG} animals after 12 weeks on one of three custom diets. Data presented as mean ± SEM. Tukey HSD was used to investigate pairwise comparisons between groups; p-value < 0.05 denoted by difference in letter.

Myocardial Total Phospholipid Fatty Acid Composition

	n6		mix		n3		2 x 3 ANOVA		
	FVB	*Fads2*^{TG}	FVB	*Fads2*^{TG}	FVB	*Fads2*^{TG}	Diet	*Fads2*	Int
18:2n6, LA	20.3±0.2**a**	18.5±0.5**a**	15.9±0.3**b**	16.5±1.1**b**	11.9±0.2**c**	12.7±0.4**c**	**<0.0001**	0.8299	0.1088
18:3n3, ALA	0.07±0.01**a**	0.10±0.02**a**	1.13±0.22**b**	1.11±0.13**b**	2.54±0.18**c**	2.56±0.10**c**	**<0.001**	0.9203	0.9865
20:4n6, AA	10.4±0.2**a**	11.4±0.6**a**	6.0±0.5**b**	6.0±0.4**b**	4.6±0.3**c**	4.5±0.2**c**	**<0.0001**	0.2588	0.3024
22:6n3, DHA	18.6±1.4**a**	18.3±1.6**a**	31.8±0.5**b**	28.3±1.5**b**	30.3±1.4**b**	29.2±1.1**b**	**<0.0001**	0.1779	0.5292
AA/LA	0.510±0.012**a**	0.615±0.032**b**	0.373±0.038**c**	0.367±0.022**c**	0.383±0.025**c**	0.358±0.013**c**	**<0.0001**	0.2134	**0.0223**

Myocardial Cardiolipin Fatty Acid Composition

	n6		mix		n3		2 x 3 ANOVA		
	FVB	*Fads2*^{TG}	FVB	*Fads2*^{TG}	FVB	*Fads2*^{TG}	Diet	*Fads2*	Int
18:2n6, LA	41.93±2.54**a**	40.05±2.17**a**	38.97±1.36**a**	40.51±1.19**a**	29.91±1.34**b**	29.47±1.48**b**	**<0.0001**	0.8726	0.6937
18:3n3, ALA	0.737±0.092**a**	0.787±0.179**a**	1.739±0.171**b**	1.840±0.118**b**	4.893±0.290**d**	3.646±0.400**c**	**<0.0001**	0.1057	**0.0317**
20:4n6, AA	5.10±0.06**a**	7.40±0.19**b**	5.12±0.19**a**	7.47±0.19**b**	5.25±0.36**a**	5.04±0.38**a**	**0.0008**	**<0.0001**	**0.0002**
22:6n3, DHA	2.24±0.36**a**	2.92±0.39**a**	7.54±0.55**b**	6.99±0.87**b**	6.83±0.97**b**	6.79±0.51**b**	**<0.0001**	0.9596	0.7279
AA/LA	0.123±0.008**a**	0.188±0.011**b**	0.131±0.010**a**	0.176±0.007**b**	0.175±0.009**b**	0.171±0.010**b**	0.1818	**0.0007**	**0.0152**

phospholipid fatty acid profile available in APPENDIX; Supplemental Table S1 and S2). Variations in myocardial TPL and cardiolipin PUFAs primarily paralleled changes in the dietary LA:ALA ratio, with significant main effects of diet found for LA, ALA, AA and DHA. A significant effect of *Fads2* genotype was only found with cardiolipin AA levels, which were greater in *Fads2*^{TG} than FVB mice fed the high *n*6 and mix (but not *n*3) diets, but similar across all three diets in FVB mice. This led to a greater cardiolipin AA/LA ratio in *Fads2*^{TG} than FVB fed the high *n*6 and mix diets, while the myocardial TPL AA/LA ratio generally reflected that of the serum phospholipids. This indicates that higher *Fads2* expression potentiates the effect of diet on cardiolipin PUFA composition, specifically favoring greater incorporation of AA when dietary

LA:ALA ratio is ≥ 1. Interestingly, a Pearson correlation demonstrated the pattern of cardiolipin AA distribution across groups predicted variations in myocardial infarct size (Figure 6A), while the AA contents of myocardial TPL and serum did not (Figure 6B and 6C), suggesting novel links between *Fads2* expression, cardiolipin AA content, and myocardial ischemic tolerance.

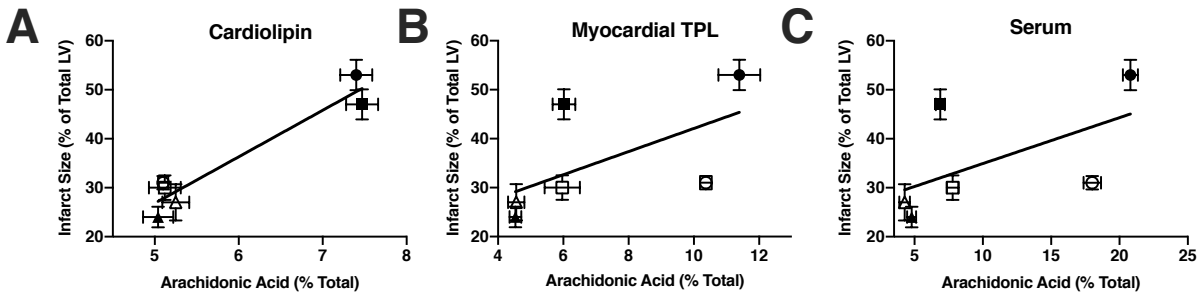

Figure 6: Cardiolipin arachidonic acid content predicts myocardial ischemia-reperfusion injury. Pearson correlation for arachidonic acid (group mean ± SEM) vs. infarct size (group mean ± SEM) for **(A)** Cardiolipin: r = 0.9619, p < 0.05; **(B)** Myocardial total phospholipid: r = 0.5991, p = ns; and **(C)** Serum: r = 0.5677, p = ns.

4. Discussion

PUFAs play pleiotropic roles in cardiovascular biology that are influenced by both diet and endogenous metabolism. Abundant epidemiological evidence supports a role of *FADS2* genotype in determining serum and tissue PUFA composition and cardiovascular risk in humans [21], but experimental studies investigating these links are lacking. In the present study, we demonstrate that moderate overexpression of *Fads2* elicits independent and diet-interactive effects on multiple cardiometabolic risk parameters in mice fed different dietary LA:ALA ratios. Most remarkably, we found that *Fads2* overexpression exacerbates myocardial ischemia-reperfusion injury only when the dietary LA:ALA ratio is ≥ 1, while its pathogenic effects on cardiovascular remodeling and glucose tolerance were largely independent of diet. These results support accumulating evidence that *FADS2* is an important independent and nutrigenetic regulator of cardiovascular risk in humans, and provide new insight to the biological bases for these interactions.

Genome wide association studies targeting the *FADS2* gene cluster in diverse human populations have identified two common haplotypes of *FADS2* associated with differing potential to generate LC-PUFAs [13]. It is predicted that ancestral human diets consisted of an equal or greater amount of essential *n*6 to *n*3 PUFA intake [4, 41] with a strong positive selection for the "high-activity" *FADS2* haplotype, possibly providing advantages in environments where essential PUFAs were scarce [13]. In the modern agricultural societies, *n*6-LA accounts for up to 90% of total dietary PUFA intake [42] resulting in dietary *n*6:*n*3 PUFA ratios up to 20:1 or higher [4, 41]. A higher desaturase activity in this LA-rich environment has been postulated to increase bioavailability of AA and its pro-inflammatory eicosanoid derivatives, perhaps contributing to the greater risk of cardiometabolic disorders in modern humans [21]. Indeed, a greater relative abundance of serum *n*6-AA to its essential precursor *n*6-LA is associated with common *FADS2* polymorphisms and predicts the development of diabetes/insulin resistance [10, 24, 43] coronary artery disease [11] and cardiovascular mortality [12], suggesting a pathogenic interaction of *FADS2* with the modern Western diet [5].

Consistent with these findings, we found that the serum AA/LA ratio was significantly increased by consumption of a high-LA (*n*6) diet in mice from the present study, and was augmented further by *Fads2* overexpression along with glucose intolerance, aortic stiffening, LV hypertrophy and myocardial ischemic injury. However, *Fads2* overexpression elicited similar pathogenic effects when mice were fed a balanced LA:ALA diet, despite having no effect on the serum AA/LA ratio compared to FVB mice. Furthermore, the higher serum AA/LA ratio in FVB mice fed the high *n*6 diet compared to the mixed diet was not associated with any increase in cardiovascular risk parameters. Taken together, these results indicate that *Fads2* genotype potentiates effects of dietary LA on cardiometabolic risk, but can influence these parameters

independent of changes in serum PUFA composition. In addition, these findings emphasize that *Fads2* expression has a greater independent effect on cardiometabolic risk than dietary PUFA composition or the serum AA/LA ratio alone.

Consistent with observational studies in humans linking estimated D6D hyperactivity to metabolic syndrome [44] and diabetes/insulin resistance [10, 24], *Fads2*^{TG} mice exhibited greater body mass and glucose intolerance compared to controls in the present study. These effects were largely independent of dietary PUFA composition, along with greater values of aortic stiffness and LV mass in *Fads2*^{TG} than FVB mice. High circulating glucose levels and insulin resistance are associated with aortic stiffening in humans [45, 46], which predicts left ventricular hypertrophy [47] and is an independent risk factor for future cardiovascular events [28]. Hyperglycemia potentiates the production of advanced glycation end-products (AGEs) in vascular tissue, which promote the crosslinking of type I collagen and elastin in the extracellular matrix and basement membrane of the vessel wall, leading to vascular stiffening [29]. Aortic accumulation of AGEs in *Fads2*^{TG} mice corresponded to higher aPWV compared to FVB controls across all three diets in the present study, providing a potential mechanism by which *Fads2* independently promotes aortic stiffening. Indeed, trends for higher aPWV and AGE expression in *Fads2*^{TG} mice paralleled those for higher peak blood glucose and AUC following the glucose tolerance test compared to FVB mice. Similarly, *Fads2* overexpression independently increased LV mass and end diastolic volume, which are consistent with an increase LV afterload and mid-systolic wall stress associated with a loss of aortic compliance. These results closely resemble the sequalae of cardiovascular aging, where aortic stiffening promotes increases in left ventricular mass and diastolic volume prior to any loss of basal contractile function [48]. We hypothesize that this phenotype occurs secondary to the glucose intolerance induced by *Fads2* overexpression through the production of

AGEs, which appears to occur largely independent of dietary PUFA composition, further supporting the independent effect *FADS2* genotype on cardiometabolic risk suggested by observational studies in humans.

It is worth pointing out that aPWV also tended to increase with greater dietary LA:ALA ratio in both FVB and *Fads2*^{TG} mice, indicating an independent effect of dietary PUFA composition on aortic stiffness. This finding is consistent with the conclusions of previous studies linking higher serum LA levels (and lower *n*3-PUFA) to higher arterial PWV in humans [49], one of which implicated effects on vascular inflammation based on parallel trends with serum C-reactive protein (CRP) [50]. Serum CRP was not measured in the present study, but has been independently associated with vascular stiffening [51] and poor glycemic control in diabetes [52], so could represent another mechanism for changes in aPWV induced by *FADS2* expression. However, it is important to note that serum LA levels did not parallel changes in aPWV in either genotype herein, and were similar or lower in *Fads2*^{TG} compared to FVB mice across the three diets. Serum AA levels did increase with dietary LA:ALA ratio in parallel with aPWV in both genotypes, but were only higher in *Fads2*^{TG} fed the high-n6 diet despite higher aPWV across all diets versus FVB mice. This emphasizes that serum *n*-6 PUFA levels may not be valid predictors of cardiovascular risk across all populations due to complex interactions of dietary PUFA intake and *FADS2* genotype on serum PUFA composition, each of which may exert independent and interactive effects on vascular stiffness by diverse mechanisms.

Myocardial infarction is often the initial manifestation of ischemic heart disease, and survival is inversely proportional to the size of the myocardial infarction sustained [53]. In this study, we used an *ex vivo* isolated perfused heart model to resolve the effects of *Fads2* expression and dietary LA:ALA on the intrinsic myocardial tolerance to ischemia-reperfusion stress. Results

indicate that greater *Fads2* expression lowers ischemic tolerance, indicated by greater myocardial infarction size following global ischemia, only when the dietary LA:ALA ratio is ≥ 1 (Figure 5). Greater risk of myocardial injury has been associated with diabetes/insulin resistance [54], aortic stiffness [55] , and a greater serum AA/LA ratio in humans [12], all of which were also observed in *Fads2*^{TG} mice in the present study. However, the trends in these parameters across diets and genotypes do not align with the diet-interactive effect of *Fads2* overexpression on ischemic injury, suggesting the involvement of other mechanisms.

Previous studies have linked increases in the myocardial phospholipid AA/LA ratio to delta-6 desaturase hyperactivity and cardiac dysfunction in heart failure and aging [17, 18], suggesting that *Fads2* genotype might impact myocardial tolerance to pathogenic stress by altering cardiac PUFA composition. Indeed, we found a diet × genotype interaction effect on the total myocardial phospholipid AA/LA ratio in the present study, but neither this trend nor that of any myocardial PUFA aligned with variations in infarct size across groups. To investigate further, we evaluated the PUFA composition of cardiolipin, a mitochondrial phospholipid that is highly enriched with LA and thought to influence cardiac responses to pathogenic stress [56], including ischemia-reperfusion injury [40]. We found that while LA was largely unaffected by *Fads2* expression, cardiolipin AA content was significantly greater in *Fads2*^{TG} than FVB mice when the dietary LA:ALA ratio was ≥ 1, closely paralleling variations in myocardial infarct size across groups (Figure 6A). Cardiac ischemia has been shown to trigger selective hydrolysis of AA from mitochondrial phospholipids [57], which can lead to the initiation of lethal arrhythmias and cell death pathways [58-60]. Genetic or pharmacological inhibition of this process reduces myocardial infarct size [61, 62], perhaps by preventing formation of AA-derived eicosanoids that trigger mitochondrial permeability transition [57, 63]. Direct oxidation of AA on cardiolipin may also

generate complex lipid derivatives implicated in pathogenic responses to tissue injury [64], further suggesting that an accumulation of AA in myocardial cardiolipin may contribute to greater infarct size in *Fads2*^{TG} mouse hearts. The mechanisms by which *Fads2* selectively increases cardiac cardiolipin AA content, and any contribution this may have to exacerbating myocardial ischemia-reperfusion injury, merit further investigation.

In the present study, we used FVB mice with moderate transgenic overexpression of *Fads2* to model human *FADS2* SNPs associated greater D6D activity/expression estimated by elevated serum AA/LA ratio. While our model demonstrated mild D6D overexpression with similar serum PUFA changes and cardiometabolic phenotypes associated with some human *FADS2* SNPs, effects observed in transgenic mice might not represent those of humans with subtle variations in dietary PUFA intake. In addition, we used an *ex vivo* isolated perfused heart system with global, no-flow ischemia to evaluate the intrinsic tolerance of the myocardium to ischemic stress. This approach enabled us to demonstrate the intrinsic effects of *Fads2* overexpression on heart, but effects on infarct size might differ from an *in vivo* coronary occlusion protocol or working heart models. Finally, we have presented and discussed several associations between cardiometabolic health parameters and serum/tissue PUFA profiles, but additional studies employing rigorous experimental gain/loss-of-function approaches targeting these interactions are required to establish causal relationships.

In summary, our results demonstrate that *Fads2* expression regulates multiple aspects of cardiovascular risk in mice both independently and through interaction with the dietary PUFA composition. Specifically, greater *Fads2* expression induces aortic stiffening and LV hypertrophy independent of the dietary LA:ALA ratio, possibly by promoting glucose intolerance and an associated accumulation of glycated proteins in vascular tissue. *Fads2* expression appears to

potentiate a pathogenic effect of dietary *n*6-PUFA on myocardial tolerance to ischemia, significantly increasing infarct size only when dietary LA was similar to or greater than ALA intake. This nutrigenetic interaction is consistent with the predictions of epidemiological studies linking *FADS2* SNPs to cardiovascular risk in humans consuming the modern Western diet, but were not explained by changes in serum or myocardial PUFA composition. Rather, variations in infarct size correlated specifically with the arachidonic acid content of cardiolipin, a mitochondrial phospholipid, suggesting novel links between *Fads2* expression, cardiac mitochondria, and myocardial ischemic tolerance that merit further investigation. In conclusion, these findings support accumulating evidence for an important influence of *FADS2* genotype on cardiometabolic risk in humans, and demonstrate a potent nutrigenetic interaction that justifies consideration of personalized nutritional plans for optimal disease prevention. These results may also help to resolve longstanding controversy over the impacts of dietary PUFAs and serum fatty acid profiles on cardiovascular health and disease.

REFERENCES

1. Siscovick, D.S., et al., *Omega-3 Polyunsaturated Fatty Acid (Fish Oil) Supplementation and the Prevention of Clinical Cardiovascular Disease: A Science Advisory From the American Heart Association.* Circulation, 2017. **135**(15): p. e867-e884.

2. Mozaffarian, D. and J.H. Wu, *Omega-3 fatty acids and cardiovascular disease: effects on risk factors, molecular pathways, and clinical events.* J Am Coll Cardiol, 2011. **58**(20): p. 2047-67.

3. Ramsden, C.E., et al., *Low omega-6 vs. low omega-6 plus high omega-3 dietary intervention for chronic daily headache: protocol for a randomized clinical trial.* Trials, 2011. **12**: p. 97.

4. Kuipers, R.S., et al., *Estimated macronutrient and fatty acid intakes from an East African Paleolithic diet.* Br J Nutr, 2010. **104**(11): p. 1666-87.

5. Patterson, E., et al., *Health implications of high dietary omega-6 polyunsaturated Fatty acids.* J Nutr Metab, 2012. **2012**: p. 539426.

6. Ramsden, C.E., et al., *Use of dietary linoleic acid for secondary prevention of coronary heart disease and death: evaluation of recovered data from the Sydney Diet Heart Study and updated meta-analysis.* BMJ, 2013. **346**: p. e8707.

7. Laaksonen, D.E., et al., *Prediction of cardiovascular mortality in middle-aged men by dietary and serum linoleic and polyunsaturated fatty acids.* Arch Intern Med, 2005. **165**(2): p. 193-9.

8. Wu, J.H., et al., *Circulating omega-6 polyunsaturated fatty acids and total and cause-specific mortality: the Cardiovascular Health Study.* Circulation, 2014. **130**(15): p. 1245-53.

9. Warensjo, E., M. Ohrvall, and B. Vessby, *Fatty acid composition and estimated desaturase activities are associated with obesity and lifestyle variables in men and women.* Nutr Metab Cardiovasc Dis, 2006. **16**(2): p. 128-36.

10. Kroger, J., et al., *Erythrocyte membrane phospholipid fatty acids, desaturase activity, and dietary fatty acids in relation to risk of type 2 diabetes in the European Prospective Investigation into Cancer and Nutrition (EPIC)-Potsdam Study.* Am J Clin Nutr, 2011. **93**(1): p. 127-42.

11. Martinelli, N., et al., *FADS genotypes and desaturase activity estimated by the ratio of arachidonic acid to linoleic acid are associated with inflammation and coronary artery disease.* Am J Clin Nutr, 2008. **88**(4): p. 941-9.

12. Warensjo, E., et al., *Markers of dietary fat quality and fatty acid desaturation as predictors of total and cardiovascular mortality: a population-based prospective study.* Am J Clin Nutr, 2008. **88**(1): p. 203-9.

13. Ameur, A., et al., *Genetic adaptation of fatty-acid metabolism: a human-specific haplotype increasing the biosynthesis of long-chain omega-3 and omega-6 fatty acids.* Am J Hum Genet, 2012. **90**(5): p. 809-20.

14. Merino, D.M., et al., *Polymorphisms in FADS1 and FADS2 alter desaturase activity in young Caucasian and Asian adults.* Mol Genet Metab, 2011. **103**(2): p. 171-8.

15. Sergeant, S., et al., *Differences in arachidonic acid levels and fatty acid desaturase (FADS) gene variants in African Americans and European Americans with diabetes or the metabolic syndrome.* Br J Nutr, 2012. **107**(4): p. 547-55.

16. O'Neill, C.M. and A.M. Minihane, *The impact of fatty acid desaturase genotype on fatty acid status and cardiovascular health in adults.* Proc Nutr Soc, 2017. **76**(1): p. 64-75.

17. Le, C.H., et al., *Delta-6-desaturase links polyunsaturated fatty acid metabolism with phospholipid remodeling and disease progression in heart failure.* Circ Heart Fail, 2014. **7**(1): p. 172-83.

18. Mulligan, C.M., et al., *Inhibition of delta-6 desaturase reverses cardiolipin remodeling and prevents contractile dysfunction in the aged mouse heart without altering mitochondrial respiratory function.* J Gerontol A Biol Sci Med Sci, 2014. **69**(7): p. 799-809.

19. Battson, M.L., et al., *Tauroursodeoxycholic Acid Reduces Arterial Stiffness and Improves Endothelial Dysfunction in Type 2 Diabetic Mice.* J Vasc Res, 2017. **54**(5): p. 280-287.

20. Battson, M.L., et al., *Gut microbiota regulates cardiac ischemic tolerance and aortic stiffness in obesity.* Am J Physiol Heart Circ Physiol, 2019. **317**(6): p. H1210-H1220.

21. Tosi, F., et al., *Delta-5 and delta-6 desaturases: crucial enzymes in polyunsaturated fatty acid-related pathways with pleiotropic influences in health and disease.* Adv Exp Med Biol, 2014. **824**: p. 61-81.

22. Malerba, G., et al., *SNPs of the FADS gene cluster are associated with polyunsaturated fatty acids in a cohort of patients with cardiovascular disease.* Lipids, 2008. **43**(4): p. 289-99.

23. Poirier, P., et al., *Obesity and cardiovascular disease: pathophysiology, evaluation, and effect of weight loss: an update of the 1997 American Heart Association Scientific Statement on Obesity and Heart Disease from the Obesity Committee of the Council on Nutrition, Physical Activity, and Metabolism.* Circulation, 2006. **113**(6): p. 898-918.

24. Warensjo, E., et al., *Associations between estimated fatty acid desaturase activities in serum lipids and adipose tissue in humans: links to obesity and insulin resistance.* Lipids Health Dis, 2009. **8**: p. 37.

25. Forouhi, N.G., et al., *Association of Plasma Phospholipid n-3 and n-6 Polyunsaturated Fatty Acids with Type 2 Diabetes: The EPIC-InterAct Case-Cohort Study.* PLoS Med, 2016. **13**(7): p. e1002094.

26. Telle-Hansen, V.H., L. Gaundal, and M.C.W. Myhrstad, *Polyunsaturated Fatty Acids and Glycemic Control in Type 2 Diabetes.* Nutrients, 2019. **11**(5).

27. *Diabetes mellitus: a major risk factor for cardiovascular disease. A joint editorial statement by the American Diabetes Association; The National Heart, Lung, and Blood Institute; The Juvenile Diabetes Foundation International; The National Institute of Diabetes and Digestive and Kidney Diseases; and The American Heart Association.* Circulation, 1999. **100**(10): p. 1132-3.

28. Vlachopoulos, C., et al., *Association of Estimated Pulse Wave Velocity With Survival: A Secondary Analysis of SPRINT.* JAMA Netw Open, 2019. **2**(10): p. e1912831.

29. Goldin, A., et al., *Advanced glycation end products: sparking the development of diabetic vascular injury.* Circulation, 2006. **114**(6): p. 597-605.

30. Chow, B. and S.W. Rabkin, *The relationship between arterial stiffness and heart failure with preserved ejection fraction: a systemic meta-analysis.* Heart Fail Rev, 2015. **20**(3): p. 291-303.

31. Mottram, P.M., et al., *Relation of arterial stiffness to diastolic dysfunction in hypertensive heart disease.* Heart, 2005. **91**(12): p. 1551-6.

32. Zito, C., et al., *Interplay between arterial stiffness and diastolic function: a marker of ventricular-vascular coupling.* J Cardiovasc Med (Hagerstown), 2014. **15**(11): p. 788-96.

33. Mehta, R.H., et al., *Clinical and angiographic correlates and outcomes of suboptimal coronary flow inpatients with acute myocardial infarction undergoing primary percutaneous coronary intervention.* J Am Coll Cardiol, 2003. **42**(10): p. 1739-46.

34. Wakatsuki, T., et al., *Coronary flow velocity immediately after primary coronary stenting as a predictor of ventricular wall motion recovery in acute myocardial infarction.* J Am Coll Cardiol, 2000. **35**(7): p. 1835-41.

35. Yamamuro, A., et al., *Coronary flow velocity pattern immediately after percutaneous coronary intervention as a predictor of complications and in-hospital survival after acute myocardial infarction.* Circulation, 2002. **106**(24): p. 3051-6.

36. Lee, S., et al., *Plasma phospholipid fatty acid composition and estimated desaturase activity in heart failure patients with metabolic syndrome.* J Clin Biochem Nutr, 2012. **51**(2): p. 150-5.

37. Nasa, Y., et al., *Changes in fatty acid compositions of myocardial lipids in rats with heart failure following myocardial infarction.* Mol Cell Biochem, 1997. **176**(1-2): p. 179-89.

38. Chicco, A.J., et al., *Linoleate-rich high-fat diet decreases mortality in hypertensive heart failure rats compared with lard and low-fat diets.* Hypertension, 2008. **52**(3): p. 549-55.

39. Han, X., et al., *Alterations in myocardial cardiolipin content and composition occur at the very earliest stages of diabetes: a shotgun lipidomics study.* Biochemistry, 2007. **46**(21): p. 6417-28.

40. Paradies, G., et al., *Mitochondrial bioenergetics and cardiolipin alterations in myocardial ischemia-reperfusion injury: implications for pharmacological cardioprotection.* Am J Physiol Heart Circ Physiol, 2018. **315**(5): p. H1341-H1352.

41. Simopoulos, A.P., *An Increase in the Omega-6/Omega-3 Fatty Acid Ratio Increases the Risk for Obesity.* Nutrients, 2016. **8**(3): p. 128.

42. Kris-Etherton, P.M., et al., *Polyunsaturated fatty acids in the food chain in the United States.* Am J Clin Nutr, 2000. **71**(1 Suppl): p. 179S-88S.

43. Russo, C., et al., *Increased membrane ratios of metabolite to precursor fatty acid in essential hypertension.* Hypertension, 1997. **29**(4): p. 1058-63.

44. Warensjo, E., U. Riserus, and B. Vessby, *Fatty acid composition of serum lipids predicts the development of the metabolic syndrome in men.* Diabetologia, 2005. **48**(10): p. 1999-2005.

45. Watson, K.E., A.L. Peters Harmel, and G. Matson, *Atherosclerosis in type 2 diabetes mellitus: the role of insulin resistance.* J Cardiovasc Pharmacol Ther, 2003. **8**(4): p. 253-60.

46. Kozakova, M., et al., *Impact of glycemic control on aortic stiffness, left ventricular mass and diastolic longitudinal function in type 2 diabetes mellitus.* Cardiovasc Diabetol, 2017. **16**(1): p. 78.

47. Roman, M.J., et al., *Impact of arterial stiffening on left ventricular structure.* Hypertension, 2000. **36**(4): p. 489-94.

48. Lakatta, E.G. and S.J. Sollott, *The "heartbreak" of older age.* Mol Interv, 2002. **2**(7): p. 431-46.

49. Reinders, I., et al., *Higher Plasma Phospholipid n-3 PUFAs, but Lower n-6 PUFAs, Are Associated with Lower Pulse Wave Velocity among Older Adults.* J Nutr, 2015. **145**(10): p. 2317-24.

50. Tomiyama, H., et al., *Relationships among the serum omega fatty acid levels, serum C-reactive protein levels and arterial stiffness/wave reflection in Japanese men.* Atherosclerosis, 2011. **217**(2): p. 433-6.

51. Yasmin, et al., *C-reactive protein is associated with arterial stiffness in apparently healthy individuals.* Arterioscler Thromb Vasc Biol, 2004. **24**(5): p. 969-74.

52. King, D.E., et al., *C-reactive protein and glycemic control in adults with diabetes.* Diabetes Care, 2003. **26**(5): p. 1535-9.

53. Braunwald, E., *Myocardial reperfusion, limitation of infarct size, reduction of left ventricular dysfunction, and improved survival. Should the paradigm be expanded?* Circulation, 1989. **79**(2): p. 441-4.

54. Jacoby, R.M. and R.W. Nesto, *Acute myocardial infarction in the diabetic patient: pathophysiology, clinical course and prognosis.* J Am Coll Cardiol, 1992. **20**(3): p. 736-44.

55. Gedikli, O., et al., *Relationship between arterial stiffness and myocardial damage in patients with newly diagnosed essential hypertension.* Am J Hypertens, 2008. **21**(9): p. 989-93.

56. Chicco, A.J. and G.C. Sparagna, *Role of cardiolipin alterations in mitochondrial dysfunction and disease.* Am J Physiol Cell Physiol, 2007. **292**(1): p. C33-44.

57. Moon, S.H., et al., *Activation of mitochondrial calcium-independent phospholipase A2gamma (iPLA2gamma) by divalent cations mediating arachidonate release and production of downstream eicosanoids.* J Biol Chem, 2012. **287**(18): p. 14880-95.

58. Haworth, R.A., K.T. Potter, and D.C. Russell, *Role of arachidonic acid, lipoxygenase, and mitochondrial depolarization in reperfusion arrhythmias.* Am J Physiol Heart Circ Physiol, 2010. **299**(1): p. H165-74.

59. Penzo, D., et al., *Arachidonic acid released by phospholipase A(2) activation triggers Ca(2+)-dependent apoptosis through the mitochondrial pathway.* J Biol Chem, 2004. **279**(24): p. 25219-25.

60. Scorrano, L., et al., *Arachidonic acid causes cell death through the mitochondrial permeability transition. Implications for tumor necrosis factor-alpha aopototic signaling.* J Biol Chem, 2001. **276**(15): p. 12035-40.

61. Moon, S.H., et al., *Cardiac Myocyte-specific Knock-out of Calcium-independent Phospholipase A2gamma (iPLA2gamma) Decreases Oxidized Fatty Acids during Ischemia/Reperfusion and Reduces Infarct Size.* J Biol Chem, 2016. **291**(37): p. 19687-700.

62. Williams, S.D. and R.A. Gottlieb, *Inhibition of mitochondrial calcium-independent phospholipase A2 (iPLA2) attenuates mitochondrial phospholipid loss and is cardioprotective.* Biochem J, 2002. **362**(Pt 1): p. 23-32.

63. Moon, S.H., et al., *Heart failure-induced activation of phospholipase iPLA2gamma generates hydroxyeicosatetraenoic acids opening the mitochondrial permeability transition pore.* J Biol Chem, 2018. **293**(1): p. 115-129.

64. Tyurina, Y.Y., et al., *A mitochondrial pathway for biosynthesis of lipid mediators.* Nat Chem, 2014. **6**(6): p. 542-52.

CHAPTER III: EXPERIMENTAL OXYGEN CONCENTRATION INFLUENCES RATES OF MITOCHONDRIAL HYDROGEN PEROXIDE RELEASE FROM CARDIAC AND SKELETAL MUSCLE PREPARATIONS [3,4]

1. Introduction

Mitochondria-derived reactive oxygen species (mtROS) have been implicated in the development of diabetes [1], cardiovascular disease [2], and neurodegenerative disorders [3], as well as in aging [4] and cancer [5]. ROS are produced by at least eleven distinct sites in mitochondria [6], the majority being represented by superoxide radicals ($O_2^{\cdot -}$) formed by the single-electron reduction of O_2 at Complexes I and III of the electron transport system (ETS) [7]. Most superoxide is rapidly converted to hydrogen peroxide (H_2O_2) by superoxide dismutase enzymes in the mitochondrial matrix and inner membrane space. H_2O_2 readily crosses mitochondrial membranes either by passive or facilitated diffusion [8], where it can react with cellular components to reversibly modify their structure/function, participate in physiological cell signaling cascades, or cause irreversible oxidative damage to lipids, proteins and DNA [9]. The rates of mitochondrial H_2O_2 production and efflux are influenced by a complex interaction of intrinsic and extrinsic factors including the redox status of ETS enzymes, the O_2 concentration ($[O_2]$), and the activity of matrix antioxidant enzymes [10, 11]. Consequently, the observed rate of mtROS production varies substantially across cell types, respiratory states, and assay conditions, rather than being a fixed proportion of mitochondrial respiration [6, 7]

---

[3]This chapter has been published in the American Journal of Physiology- Regulatory, Integrative, and Comparative Physiology; DOI:10.1152/ajpregu.00227.2019

[4]Authors List: Li Puma LC, Hedges M, Heckman JM, Mathias AB, Engstrom MR, Brown AB, Chicco AJ

Several approaches have been developed for monitoring mtROS production and release from various sample types *in vitro* [12]. Measurement of H_2O_2 efflux from tissue mitochondrial preparations is among the most common and reliable quantitative methods, utilizing fluorophores such as Amplex® UltraRed to monitor changes in media H_2O_2 levels [13]. Historically, this approach has been employed in isolated mitochondria under ambient (room air equilibrated) [O_2] without ADP (State 4 or "LEAK" respiration), where mitochondria are energized with substrates that maximize mtROS production to generate the most robust signal (e.g., succinate + rotenone) [14]. However, the rate of mtROS release is much lower during oxidative phosphorylation (OXPHOS) and varies significantly with different substrate combinations [6]. Increasing interest in the relationship between mtROS production and O_2 consumption rates under more physiological conditions has led to new instrumentation and methodology for simultaneous monitoring of O_2 and H_2O_2 flux in various mitochondrial preparations [15, 16]. These technical advances have the potential to improve our understanding of mtROS roles in health and disease, but also raise important questions about the design and interpretation of experiments to avoid inconsistent or erroneous results [15].

Perhaps the most critical variable to consider in this context is the [O_2] of the assay media, which steadily declines as O_2 is reduced to water by cytochrome *c* oxidase, generating the assayed rate of mitochondrial oxygen consumption (JO_2). The extent to which media [O_2] declines depends on the concentration of mitochondria and substrates added, the length of the assay protocol, and O_2 diffusion limitations imposed by some sample preparations [17, 18]. Accordingly, dynamic changes in assay [O_2] may differentially affect measurements of JO_2 and ROS production/release (JH_2O_2) depending on the sensitivities of these processes to [O_2], the timing of data collection, and the sample type being evaluated. For example, use of permeabilized

muscle fibers is preferred over isolated organelles in some contexts to avoid disruption of mitochondrial connectivity [19] or when sample quantity is limited, but requires hyperoxic assay conditions to overcome a strong O_2 diffusion limitation on JO_2 [20, 21]. Isolated mitochondria lack this diffusion limitation, so are typically studied at ambient [O_2], but generate much more ROS than permeabilized cells [22]. Tissue homogenates have also been used to assess heart [23] and muscle [24] mitochondrial function, but contain other cellular components that could alter the relationships between assay [O_2], JO_2, and JH_2O_2.

The present study was undertaken to systematically characterize the feasibility and limitations of simultaneously measuring mitochondrial JO_2 and JH_2O_2 in cardiac and skeletal muscle mitochondrial preparations across the wide range of [O_2] typically encountered during extended high-resolution fluo-respirometry protocols. A particular focus was placed on the importance of background calibration experiments, the metabolic shift from LEAK (low JO_2, high JH_2O_2) to OXPHOS (high JO_2, low JH_2O_2) respiratory states, and the stability of JH_2O_2/O_2 measurements (H_2O_2 released per O_2 consumed) during OXPHOS-linked respiration over time. We hypothesized that assay [O_2] would differentially influence JH_2O_2 and JO_2, and that these kinetics would vary depending on the sample preparation being studied.

2. Materials and Methods

2.1 Animals Models

Adult (6-8-month-old) male FVB mice were obtained from Jackson Labs for use in these studies. Animals were housed in a temperature and humidity controlled facility on a 12:12 hour light:dark cycle and provided water and chow (Purina 2918) *ad libitum*, and were sacrificed for tissue collection by midline thoracotomy and removal of the heart following confirmation of deep

anesthesia by sodium pentobarbital injection (100 mg/kg i.p.). All procedures were approved by the Colorado State University Care and Use Committee and conform to the Guide for the Care and Use of Laboratory Animals published by the U.S. National Institutes of Health (NIH Publication No. 85-23, revised 1996).

2.2 Mitochondrial Isolation

Mitochondria (Mt) were isolated from heart and skeletal muscle tissues using standard differential centrifugation methods essentially as previously described [25]. All procedures were performed on ice or controlled at 4°C immediately upon harvesting fresh tissue. Hearts were excised and trimmed free of connective tissue, atria, and valves to provide myocardial tissue, then rinsed and minced in ice-cold Chappell-Perry (CP1) buffer consisting of (in mM) 100 KCl, 50 MOPS, 1 EDTA, 5 EGTA, 5 $MgSO_4 \cdot 7H_2O$, and 1 ATP, pH 7.4 with KOH [26]. Minced tissue was then homogenized for 10 secs at medium speed using a polytron, and incubated in CP1 containing trypsin (~5mg/g tissue) for 7 minutes to disrupt myofibrils in order to extract both interfibrillar and subsarcolemmal mitochondria. Trypsinized homogenates were then subjected to 6 passes with glass-Teflon Potter-Elvehjem homogenizer prior to centrifugation at 600 x g. The supernatant (containing mitochondria) was collected and centrifuged at 7000 x g to pellet mitochondria, followed by three 7000 x g clarifying spins in CP1 + 2 mg/ml albumin (twice), then once in KME buffer containing 100 mM KCl, 50 mM MOPS, 0.5 mM EGTA. Skeletal muscle (plantaris + gastrocnemius) mitochondria were isolated by a similar procedure except that no polytron was used, and EGTA was excluded until after the trypsin step. Final mitochondrial pellets were suspended in KME at approximately 5-10 mg protein/mL as determined by BCA protein assay (Thermo Fisher Scientific, San Jose, CA), then added to respiratory chambers at 37.5 μg protein/mL.

2.3 Permeabilized Fiber Preparation

Tissue sections (5-10 mg) of left ventricular myocardium or the soleus (entire muscle) were trimmed free of connective tissue and gently teased with needle tip forceps in ice-cold BIOPS preservation solution containing (in mM) 10 Ca-EGTA (0.1 μM free calcium), 20 imidazole, 20 taurine, 50 K-MES, 0.5 DTT, 6.56 $MgCl_2$, 5.77 ATP, 15 phosphocreatine, pH 7.1. Teased fiber bundles were then incubated with 50 μg/ml saponin on ice for 20 minutes with gentle rocking to permeabilize cell membranes while leaving mitochondrial membranes intact [20, 27]. Permeabilized fiber (Pf) bundles were then transferred to mitochondrial respiration medium (MiR05) containing (in mM) 0.5 EGTA, 3 $MgCl_2$ hexahydrate, 60 lactobionic acid, 20 taurine, 10 KH_2PO_4, 20 HEPES, 110 sucrose, and 0.1% BSA, pH 7.1 with KOH, and rinsed by rocking for 10 minutes on ice, followed by another identical 15-minute rinse. Permeabilized fiber bundles were gently blotted dry for 10-15 seconds on Whatman paper and weighed immediately before adding 0.9-1.1 mg (heart) or 2-2.5 mg (skeletal muscle) to each Oroboros oxygraph chamber for experiments.

2.4 Tissue Homogenate Preparation

Sections of left ventricular myocardium (35-50 mg) or skeletal muscle (plantaris + gastrocnemius) were excised and placed in ice-cold CP1 buffer (heart) or CP1 buffer excluding EGTA (muscle), then minced with scissors and rinsed 1-2 times to remove residual blood cells and debris. Buffers were then aspirated and MiR05 was added to a dilution of 20 mg / mL. Minced tissue was then homogenized on ice using a polytron on medium speed for 15 sec, after which 200 μL of the homogenate (Hm) was immediately added to the oxygraph chambers to provide a final tissue concentration of 2 mg/mL MiR05 for fluoro-respirometry experiments.

2.5 Simultaneous measurement of mitochondrial respiration and H_2O_2 release

An Oxygraph O2k-FluoRespirometer (Oroboros Instruments, Innsbruck, AT) consisting of two temperature-controlled chambers (37°C), each containing a polarographic oxygen sensor and a custom-fitted fluorometer (O2k-Fluo LED2 module), was used to simultaneously monitor changes in buffer [O_2] and H_2O_2 content as previously described in detail [15, 16]. Experiments were performed in 2 mL of the MiR05 respiration medium described above, based on rigorous testing of multiple common mitochondrial incubation media that determined MiR05 to have the highest stability and sensitivity for simultaneous JO_2 and JH_2O_2 measurements during prolonged respirometry protocols [28]. Standardized instrumental and chemical calibrations were applied using Datlab software for accurate measurement of chamber O_2 content and flux according to the manufacturer instructions (Oroboros Instruments, Innsbruck, Austria), which includes corrections for background diffusion of oxygen into the chamber, the oxygen solubility in MiR05 (0.92), and background consumption of oxygen by the electrodes across a broad range (50-450 μM) of chamber O_2 concentrations. Sample mitochondrial oxygen flux (JO_2) was monitored in real-time by resolving changes in the negative time derivative of the chamber oxygen concentration, normalized to the protein content (mitochondria) or tissue mass (fibers and homogenates) added to the chamber.

The net rate of mitochondrial H_2O_2 release (JH_2O_2) was measured simultaneously during respirometry experiments by monitoring the accumulation of chamber resorufin (Ex/Em 571/585 nm), the stable fluorescent product of 1:1 oxidation of Amplex UltraRed (AmR; 5 μM) by H_2O_2 in the presence of horseradish peroxidase (HRP; 1 U/mL) [13]. Care was taken to avoid exposure of the AmR and chamber to light during experiments, given the well-established photosensitivity of this probe [29]. Resorufin fluorescence was calibrated to chamber [H_2O_2] using freshly prepared H_2O_2 standards (0.1-1 μM) stabilized with 10 μM HCl as previously described in detail

[15]. Briefly, the increase in chamber fluorescence resulting from titrations of known H_2O_2 concentration was used to convert the fluorescence signal to chamber H_2O_2 content, being careful to avoid or account for the contribution of chemical background fluorescence in these measurements (APPENDIX; Supplemental Figure S1). Importantly, this chemical background (resorufin) fluorescence, which results largely from the interaction of AmR-HRP with MiR05 buffer components and respiratory substrates [15, 28], accumulates in the chamber over time to account for a significant proportion of the total (cumulative) and rate of fluorescence developed during experimental protocols (discussed later). While the contributions of individual substrates and buffer components to the rates of background fluorescence has been characterized previously [15], it is recommended that this be established for each instrument, buffer and substrate combinations used for fluo-respirometry experiments.

In accordance with this recommendation, we recorded the stable background fluorescence rate of MiR05 buffer in the presence of substrates used during our experimental protocols (in mM: 1 malate, 5 pyruvate, 10 glutamate, and 20 succinate, with or without 2.5 ADP), and accounted for (essentially subtracted) the background in calculations of authentic mitochondrial JH_2O_2 from biological samples. However, we found that this rate of chemical background fluorescence is sensitive to chamber O_2 concentration, declining linearly by approximately 6% for every 50 μM decrease in chamber [O_2] (Figure 7A). This indicates that accurate determination of sample JH_2O_2 requires corrections for background fluorescence rates measured at the chamber [O_2]s encountered during experimental protocols, accounting for wide variations in experimental [O_2] with multiple background measurements and/or estimates calculated by linear regression, which were applied in our experimental studies.

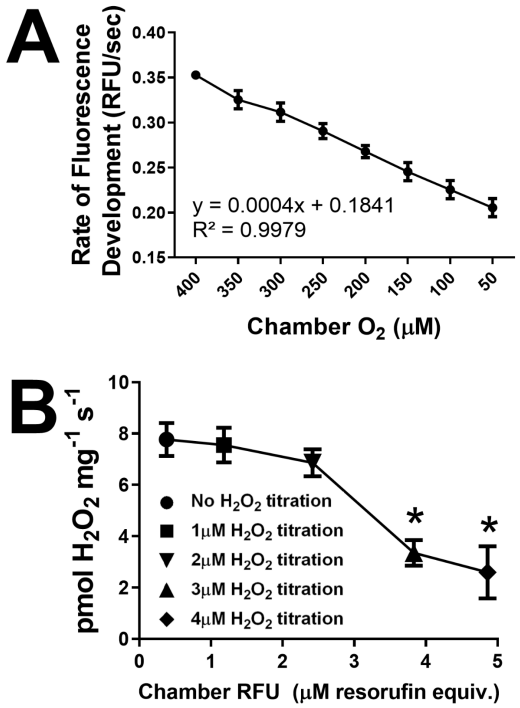

Figure 7. Amplex Red-HRP chemical background considerations. **A)** The background rate of resorufin fluorescence developed by chemical interactions with components of the MiR05 buffer with respiratory substrates (in the absence of sample) declines linearly with chamber [O_2] ($N = 4$). **B)** Corrected rates of H_2O_2 release from cardiac mitochondria at 250 μM O_2 following 0 - 4 μM H_2O_2 pre-injections (prior to adding mitochondria) to augment accumulation of chamber resorufin fluorescence facilitated by 5 μM AmR and 1 U/mL HRP (N = 4-8/point). *$P < 0.05$ versus No H_2O_2 titration by repeated measures ANOVA.

In addition, we found that the background-corrected rates of H_2O_2 formation by biological samples at a particular [O_2] (cardiac mitochondria at 250 μM O_2) significantly declined when chamber resorufin levels exceeded 2-3 μM, which was explored by increasing resorufin with H_2O_2 titrations prior to addition of sample in preliminary studies (Figure 7B). This likely reflects the decreasing linearity of the resorufin fluorescence signal observed above these levels [15], and perhaps product-inhibition of the HRP reaction rate by resorufin accumulation (and depletion of the AmR probe) in the chamber over time. Consequently, our experiments were designed to avoid cumulative resorufin concentrations greater than 2 μM by limiting H_2O_2 calibration steps to three

0.1 μM titrations and terminating experimental protocols before raw chamber fluorescence exceeded this level. It is worth noting that AmR can also be converted to resorufin by H_2O_2-independent reactions in some biological samples [30, 31]. These are expected to be minimal in the mitochondrial preparation used in the present study, but should also be considered when interpreting the precise implications of experimental results from using this probe.

2.6 Experimental protocols

2.6.1 Transition from LEAK to OXPHOS states

To evaluate the relationship between JO_2 and JH_2O_2 by energized mitochondria during the metabolic shift from a high-membrane potential/low ATP demand (LEAK) state to a lower-membrane potential/high ATP demand (OXPHOS) state, sample preparations were studied before and after the addition of 2.5 mM ADP. Mitochondrial were energized with saturating concentrations of substrates that fully reconstitute forward flux of the citric acid cycle, ultimately supplying electrons to the ETS from NADH and succinate (NS pathway) through Complexes I and II (in mM): 1 malate, 5 pyruvate, 10 glutamate, and 20 succinate. Samples were prepared as above and added to the oxygraph chambers immediately before (fibers and homogenates) or after (mitochondria) the addition of 1-2 mL of 100% O_2 gas to the air vortex created by stirring the chamber media with the stopper partially inserted, allowing media [O_2] to increase rapidly. Chambers were fully closed when media [O_2] reached approximately 400 μM, after which AmR, HRP, and substrates were titrated in sequence without ADP to establish JO_2 and JH_2O_2 under LEAK state conditions. Flux data were derived from at least 20 consecutive measurements recorded at 4-second intervals between 350-400 μM [O_2] (mean 375 μM) at 37°C for all samples to enable consistent comparisons across different preparations and tissues. Following data collection in the LEAK state, O_2 was increased to >400 μM again prior to adding ADP to re-

establish stable JO_2 and JH_2O_2 data in the OXPHOS state between 350-400 μM [O_2]. Hyperoxic conditions were selected for these experiments to overcome potential O_2 diffusion limitations of JO_2 previously reported in permeabilized muscle fibers [20], which was further investigated in subsequent studies.

2.6.2 Effect of chamber [O_2] on OXPHOS-linked JO_2 and JH_2O_2

Given increasing interest in studying mitochondrial bioenergetics under dynamic, physiologically-relevant conditions, we evaluated JO_2 and JH_2O_2 of sample preparations in the fully reconstituted NS-supported OXPHOS state across a wide range of [O_2]s typically encountered during multi-substrate respirometry protocols. Samples were prepared and loaded into the oxygraph chambers, then oxygenated to 200-450 μM and energized with the same substrate combination above + ADP to establish stable OXPHOS-linked JO_2 and JH_2O_2. Flux was continuously monitored as chamber [O_2] declined, and recorded at 50 μM intervals to generate at least 4 measurements between 400-50 μM for all sample preparations from at least 4 separate animals. Consecutive readings on individual samples were limited to cumulative chamber fluorescence levels equating to < 2 μM resorufin (H_2O_2) to avoid potentially confounding effects of AmR depletion or resorufin accumulation on assayed rates of JH_2O_2 (ref. [15]; Figure 7B). While recordings below 50 μM O_2 are of potential interest given the low intracellular PO_2s encountered *in vivo* [32], we found that the stability of the JO_2 signal and resolution of mitochondrial JH_2O_2 above chemical background fluorescence declined variably across mitochondrial preparations below this level (APPENDIX; Supplemental Figure S2 and S3). Moreover, performing fluorespirometry experiments below 50 μM O_2 is difficult or impractical without frequently replenishing or clamping chamber O_2 content, which interferes with stable

assessment of JO_2 and JH_2O_2. Therefore, we limited our presentation of data to 50 μM intervals between 50-400 μM O_2 for these experiments.

2.7 Statistical Analyses

All data are presented as means ± SEM. Data from LEAK and OXPHOS states were compared by independent sample (between tissues) or paired (within tissue) *t*-tests. One-way analyses of variance (ANOVA) were used to compare data across the three tissue mitochondrial preparations under discrete respiratory states and chamber O_2, contents, with repeated measures applied for comparisons across multiple O_2 concentrations. One-sided *t*-tests were used to compare differences between flux rates at 50 and 100 μM O_2 intervals when the ANOVA was significant to represent the range of O_2 concentration typically encountered during a multi-substrate respirometry protocol without reoxygenation. P values < 0.05 were considered statistically significant for all analyses.

3. Results

3.1 Cardiac and skeletal muscle JO_2 and JH_2O_2 in LEAK and OXPHOS states.

As expected, JO_2 increased significantly (2-4-fold) from the NS-supported LEAK (no ADP) to OXPHOS (ADP-stimulated) states in all sample preparations (Figure 8A-C), while JH_2O_2 significantly declined (50-90%) under identical (375 μM) chamber O_2 levels (Figure 8D-F). Representative raw data tracings from these studies are presented in APPENDIX; Supplemental Figure S4. In general agreement with previous studies [14-16], JH_2O_2 in the LEAK state ranged from 0.9 – 2.3 % of JO_2 across all sample preparations, then declined to 0.04 – 0.17 % of JO_2 in the OXPHOS state (Figure 8G-I). JO_2 was significantly higher in cardiac versus skeletal muscle Hm during OXPHOS (Figure 8A), and during both LEAK and

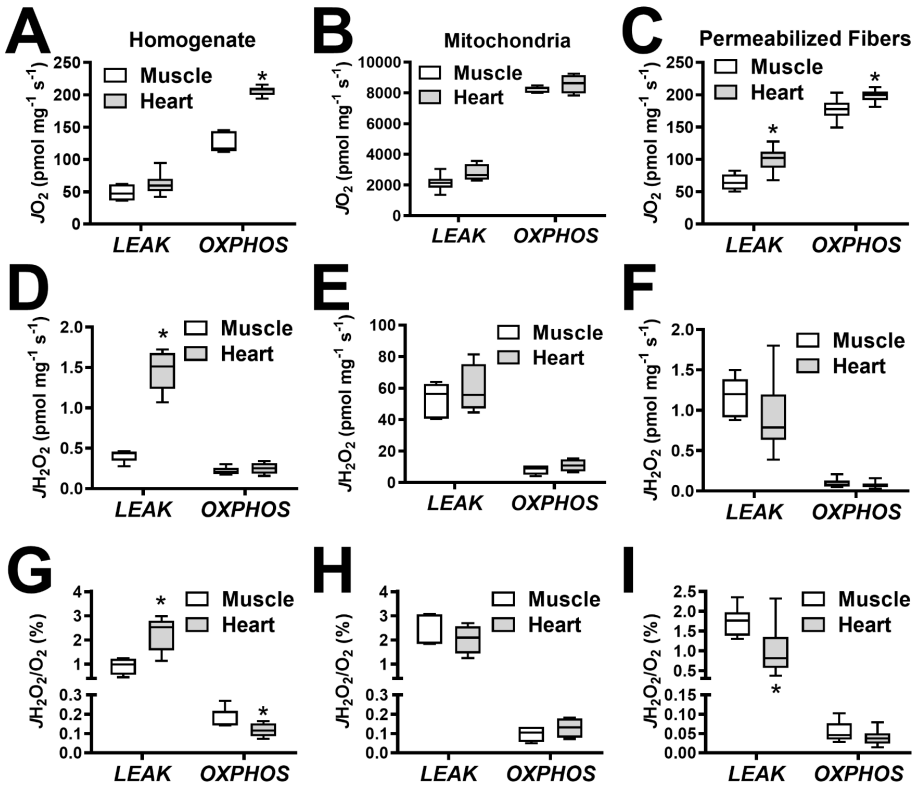

Figure 8. JO_2 and JH_2O_2 from muscle and heart preparations in LEAK and OXPHOS states. Oxygen consumption rates from heart homogenates were higher than muscle during OXPHOS **(A)**, but similar between tissues in isolated mitochondria **(B)**, and higher in heart during both LEAK and OXPHOS in permeabilized fibers **(C)**. Hydrogen peroxide release rates were higher from heart compared to muscle homogenates in the LEAK state **(D)**, but similar for both states between tissues in isolated mitochondria **(E)** and permeabilized fibers **(F)**. Rates of hydrogen peroxide release expressed as a percent of oxygen consumption were higher from heart homogenates during LEAK, but lower during OXPHOS **(G)**, similar between tissues in isolated mitochondria **(H)**, and lower in heart permeabilized fibers during LEAK **(I)**. All data were collected between 350-400 μM [O_2] at 37°C and presented as means ± SEM (N=4-10/group). Boxes illustrate the range (whiskers) and mean (middle bar) of individual values. *$P < 0.05$ versus muscle by independent samples *t*-test.

OXPHOS in Pf preparations (Figure 8B) ($P<0.01$). This likely reflects the higher mitochondrial density of cardiac compared to skeletal muscle given similar JO_2 per mg protein in isolated Mt from both tissues (Figure 8C). JH_2O_2 was generally similar in cardiac versus skeletal muscle preparations, but was >3-fold higher in cardiac Hm in the LEAK state (Figure 8D), contributing

to >2-fold higher JH_2O_2/O_2 under these conditions (Figure 8G). However, JH_2O_2/O_2 was 74% higher from skeletal muscle versus cardiac Hm in the OXPHOS state (Figure 8G) and from Pf in the *LEAK* state (Figure 8H), with similar values between tissues in Mt (Figure 8I). Taken together, these results highlight the variability in JO_2 and JH_2O_2 introduced by studying complex tissue preparations when flux data is normalized to sample mass, which is avoided when comparing isolated mitochondria normalized to sample protein content.

3.2 Influence of sample preparation on ADP control of JO_2 and JH_2O_2.

The relative shift (or "ADP control") of mitochondrial function from LEAK to OXPHOS states can provide useful insight to tissue metabolic control and sample quality under various biological and experimental conditions. We predicted that ADP control of JO_2 and JH_2O_2 would vary across mitochondrial preparations, and found notable tissue-specific differences in both outcomes (Figure 9). The extent of ADP-control over NS-linked JO_2 in cardiac preparations were as follows: Hm = Mt > Pf (P<0.05; Figure 9A), with no differences in JH_2O_2 (Figure 9B) or JH_2O_2/O_2 (Figure 9C) across the three cardiac preparations. Variation across skeletal muscle preparations were as follows: for JO_2, Hm = Pf < Mt (Figure 9D); for JH_2O_2 and JH_2O_2/O_2, Hm < Mt = Pf (Figure 9E and F). Therefore, ADP control of JO_2 is generally higher in Mt than Pf from both tissues, with tissue-specific differences in Hm compared to other preparations. The associated decline in JH_2O_2 from LEAK to OXPHOS is consistent across sample preparations in heart, but is attenuated in skeletal muscle Hm compared Mt and Pf.

3.3 Chamber oxygen content strongly influences JH_2O_2 across sample preparations

Systematic evaluation of OXPHOS-linked JO_2 in cardiac samples across a wide range of chamber O_2 concentrations revealed a persistent decrease from 400 to 50 μM O_2 in all three preparations by ANOVA (P < 0.05; Figure 10A-C). However, the extent of decline over 50-100

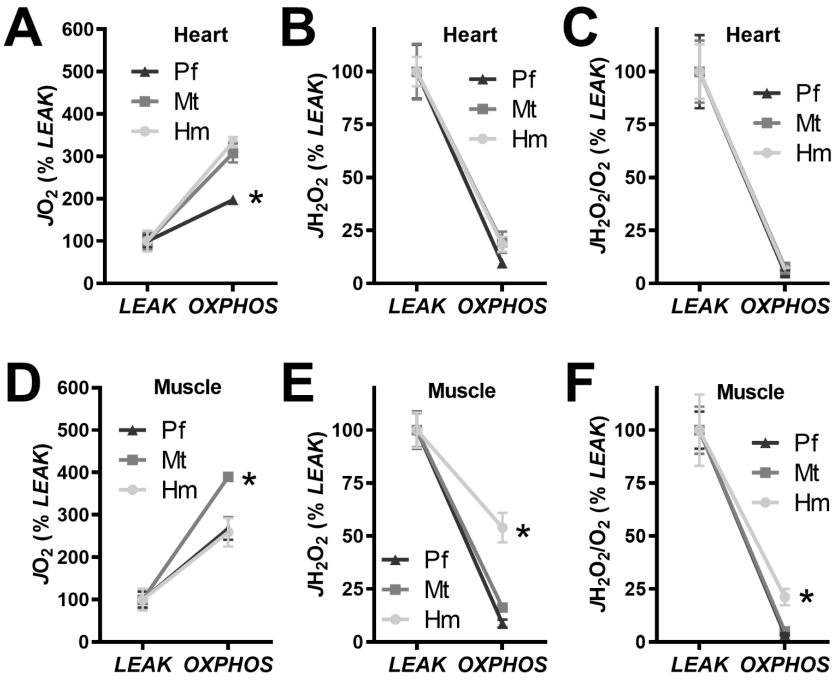

Figure 9. Effect of sample preparation on the shifts in JO_2 and JH_2O_2 from LEAK to OXPHOS states. In cardiac preparations, oxygen consumption increased from LEAK to OXPHOS to a lesser extent in permeabilized fibers (PF) than homogenates (Hm) and isolated mitochondria (Mt) **(A)**, while hydrogen peroxide release rates declined similarly to <25% of LEAK rates across all sample preparations when expressed as pmol H_2O_2/mg/sec **(B)** or a percent of oxygen consumption **(C)**. In skeletal muscle preparations, oxygen consumption rates increased to a greater degree in Mt comparted to Hm and Pf **(D)**, while the decline in hydrogen peroxide release was greater in Mt and Pf than Hm expressed in absolute **(E)** and relative terms **(F)**. All data were collected between 350-400 μM [O_2] at 37°C and presented as means ± SEM (N = 4-10/group). *P < 0.05 versus other preparations by one-way ANOVA.

O_2 intervals was negligible in Hm and Mt (< 5% per 100 μM O_2; P=NS), and only 10-15% over the entire 350 μM range. OXPHOS-linked JO_2 in Pf was relatively stable across higher chamber O_2 concentrations, but significantly declined by 250 μM O_2, and was increasingly sensitive to [O_2] changes below this concentration (Figure 10C), consistent with the strong O_2 diffusion limitation of JO_2 in permeabilized fiber bundles [20]. In contrast with JO_2, JH_2O_2 declined by ~75% in all three sample preparations from 400 to 50 μM O_2 (Figure 10D-F), with variable effects of sample

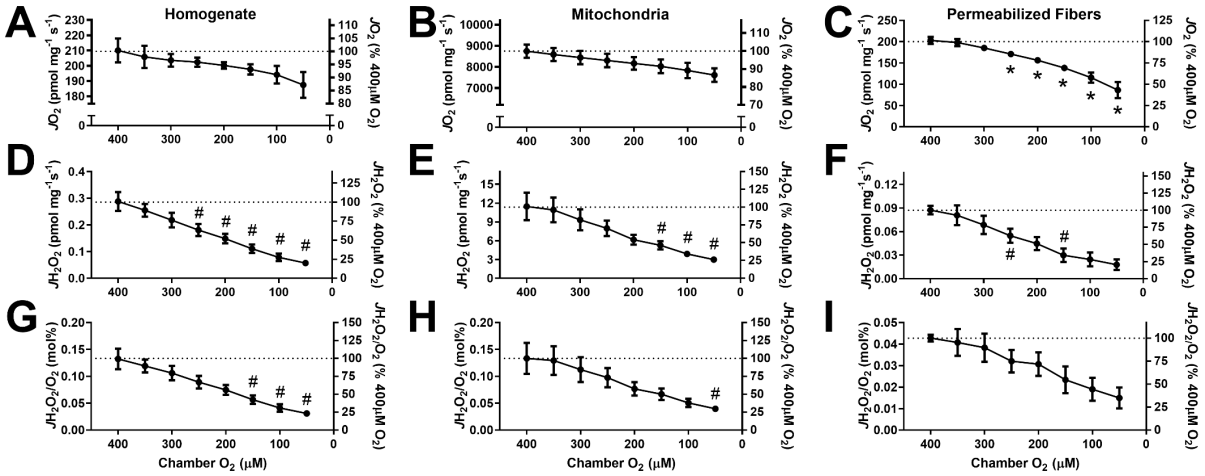

Figure 10. Influence of chamber oxygen content on JO_2 and JH_2O_2 during OXPHOS in cardiac sample preparations. Oxygen consumption rates (JO_2) declined slightly (10-15%) in homogenates **(A)** and isolated mitochondria **(B)** as chamber oxygen content decreased from 400 to 50 μM, but decreased significantly for every 50 μM decrease in chamber oxygen content below 300 μM in permeabilized fibers **(C)**. Hydrogen peroxide release rates (JH_2O_2) declined ~75% in all sample preparations as chamber oxygen content decreased from 400 to 50 μM when expressed as pmol H_2O_2/mg/s **(D-F)** or as a proportion of JO_2 **(G-I)**, with variable effects of sample preparation on the significance of differences across 100 μM [O_2] intervals below 300 μM. Data are means ± SEM (N=4-12/group) presented as absolute flux (left y-axes) and as a percent of the 400 μM O_2 value (right y-axes). Differences in flux were analyzed by independent sample *t*-tests to evaluate the impact of variable [O_2] on comparisons made between two experimental samples during a typical fluo-respirometry protocol. *$P < 0.05$ versus 50 μM higher [O_2]. #$P < 0.05$ versus 100 μM higher [O_2].

preparation on the significance of decreases across 100 μM O_2 intervals below 300 μM. JH_2O_2 expressed as a proportion of JO_2 also declined linearly with chamber O_2 concentration (Figure 10 G-I), but was more resistant to significant changes over 100 μM O_2 intervals than absolute JH_2O_2.

Responses of skeletal muscle preparations to chamber O_2 concentration were similar to cardiac samples, with significant declines in OXPHOS-linked JO_2 from 400 to 50 μM O_2 in all three preparations by ANOVA (Figure 11A-C), but negligible effects in Hm and Mt over 50-100 μM intervals. JO_2 in Pf was Muscle JH_2O_2 declined by ~75% in Hm and Pf, and nearly 100% in Mt from 400 to 50 μM O_2 (Figure 11D-F), with sensitivity over 50-100 μM O_2 intervals being

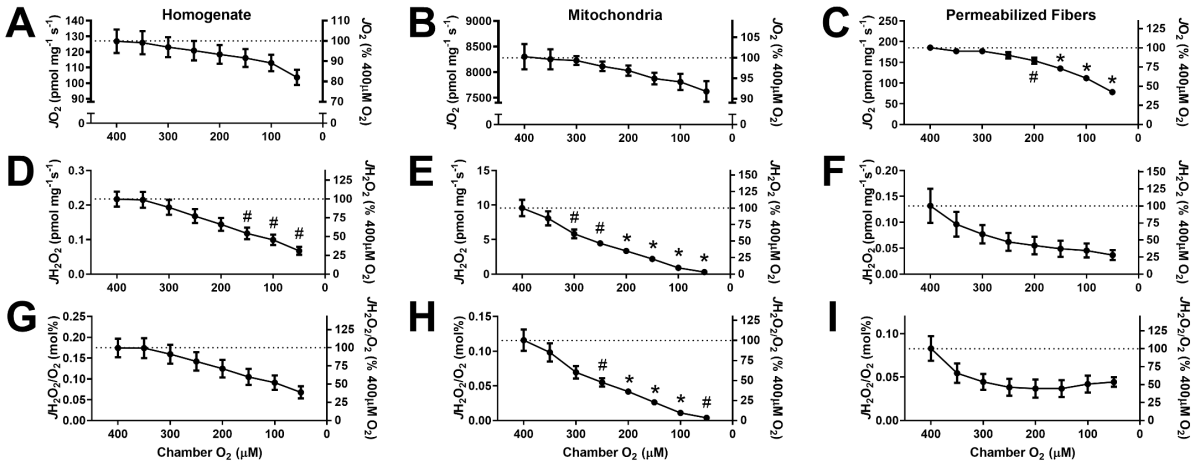

Figure 11. Influence of chamber oxygen content on JO_2 and JH_2O_2 during OXPHOS in skeletal muscle sample preparations. Oxygen consumption rates (JO_2) declined slightly in homogenates **(A)** and isolated mitochondria **(B)** as chamber [O_2] decreased from 400 to 50 μM, but declined significantly for every 50-100 μM decrease in chamber [O_2] below 250 μM in permeabilized fibers **(C)**. Hydrogen peroxide release rates (JH_2O_2) declined markedly in all sample preparations as chamber [O_2] decreased from 400 to 50 μM when expressed as pmol H_2O_2/mg/s **(D-F)** or as a proportion of JO_2 **(G-I)**, with variable effects of sample preparation on the significance of differences across [O_2] intervals below 350 μM. Data are means ± SEM (N = 4-12/group) presented as absolute flux (left y-axes) and as a percent of the 400 μM O_2 value (right y-axes). Differences in flux were analyzed by independent sample t-tests to evaluate the impact of variable [O_2] on comparisons made between two experimental samples during a typical fluo-respirometry protocol. *$P < 0.05$ versus 50 μM higher [O_2]. #$P < 0.05$ versus 100 μM higher [O_2].

highest in Mt > Hm > Pf. This led to variable sensitivity of JH_2O_2/JO_2 responses to chamber O_2 across muscle preparations (Figure 11G-I), with the greatest observed in Mt > Hm > Pf. Taken together, these results demonstrate a strong influence of chamber O_2 content on JH_2O_2 in all mitochondrial preparations, leading to highly variable rates of JH_2O_2/JO_2 due to different O_2-sensitivities of JO_2 across tissues and sample preparations.

It is worth noting that the chemical background fluorescence discussed above (Figure 7A) accounted for 34 to 93% of the total rate of resorufin fluorescence developed by biological samples depending on the mitochondrial preparation used, tissue of origin, and chamber [O_2] during the

recording (APPENDIX; Supplemental Figure S3A), highlighting the importance of appropriate background corrections discussed in the Methods. The O_2-dependence of mitochondrial JH_2O_2 was found to be greater than that of the chemical background signal, which results in an increasing contribution of chemical background flux to the total rate of fluorescence developed by all sample preparations as chamber [O_2] declines (APPENDIX; Supplemental Figure S3B;).

4. Discussion

Mitochondria are responsible for the vast majority of oxygen consumption by aerobic organisms. Electrons from oxidized metabolic substrates are carried by reduced cofactors to the electron transfer system, where they travel through inner membrane protein complexes to oxygen at cytochrome *c* oxidase. This process facilitates formation of an inner membrane proton gradient that is harnessed by the ATP synthase to phosphorylate ADP, and results in both JO_2 (H_2O formation) and ROS production at rates that vary depending on the tissue, substrate, and metabolic state examined [6]. Oxygen tension is an important regulator of ROS production *in vivo* [33, 34] and *in vitro* [35-37], but the present study is the first to systematically evaluate the sensitivity of simultaneous JO_2 and JH_2O_2 measurements from tissue mitochondrial preparations to variations in experimental O_2 content. Results demonstrate a generally linear association between sample JH_2O_2 and chamber O_2 content in all cardiac and skeletal muscle preparations evaluated, despite preparation-specific variations in the O_2-sensitivity of JO_2. This manifests as a steady decline in assayed JH_2O_2 rates as chamber O_2 is consumed by the sample during OXPHOS-linked JO_2, and wide variations in calculated rates of JH_2O_2/O_2 across sample preparations at different chamber O_2 concentrations. This has important implications for studies that employ extended respirometry protocols or sample comparisons that result in variations in chamber O_2 content >50 μM. For

example, samples with slower JO_2 may have higher JH_2O_2 in the later stages of an extended multi-substrate protocol simply by maintaining higher chamber O_2 content over time. Therefore, it is critical to consider the intrinsic (sample preparation) and extrinsic factors (experimental conditions) that influence sample of JO_2 and JH_2O_2 in order to draw valid conclusions about mitochondrial function and dysfunction, particularly when monitoring these parameters simultaneously.

High-resolution respirometry protocols are being increasingly employed to investigate mitochondrial responses to multiple substrate, inhibitor and uncoupler titrations within the same experiment; resulting in considerable changes in chamber O_2 content ranging from < 50 μM to > 500 μM during assay periods that routinely exceed 60 minutes [16, 20]. Re-oxygenation of the chamber has been recommended to overcome O_2 diffusion limitations of JO_2 below a selected threshold [O_2] for permeabilized muscle fibers, but not for isolated mitochondria, homogenates or most cultured cells [17]. The present study corroborates these findings, demonstrating negligible O_2-sensitivity of JO_2 in Mt and Hm from heart and skeletal muscle over 100 μM O_2 assay ranges, while JO_2 in Pf declines linearly with chamber O_2 concentrations below ~250 μM. Therefore, the nearly linear dependence of JH_2O_2 on chamber [O_2] from 400-50 μM in all sample preparations indicates that mtROS producing sites are far more sensitive to changes in O_2 tension than cytochrome *c* oxidase, as previously demonstrated in isolated mitochondria and submitochondrial particles oxidizing a variety of substrates [37]. Mt and Hm generated nearly 2-fold greater JH_2O_2/O_2 than Pf in the OXPHOS state, suggesting that O_2 diffusion also limits superoxide production from mitochondrial embedded within intact myofibrils. However, it is also important to emphasize that JH_2O_2 reflects a net balance of mtROS production and consumption by exogenous antioxidant systems [38]. This could explain why Hm and Pf, both of which retain

intracellular antioxidant enzymes, had lower JH_2O_2/O_2 than Mt during the LEAK state when mtROS production is maximized. Regardless of the mechanisms responsible, these findings should be considered along with the advantages and disadvantages of different muscle mitochondrial preparations for respirometry discussed by Perry et al. [39] and others [19], particularly in studies when mtROS production or damage is a primary interest.

A notable finding from the present study is that Mt isolated from slow-oxidative skeletal muscle exhibit similar NS-supported JO_2 as cardiac Mt during both LEAK and OXPHOS states (expressed per mg protein), while JO_2 was much higher in cardiac versus skeletal muscle Hm and Pf (expressed relative to tissue wet weight). This implicates greater mitochondrial density as the primary basis for the higher oxidative capacity of cardiac compared to skeletal muscle tissue [40, 41], and emphasizes the importance of considering both intrinsic and extrinsic factors that influence mitochondrial function when selecting sample preparations for experiments. In both tissues, Mt exhibited higher ADP control of JO_2 than Pf, perhaps reflecting an ADP diffusion limitation in Pf. However, ADP control of JO_2 in Hm paralleled Mt in heart, and Pf in muscle. This might reflect a confounding effect of interstitial or cytosolic components present in skeletal muscle compared to cardiac Hm and Pf, which should also be considered when selecting and interpreting data from these sample preparations. Also noteworthy is the higher JH_2O_2 and particularly JH_2O_2/O_2 during LEAK in heart versus skeletal muscle Hm, which followed an opposite trend in Pf. This is unlikely due to greater damage of cardiac mitochondria by homogenization since JH_2O_2/O_2 was lower than muscle Hm during OXPHOS. Elucidating the mechanisms responsible for these variations across tissue preparations and respiratory states is beyond the scope of this study, but the results emphasize the importance of considering and

perhaps evaluating the distinct properties of these tissue preparations when designing and interpreting studies of mitochondrial function.

It is often erroneously assumed that mtROS are produced as a fixed 1-2% of mitochondrial JO_2 based on early reports by Boveris and Chance [14], despite qualification by the authors that this only applied to specific experimental conditions (similar to the LEAK state herein). Recent reviews have further clarified this point, emphasizing the influence substrates, respiratory state and membrane potential on mtROS production [6, 7]. The present study demonstrates a robust increase in JO_2 from NS-supported LEAK to OXPHOS states, while JH_2O_2 robustly decreases, reflecting the expected effects of a decline in mitochondrial membrane potential (MMP) facilitated by activation of the ADP phosphorylation system (ATP synthase and the adenine nucleotide translocase). In the LEAK state, the ETS is fully reduced by substrate supply in the absence of energy demand (no ADP), resulting in a high MMP that maximizes electron leak to O_2 (mtROS production), but severely limits the rate of electron flow to cytochrome *c* oxidase (JO_2). The addition of ADP releases this electron "back up" and MMP by facilitating dissipation of the inner membrane proton gradient through the ATP synthase, thereby decreasing mtROS formation and increasing JO_2 in the OXPHOS state [6, 7]. The extents of ADP control over JO_2 and JH_2O_2 reveal the sensitivity of mitochondria to changes in energy supply and demand, analogous to the transition from a post-prandial resting state to the elevated energy demands of heavy physical exercise. JH_2O_2/O_2 consistently declined to < 0.2% of JO_2 in response to increased energy demand (ADP) across all sample preparations, demonstrating the potent effects of respiratory state on mtROS release in heart and skeletal muscle. mtROS production rates are likely to be even lower under physiological conditions *in vivo* due to lower tissue PO_2 and substrate availability, but may achieve these or higher rates in pathological conditions such as tissue ischemia-reperfusion [6, 7].

Another important consideration highlighted by our study is the demonstration that development of AmR background fluorescence is also sensitive to chamber O_2 content. Resorufin is generated in the absence of sample by the chemical interaction of AmR-HRP with sucrose, taurine and lactobionate in the MiR05 respiration buffer independent of AmR concentration or substrates present [15]. Herein, we show that this chemical background flux (rate of fluorescence development) declines linearly with media oxygen concentration (Figure 7A), emphasizing the importance of performing chemical background corrections across a range of media oxygen contents encountered during planned experiments. Importantly, this background may vary with different buffer formulations, which might also influence assayed rates of mitochondrial JO_2 and JH_2O_2 [15, 39]. We found that resorufin fluorescence generated in response to 0.1-1 μM H_2O_2 titrations was consistent across chamber O_2 contents as previously reported [15, 28] (data not shown), but that an accumulation of resorufin can limit assayed rates of JH_2O_2 from biological samples. AmR concentrations of 5-10 μM have been recommended for fluo-respirometry experiments to avoid depletion of the probe during extended protocols and potential inhibitory effects on mitochondrial respiration above 20 μM [15]. However, while resorufin fluorescence in MiR05 buffer increases linearly with chemical concentrations up to ~2-3 μM, it progressively declines thereafter by up to 20% at 5 μM [15]. Our studies demonstrate that the assayed rate of mitochondrial JH_2O_2 supported by 5 μM AmR at 250 μM O_2 declines by over 50% when cumulative fluorescence exceeds 3.5 μM resorufin (Figure 7B). Taken together, these findings indicate that cumulative chamber resorufin fluorescence corresponding to >2-3μM H_2O_2 should be avoided when using 5 μM AmR by limiting the length of the assay protocol, decreasing the quantity of sample added, or using lower concentrations of H_2O_2 standards during calibration experiments (e.g., 0.1 μM).

In summary, the present study demonstrates a strong dependence of mitochondrial JH_2O_2 from heart and skeletal muscle preparations on experimental O_2 concentration. This leads to significant variations in observed rates of mtROS release from samples in a closed respirometry chamber that depend upon the initial assay [O_2], rate of sample JO_2, and sample preparation used, particularly when expressed as a proportion of JO_2. Rates of mtROS release also vary substantially depending on the respiratory state examined, declining from ~1-2% of JO_2in the LEAK state to < 0.2% in the OXPHOS state, with variable responses of different sample preparations to shifts in energy demand (ADP). Therefore, it is recommended that JO_2 and JH_2O_2 data be recorded within a common narrow range of chamber [O_2] across all experimental groups and respiratory states being compared during fluo-respirometry experiments. We also show that background rates of fluorescence development by AmR in MiR05 respiration media are O_2-dependent, and that accumulation of resorufin (or depletion of AmR) can limit observed rates of JH_2O_2 from biological samples independent of chamber [O_2]. Therefore, careful design of background corrections, H_2O_2 calibrations, and assay protocols are needed to ensure accurate reporting of sample JH_2O_2 rates under dynamic experimental conditions. Collectively, these studies expand upon recent methodological reports demonstrating the feasibility and potential pitfalls of simultaneously monitoring mitochondrial JO_2 and JH_2O_2 of biological samples [15, 16], and provide a basis for selecting cardiac and skeletal muscle sample preparations for studies addressing the role mtROS in physiology and disease.

REFERENCES

1. Nishikawa, T. and E. Araki, *Impact of mitochondrial ROS production in the pathogenesis of diabetes mellitus and its complications.* Antioxid Redox Signal, 2007. **9**(3): p. 343-53.

2. Kornfeld, O.S., et al., *Mitochondrial reactive oxygen species at the heart of the matter: new therapeutic approaches for cardiovascular diseases.* Circ Res, 2015. **116**(11): p. 1783-99.

3. Wang, X., et al., *Oxidative stress and mitochondrial dysfunction in Alzheimer's disease.* Biochim Biophys Acta, 2014. **1842**(8): p. 1240-7.

4. Gomez-Cabrera, M.C., et al., *Mitochondria as sources and targets of damage in cellular aging.* Clin Chem Lab Med, 2012. **50**(8): p. 1287-95.

5. Idelchik, M., et al., *Mitochondrial ROS control of cancer.* Semin Cancer Biol, 2017. **47**: p. 57-66.

6. Wong, H.S., et al., *Production of superoxide and hydrogen peroxide from specific mitochondrial sites under different bioenergetic conditions.* J Biol Chem, 2017. **292**(41): p. 16804-16809.

7. Murphy, M.P., *How mitochondria produce reactive oxygen species.* Biochem J, 2009. **417**(1): p. 1-13.

8. Bienert, G.P., J.K. Schjoerring, and T.P. Jahn, *Membrane transport of hydrogen peroxide.* Biochim Biophys Acta, 2006. **1758**(8): p. 994-1003.

9. Sies, H., *Role of metabolic H2O2 generation: redox signaling and oxidative stress.* J Biol Chem, 2014. **289**(13): p. 8735-41.

10. Cortassa, S., B. O'Rourke, and M.A. Aon, *Redox-optimized ROS balance and the relationship between mitochondrial respiration and ROS.* Biochim Biophys Acta, 2014. **1837**(2): p. 287-95.

11. Treberg, J.R., C.L. Quinlan, and M.D. Brand, *Hydrogen peroxide efflux from muscle mitochondria underestimates matrix superoxide production--a correction using glutathione depletion.* FEBS J, 2010. **277**(13): p. 2766-78.

12. Dikalov, S.I. and D.G. Harrison, *Methods for detection of mitochondrial and cellular reactive oxygen species.* Antioxid Redox Signal, 2014. **20**(2): p. 372-82.

13. Starkov, A.A., *Measurement of mitochondrial ROS production.* Methods Mol Biol, 2010. **648**: p. 245-55.

14. Boveris, A. and B. Chance, *The mitochondrial generation of hydrogen peroxide. General properties and effect of hyperbaric oxygen.* Biochem J, 1973. **134**(3): p. 707-16.

15. Krumschnabel, G., et al., *Simultaneous high-resolution measurement of mitochondrial respiration and hydrogen peroxide production.* Methods Mol Biol, 2015. **1264**: p. 245-61.

16. Makrecka-Kuka, M., G. Krumschnabel, and E. Gnaiger, *High-Resolution Respirometry for Simultaneous Measurement of Oxygen and Hydrogen Peroxide Fluxes in Permeabilized Cells, Tissue Homogenate and Isolated Mitochondria.* Biomolecules, 2015. **5**(3): p. 1319-38.

17. Gnaiger, E., *Capacity of oxidative phosphorylation in human skeletal muscle: new perspectives of mitochondrial physiology.* Int J Biochem Cell Biol, 2009. **41**(10): p. 1837-45.

18. Scandurra, F.M. and E. Gnaiger, *Cell respiration under hypoxia: facts and artefacts in mitochondrial oxygen kinetics.* Adv Exp Med Biol, 2010. **662**: p. 7-25.

19. Picard, M., et al., *Mitochondria: isolation, structure and function.* J Physiol, 2011. **589**(Pt 18): p. 4413-21.

20. Pesta, D. and E. Gnaiger, *High-resolution respirometry: OXPHOS protocols for human cells and permeabilized fibers from small biopsies of human muscle.* Methods Mol Biol, 2012. **810**: p. 25-58.

21. Gnaiger, E., *Oxygen conformance of cellular respiration. A perspective of mitochondrial physiology.* Adv Exp Med Biol, 2003. **543**: p. 39-55.

22. Picard, M., et al., *Mitochondrial structure and function are disrupted by standard isolation methods.* PLoS One, 2011. **6**(3): p. e18317.

23. Pham, T., et al., *Mitochondrial inefficiencies and anoxic ATP hydrolysis capacities in diabetic rat heart.* Am J Physiol Cell Physiol, 2014. **307**(6): p. C499-507.

24. Ziak, J., et al., *Assessing the function of mitochondria in cytosolic context in human skeletal muscle: adopting high-resolution respirometry to homogenate of needle biopsy tissue samples.* Mitochondrion, 2015. **21**: p. 106-12.

25. Heim, A.B., et al., *Tissue-specific seasonal changes in mitochondrial function of a mammalian hibernator.* Am J Physiol Regul Integr Comp Physiol, 2017. **313**(2): p. R180-R190.

26. Palmer, J.W., B. Tandler, and C.L. Hoppel, *Biochemical properties of subsarcolemmal and interfibrillar mitochondria isolated from rat cardiac muscle.* J Biol Chem, 1977. **252**(23): p. 8731-9.

27. Chicco, A.J., et al., *Adaptive remodeling of skeletal muscle energy metabolism in high-altitude hypoxia: Lessons from AltitudeOmics.* J Biol Chem, 2018. **293**(18): p. 6659-6671.

28. Komlodi, T., et al., *Comparison of Mitochondrial Incubation Media for Measurement of Respiration and Hydrogen Peroxide Production.* Methods Mol Biol, 2018. **1782**: p. 137-155.

29. Summers, F.A., et al., *Photooxidation of Amplex Red to resorufin: implications of exposing the Amplex Red assay to light.* Methods Enzymol, 2013. **526**: p. 1-17.

30. Debski, D., et al., *Mechanism of oxidative conversion of Amplex(R) Red to resorufin: Pulse radiolysis and enzymatic studies.* Free Radic Biol Med, 2016. **95**: p. 323-32.

31. Miwa, S., et al., *Carboxylesterase converts Amplex red to resorufin: Implications for mitochondrial H2O2 release assays.* Free Radic Biol Med, 2016. **90**: p. 173-83.

32. Kreutzer, U. and T. Jue, *Critical intracellular O2 in myocardium as determined by 1H nuclear magnetic resonance signal of myoglobin.* Am J Physiol, 1995. **268**(4 Pt 2): p. H1675-81.

33. Kulkarni, A.C., P. Kuppusamy, and N. Parinandi, *Oxygen, the lead actor in the pathophysiologic drama: enactment of the trinity of normoxia, hypoxia, and hyperoxia in disease and therapy.* Antioxid Redox Signal, 2007. **9**(10): p. 1717-30.

34. Shimada, I., et al., *Hyperoxia causes diffuse alveolar damage through mechanisms involving upregulation of c-Myc/Bax and enhanced production of reactive oxygen species.* Respir Investig, 2016. **54**(1): p. 59-68.

35. Brueckl, C., et al., *Hyperoxia-induced reactive oxygen species formation in pulmonary capillary endothelial cells in situ.* Am J Respir Cell Mol Biol, 2006. **34**(4): p. 453-63.

36. Pendyala, S., et al., *Role of Nox4 and Nox2 in hyperoxia-induced reactive oxygen species generation and migration of human lung endothelial cells.* Antioxid Redox Signal, 2009. **11**(4): p. 747-64.

37. Grivennikova, V.G., A.V. Kareyeva, and A.D. Vinogradov, *Oxygen-dependence of mitochondrial ROS production as detected by Amplex Red assay.* Redox Biol, 2018. **17**: p. 192-199.

38. Munro, D. and J.R. Treberg, *A radical shift in perspective: mitochondria as regulators of reactive oxygen species.* J Exp Biol, 2017. **220**(Pt 7): p. 1170-1180.

39. Perry, C.G., et al., *Methods for assessing mitochondrial function in diabetes.* Diabetes, 2013. **62**(4): p. 1041-53.

40. Lemieux, H. and C.L. Hoppel, *Mitochondria in the human heart.* J Bioenerg Biomembr, 2009. **41**(2): p. 99-106.

41. Park, S.Y., et al., *Cardiac, skeletal, and smooth muscle mitochondrial respiration: are all mitochondria created equal?* Am J Physiol Heart Circ Physiol, 2014. **307**(3): p. H346-52.

CHAPTER IV: *FADS2* EXPRESSION REGULATES MYOCARDIAL ISCHEMIC INJURY AND MITOCHONDRIAL RESPONSE TO CALCIUM OVERLOAD [5,6]

1. Introduction

Heart disease is the most common cause of death in western societies, where someone experiences an acute myocardial infarction (AMI) every 40 seconds [1]. AMI leads to cardiac complications such as arrhythmias [2], heart failure [3], mechanical complications [4], and survival is inversely proportional to the size of the myocardial infarction sustained [5]. Therefore, identifying factors that influence the extent of myocardial injury during ischemia reperfusion is of critical importance.

Single nucleotide polymorphisms (SNPs) in the *FADS2* gene cluster predict cardiovascular morbidity in humans, implicating endogenous metabolism of polyunsaturated fatty acids (PUFAs) in the regulation of cardiovascular health and disease [6]. Studies in animal models have linked greater *Fads2* expression or activity of its gene product delta-6 desaturase (D6D) to the development of hypertensive heart disease [7], age-related cardiac dysfunction [8], and ischemia-reperfusion (IR) injury (Li Puma, in preparation) perhaps by altering the distribution of PUFA in myocardial phospholipids. In particular, higher *Fads2*/D6D activity appears to increase endogenous synthesis of arachidonic acid (AA; *n*6) from dietary linoleic acid (LA; *n*6), the most abundant PUFA in modern Western diet, leading to increases in the serum and myocardial AA/LA ratio. This is consistent with evidence from epidemiological studies linking higher serum AA/LA ratio to *FADS2* SNPs and cardiovascular mortality in humans [9], suggesting an important

---

[5]This chapter has been prepared for submission to American Journal of Physiology- Heart

[6]Author's List: Li Puma LC, Specht KS, Heckman JM, Chicco AJ

nutrigenetic interaction between *FADS2* and the modern diet on cardiovascular risk [10]. However, the mechanisms by which *Fads2* alters myocardial responses to pathogenic stress are unclear. Recently, we found that greater *Fads2* expression promotes a selective incorporation of AA into cardiac mitochondrial membranes, which closely paralleled the extent of myocardial injury following IR, suggesting a potential role of mitochondria in this response (Li Puma, in preparation).

The pathogenesis of myocardial IR injury is a complex process that develops from a transient deprivation of coronary blood supply to heart muscle. During ischemia, a decrease in oxygen delivery impairs mitochondrial oxidative phosphorylation, leading to depletion of ATP, an increase in cytosolic calcium levels (Ca^{++}), and activation of membrane phospholipases [11, 12]. Reperfusion results in a sudden reoxygenation of the myocardium that supports a rapid increase in mitochondrial membrane potential and mitochondrial Ca^{++} accumulation, leading to excessive production of reactive oxygen species (ROS) and opening of the mitochondrial permeability transition pore (mPTP) [11, 12]. These processes mediate the majority of cardiomyocyte death during IR, particularly mPTP opening, which enables mitochondrial ROS release to the cytosol and participates in both apoptotic and necrotic death pathways [13-16].

Activation of phospholipases can occur via ischemia and ischemia-reperfusion [17], in part via Ca^{++} accumulation [18], acyl-CoA generation [19], and oxidized-fatty acids [20]. In particular, phospholipid hydrolysis of AA and generation of its eicosanoid derivatives in cardiac tissue have been linked to tachyarrhythmias [21], fibrosis and hypertrophy [22, 23], and IR injury [24, 25]; though evidence demonstrates they may also have cardioprotective effects [26]. Recently, $iPLA_2\gamma$ has been characterized as a prominent phospholipase in cardiomyocytes activated during IR, where it catalyzes Ca^{++} dependent release of AA specifically from mitochondrial membranes [27].

Mitochondrial AA can be converted to eicosanoids by lipoxygenase and cytochrome P450 enzymes that increase mPTP sensitivity and contribute to the development of myocardial injury [24]. Therefore, *Fads2* expression may exacerbate IR injury by increasing mitochondrial AA content and altering functional responses to Ca^{++} overload. The present study tested this hypothesis by evaluating cardiac mitochondrial responses to Ca^{++}-overload in mice with genetic gain and loss of *Fads2* expression, modeling variations in *FADS2* genotype across human populations. The roles of mitochondrial $iPLA_2$ and AA metabolism were also investigated pharmacologically, providing new insight to the mechanisms by which myocardial PUFA levels influence cardiac responses to pathogenic stress.

2. Materials and Methods

2.1 Animal Models

Transgenic mice with global over-expression of murine *Fads2* (*Fads2*^{TG}) driven by the cytomegalovirus (CMV) promoter were generated on an FVB background and bred through at least the tenth backcrossed generations in a colony maintained at Colorado State University (Li Puma, in preparation). A parallel colony of FVB wild-type mice in the sixth generation maintained at Colorado State University served as the control (FVB) mice for these studies. Heterozygous D6D-null mice (*Fads2*^{KD}) founder mice (C57Bl/6j background) were gifted to our laboratory by Dr. Manabu Nakamura at the University of Illinois [28] which were used to generate a colony of *Fads2*^{KD} and *Fads2*$^{+/+}$ (WT) mice currently in the fourth generation at Colorado State University. *Fads2*^{KD} pups were genotyped using DNA extracted from 5mm tail snips via PCR. Four primer sets flanking exon 1 of *Fads2* were used to amplify both KO and WT regions [28]. Animals were housed in a temperature and humidity controlled facility on a 12:12 hour light:dark cycle and

provided water and diets (Purina 2918) *ad libitum* until sacrifice (6-8 months of age) by midline thoracotomy and removal of the heart following confirmation of deep anesthesia with sodium pentobarbital injection (100 mg/kg i.p.). All procedures were approved by the Colorado State University Care and Use Committee and conform to the Guide for the Care and Use of Laboratory Animals published by the U.S. National Institutes of Health (NIH Publication No. 85-23, revised 1996).

2.2 Myocardial Ischemia-Reperfusion Injury

Myocardial tolerance to ischemia-reperfusion (IR) stress was evaluated *ex vivo* using an isolated perfused heart system to investigate intrinsic myocardial responses independent of circulating factors or systemic perturbations as previously described [29]. Briefly, mice were placed under deep anesthesia with intraperitoneal injection of a heparinized pentobarbital 50 mg/kg solution prior to sacrifice by midline thoracotomy and rapid heart excision by cutting the pulmonary trunk, pulmonary arteries, the aortic arch distal to the brachiocephalic trunk, and the superior/inferior vena cava. Hearts were immediately placed in ice-cold Krebs-Henseleit buffer (in mM: 117.4 NaCl, 4.7 KCl, 1.9 $CaCl_2$, 1.2 $MgSO_4$, 1.2 KH_2PO_4, 5 pyruvate, 11 glucose, 0.5 EDTA, 25 $NaHCO_3$, and pH to 7.4 with 95/5% O_2/CO_2) to remove any excess lung or adipose tissue. Hearts were then cannulated via the ascending aorta and retrogradely perfused in Langendorff mode generating a constant perfusion pressure of ~80 mmHg. All hearts underwent 20 minutes of stabilization prior to 45 minutes of global, no-flow ischemia, then reperfused for 120 minutes prior to infarct size assessment by Triphenyltetrazolium Chloride (TTC) staining described below. Coronary effluent was collected directly from perfused hearts immediately prior to ischemia and 5, 10, 15, 30, 60, 90, and 120 minutes after reperfusion. To quantitate the extent of myocardial infarction following the I-R protocol, hearts were removed from the cannula and dissected to

isolate the left ventricle and septum. The left ventricle was then weighed prior to placing into a matrix and sliced transversely into five, 1mm transverse slices. Each slice was weighed prior to incubation in 0.1% TTC solution for 10 minutes in a shaking incubator at 37C. Slices were then fixed in 10% Formalin for one hour prior to imaging using a camera attached to a dissecting scope (Ken-A-Vision). TTC stains active tissue brick-red, while infarcted tissue appears white/yellow. NIH ImageJ software was used to calculate the ratio of active to dead tissue. Infarct size (percent of total LV) was calculated by averaging the ratio of white/red on each side of the slice and then weighting that average by the percent that slice made up of the total LV: (((%Infarct Side A) + (%Infarct Side B))/2) * ((Mass of Slice/Total LV Mass) *100) and then each slice added together to get percent infarct of the LV.

To evaluate mitochondrial function after exposure to IR, hearts were cannulated as described above and underwent 20 minutes of stabilization prior to 45 minutes of global, no-flow ischemia, then reperfused for 45 minutes prior to isolation of mitochondria (as described below). All procedures were performed by the same experienced technician.

2.3 Mitochondrial Isolation

Mitochondria were isolated from myocardial tissue using standard differential centrifugation methods essentially as previously described [8]. All procedures were performed on ice or controlled at 4°C immediately upon harvesting fresh tissue. Hearts were excised and trimmed free of connective tissue, atria, and valves to provide myocardial tissue, then rinsed and minced in ice-cold Chappell-Perry (CP1) buffer consisting of (in mM) 100 KCl, 50 MOPS, 1 EDTA, 5 EGTA, 5 $MgSO_4 \cdot 7H_2O$, and 1 ATP, pH 7.4 with KOH. Minced tissue was then homogenized for 10 secs at medium speed using a polytron, and incubated in CP1 containing trypsin (~5 mg/g tissue) for 7 minutes to disrupt myofibrils in order to extract both interfibrillar

and subsarcolemmal mitochondria. Trypsinized homogenates were then subjected to six passes with glass-Teflon Potter-Elvehjem homogenizer prior to centrifugation at 600 x g. The supernatant (containing mitochondria) was collected and centrifuged at 7000 x g to pellet mitochondria, followed by three 7000 x g clarifying spins in CP1 + 2 mg/ml albumin (twice), then once in KME buffer containing 100 mM KCl, 50 mM MOPS, 0.5 mM EGTA. Final mitochondrial pellets were suspended in KME at approximately 5-10 mg protein/mL as determined by BCA assay (Thermo Fisher Scientific, San Jose, CA), then added to respiratory chambers at 15 µg protein/mL.

2.4 Mitochondrial Phospholipid Fatty Acid Composition

Analysis of the fatty acids present on mitochondrial phospholipids was performed by gas chromatography as previously described [7]. Briefly, mitochondria (50ug) were homogenized in ice-cold methanol (1:10 w/v) and centrifuged to pellet the non-lipid material. Lipids in the methanol supernatant were transferred to a glass tube containing sodium methoxide solution (25% w/v) to synthesize fatty acid methyl esters from phospholipid FAs. Hexane was then added, the solution dried under nitrogen gas, and resuspended in hexane. Samples were analyzed using an Agilent Technologies DB-225 30 m × 0.250 mm × 0.25 µm column (model 122-2232, J&W Scientific) on an Agilent 6890 Series gas chromatograph with a flame ionization detector at a flow rate of 1.7 mL/min and split ratio of 15:1 in 25 minutes.

2.5 Simultaneous measurement of mitochondrial respiration and H_2O_2 release

An Oxygraph O2k-FluoRespirometer (Oroboros Instruments, Innsbruck, AT) consisting of two temperature-controlled chambers (37^{o}C), each containing a polarographic oxygen sensor and a custom-fitted fluorometer (O2k-Fluo LED2 module), was used to simultaneously monitor changes in buffer O_2 and H_2O_2 content as previously described in detail [30-32]. Experiments were performed in 2 mL of MiR05 containing (in mM) 0.5 EGTA, 3 $MgCl_2$ hexahydrate, 60

lactobionic acid, 20 taurine, 10 KH_2PO_4, 20 HEPES, 110 sucrose, and 0.1% BSA, pH 7.1 with KOH. Standardized instrumental and chemical calibrations were applied using Datlab software for accurate measurement of mitochondrial oxygen consumption rate (JO_2) as previously described [32] The net rate of mitochondrial H_2O_2 release (JH_2O_2) was determined during respirometry by monitoring the accumulation of chamber resorufin (Ex/Em 571/585 nm), the stable fluorescent product of 1:1 oxidation of Amplex UltraRed (AmR; 5 μM) by H_2O_2 in the presence of horseradish peroxidase (HRP; 1 U/mL). Mitochondria (30 μg protein) were energized with saturating concentrations of substrates that fully reconstitute forward flux of the TCA cycle (1 mM malate, 5 mM pyruvate, 10 mM glutamate, and 20 mM succinate) in the presence of ADP (2.5 mM), ultimately supplying electrons to the electron transfer system from NADH and succinate through Complexes I and II to maximize rates of JO_2 and JH_2O_2 during ATP synthesis. To measure JO_2 and JH_2O_2 in response to Ca^{++}-overload, free-Ca^{++} was added to chambers in successive steps every two minutes to allow stabilization of JO_2 and JH_2O_2 in between titrations. Stocks of 25 mM free-Ca^{++} were used to generate the concentrations stated in figures, taking into consideration volume and EGTA concentration of solutions. Data collection was restricted to a narrow [O_2] range of 100 μM, with the chamber being reoxygenated with 100% O_2 if chamber [O_2] ever dropped below 300 μM to reduce limitation of chamber O_2 concentration on JH_2O_2 [32].

2.6 Mitochondrial Swelling Assay

Isolated cardiac mitochondria were kept on ice in KME until preparation of mitochondrial swelling assay. Mitochondria were added to 2X swelling buffer (in mM: 500 sucrose, 20 Tris-Mops, 0.02 EGTA, 10 pyruvate, 2 malate, pH: 7.4 with KOH) for a final amount of 33 μg per well. For experiments examining the effects of phospholipase or oxygenase inhibition, mitochondria in 2X swelling buffer were pretreated with the following inhibitors (final concentration in 200 μL):

500nM Cyclosporin A; mPTP pore inhibitor, 30 μM (*R*)- BEL ((*E*)-6-(bromomethylene)-3-(1-naphthalenyl)-2*H*- tetrahydropyran-2-one); iPLA$_2$γ inhibitor, 10 μM baicalein (5,6,7-trihydroxyflavone); pan-lipoxygenase inhibitor, 10 μM indomethacin; pan-cyclooxygenase inhibitor, 40 μM MSPPOH (*N*-(methylsulfonyl)-2-(2-propynyloxy)- benzenehexanamide); CYP450 epoxygenase inhibitor, 40 μM SKF-525A; pan-CYP450 inhibitor, or dimethyl sulfoxide (DMSO) vehicle alone for 10 min at room temperature. Mitochondrial swelling was initiated by addition of free-Ca^{++} to a final concentration of 200 uM. Decreases in the absorbance of 540 nm indicative of mitochondrial swelling were measured every 60 seconds for 30 minutes using a spectrophotometer (Agilent, CA, USA).

2.7 Statistics

Statistical analysis was performed using Graphpad Prism 8 (Graphpad Software, CA, USA). Groups were compared by a 2 genotype X 2 treatment ANOVA to resolve main and interactive effects of *Fads2* expression and treatment (IR/ intervention) on all parameters. Pairwise comparisons between individual groups were made by Tukey post-hoc analyses following a significant ANOVA, or students *t*-test when only two groups were compared. Statistical significance was set at $P < 0.05$ for all analyses.

3. Results

3.1 Overexpression of Fads2 exacerbates ischemia-reperfusion injury.

We have previously shown that *Fads2*^{TG} mice develop larger myocardial infarcts compared to FVB wild-type mice when fed custom-engineered diets where the *n*6:n*3* PUFA ratios was 57:1 and 1:1 and 0% LC-PUFAs (Li Puma in preparation). To confirm that this phenotype persists when mice are fed a standard, grain-based chow diet (12:1 *n*6:*n*3 ratio, of which 13% of PUFAs were

LC-PUFAs), hearts from FVB and *Fads2*^{TG} mice were exposed to the same 45/120 minute global IR protocol in the present study. As expected, left ventricles from *Fads2*^{TG} mice had 42% greater myocardial infarct sizes than FVB controls (Figure 12A; $P < 0.05$), confirming that greater *Fads2* expression lowers intrinsic myocardial tolerance to IR stress.

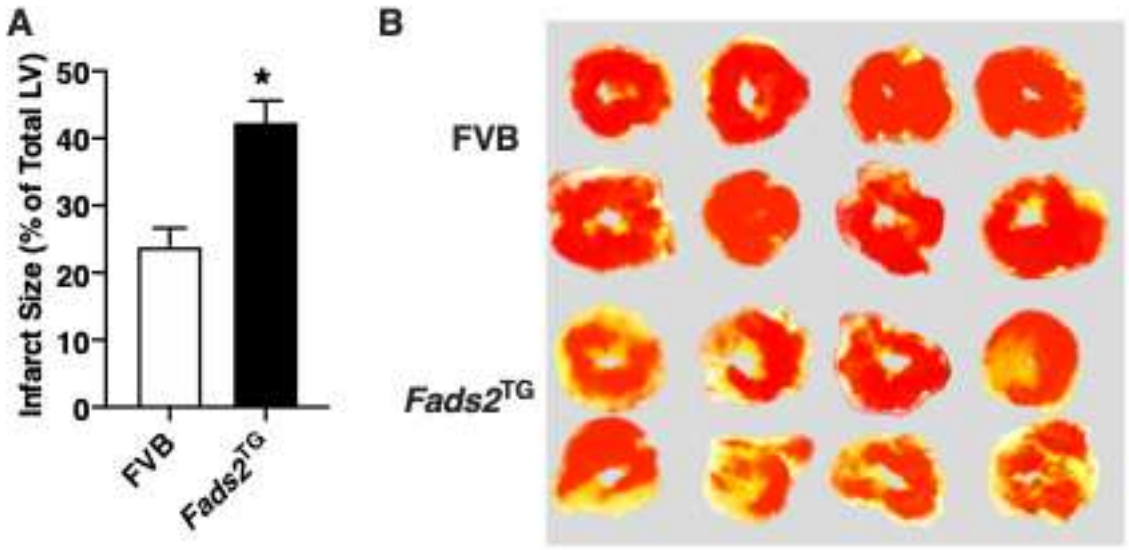

Figure 12: Overexpression of *Fads2* exacerbates myocardial ischemia-reperfusion injury. A) Left ventricular (LV) infarct size in isolated hearts from FVB and *Fads2*^{TG} mice exposed to 45/120 minutes of *ex vivo* ischemia/reperfusion, expressed as percent of total LV mass (N=8/group). **B**) Representative images of stained transverse left ventricular sections that generated data in panel A (infarcted tissue is yellow). Data are means ± SEM. *$P < 0.05$ using a Student's *t*-test.

3.2 Fads2 overexpression increases arachidonic acid in mitochondrial phospholipids.

In our previous study (Li Puma, in preparation) we demonstrated a close positive correlation between myocardial infarct size and the AA content of cardiolipin, the signature phospholipid of the inner mitochondrial membrane. Therefore, we predicted that *Fads2* overexpression would increase AA in the total mitochondrial phospholipid fraction in chow-fed mice. Indeed, AA was significantly greater in *Fads2*^{TG} compared to FVB mitochondria, which could be accounted for largely by a reciprocal decrease in LA (Table 5). PUFA ratios reflective

Table 5: *Fads2* overexpression increases arachidonic acid in mitochondrial phospholipids. Gas chromatographic analysis of major fatty acids present on phospholipids extracted from FVB and *Fads2*^{TG} myocardial mitochondria (*N*=5/group). Data are means ± SEM expressed as % of total fatty acids. A Student's *t*-test used to investigate differences between groups; **P* < 0.05 using a Student's *t*-test.

	FVB	***Fads2*^{TG}**
16:0, Palmitic	14.0±0.2	14.5±0.2
16:1, Palmitoleic	0.37±0.05	0.45±0.05
18:0, Stearic	21.9±0.2	22.3±0.3
18:1n9, Oleic	6.02±0.19	4.54±0.14*
18:1n7, Vaccenic	1.80±0.07	1.41±0.06*
18:2n6, LA	18.6±0.5	13.2±0.4*
18:3n3, ALA	0.61±0.03	0.62±0.02
20:3n6, DGLA	0.48±0.02	0.48±0.02
20:4n6, AA	7.63±0.12	12.6±0.2*
22:5n3, DPA	1.10±0.07	1.44±0.10*
22:6n3, DHA	27.3±0.3	27.8±0.2
DGLA/LA	0.026±0.002	0.037±0.002*
AA/LA	0.41±0.01	0.96±0.03*
DPA/ALA	1.83±0.15	2.34±0.18*
DHA/ALA	45.2±1.7	45.2±1.6

of higher D6D activity (DGLA/LA, AA/LA, and DPA/ALA) were also significantly greater in *Fads2*^{TG} mitochondria compared to FVB control, consistent with greater endogenous synthesis of AA and other long-chain PUFA in *Fads2*^{TG} mice.

Interestingly, the greater proportion of AA in *Fads2*^{TG} mitochondrial membranes was ablated by exposure to a truncated (45/90 min) IR protocol (Figure 13A), with no significant effect on other membrane fatty acid levels (APPENDIX; Supplemental Table S3). This was associated with a significant decrease in JO_2 (Figure 13B) and greater loss of mitochondrial membrane integrity (Figure 13C) compared to pre-IR values and FVB mitochondria. These results suggest

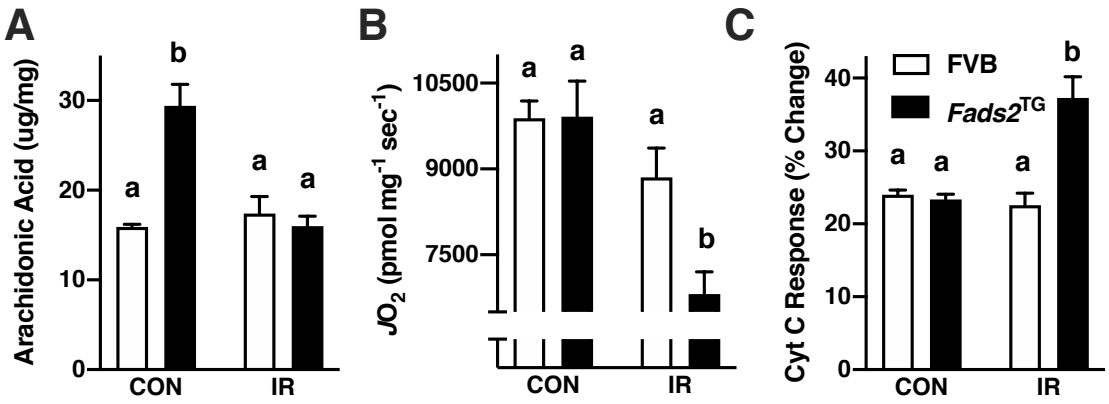

Figure 13: Ischemia-reperfusion decreases AA from *Fads2*^{TG} mitochondrial phospholipids and impacts mitochondrial energetics. Intact mitochondria from FVB and *Fads2*^{TG} myocardium were isolated immediately after an abbreviated (45/90 min) ischemia-reperfusion protocol. **A**) Amount (μg lipid/mg mitochondria) of arachidonic acid present in FVB and *Fads2*^{TG} mitochondrial phospholipids before and after IR; *N*=5/group. **B**) Maximal oxygen consumption rate (JO_2) of isolated mitochondria reconstituted with TCA cycle intermediates and ADP; *N*=5/group. **C**) Percent increase in JO_2 induced by addition of cytochrome c to the oxygraph chamber, reflecting the extent of mitochondrial outer membrane damage in the sample; *N*=5/group. $P < 0.05$ denoted by difference in letter.

that the excess AA present on mitochondrial membranes of *Fads2*^{TG} mouse hearts prior to ischemia is hydrolyzed during the early stages of IR, which corresponds to a loss of mitochondrial functional integrity consistent with the larger infarct sizes observed following the longer IR protocol (Figure 12).

3.3 Fads2^{TG} cardiac mitochondria exhibit lower tolerance to Ca^{++} overload.

Beat-to-beat Ca^{++} levels in the cytosol oscillate between 1-2 uM [33]; however, it has been demonstrated that the dyadic space between the sarcoplasmic reticulum and mitochondria can reach 200 uM free-Ca^{++} and greater, entering the matrix through the mitochondrial calcium uniporter [34-36]. Mitochondrial Ca^{++} overload contributes to IR injury by impairing myocardial bioenergetics, increasing mitochondrial ROS release, and inducing mPTP opening [11, 16]. We hypothesized that mitochondria from mice with greater *Fads2* expression would be less tolerant to Ca^{++}-overload, reflected by lower JO_2 and/or higher JH_2O_2. Naïve myocardial mitochondria were

isolated and reconstituted with TCA cycle intermediates and ADP and allowed to stabilize oxidative phosphorylation prior to Ca^{++} titrations in our oxygraph chambers. As predicted, JO_2 declined in *Fads2*^{TG} mitochondria at a lower cumulative Ca^{++} concentration compared to FVB mitochondria, and decreased at a greater rate with subsequent titrations (Figure 14A). In addition, Ca^{++} titrations increased JH_2O_2 to a greater extent in *Fads2*^{TG} compared to FVB mitochondria (Figure 14B), resulting in much greater JH_2O_2 expressed as a fraction of JO_2 (Figure 14C). These findings indicate that *Fads2* overexpression reduces cardiac mitochondrial tolerance to Ca^{++}-overload, leading to impaired bioenergetics and greater ROS release that may exacerbate myocardial injury during IR. Mitochondrial functional impairments are linked to myocardial necrosis primarily through mPTP opening [13], which was investigated further in the context of mitochondrial AA metabolism.

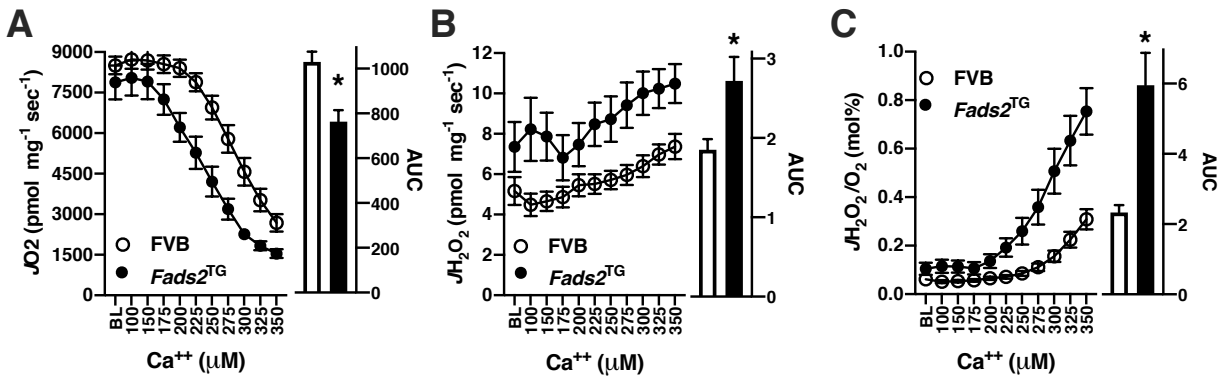

Figure 14: *Fads2* overexpression decreases cardiac mitochondrial Ca^{++} tolerance. Mitochondria isolated from FVB and *Fads2*^{TG} mouse hearts were reconstituted with TCA cycle intermediates in presence of ADP to support maximal oxygen consumption (JO_2; **A**) and H_2O_2 release (JH_2O_2; **B**) before sequential titrations of calcium (N=10/group). **C**) JH_2O_2 expressed as percent of JO_2. *$P < 0.05$ compared to FVB by Sidak *post-hoc* analyses following a significant repeated-measures ANOVA.

3.4 Mitochondrial arachidonic acid metabolism links greater Fads2 expression to Ca^{++} dependent mPTP opening.

Mitochondrial Ca^{++}-overload activates phospholipases and generation of AA-derived eicosanoids that augments mPTP opening and contributes to myocardial IR injury [18, 24]. Based on our evidence for greater AA content in *Fads2*^{TG} mitochondria that may be hydrolyzed during IR (Figure 13), we hypothesized that *Fads2* overexpression would augment mPTP opening in response to Ca^{++}-overload in a manner dependent upon the mobilization and metabolism of mitochondrial AA. mPTP opening was assessed by cyclosporine A (CsA)-sensitive swelling of cardiac mitochondria from *Fads2*^{TG} and FVB mice exposed to 200 μM free-Ca^{2++} in the presence of pharmacological inhibitors of phospholipid AA hydrolysis and metabolism. Ca^{++} challenge significantly increased swelling of *Fads2*^{TG} mitochondria compared to FVB, which was abolished in both genotypes by CsA, confirming the involvement of mPTP opening (Figure 15A). Inhibition of $iPLA_2$ with bromoenol lactone (BEL) mitigated mitochondrial swelling to a similar extent in both genotypes, and attenuated the trend for greater swelling in *Fads2*^{TG} versus FVB (Figure 15B). Inhibition of 12/15 lipoxygenase with Baicalein completely abolished the differences between genotypes, and reduced mitochondrial swelling in both groups to a similar extent as CsA (Figure 15C). Interestingly, inhibition of cyclooxygenase with Indomethacin (Figure 15D) and CYP450 epoxygenase with MSPPOH (Figure 15E) exacerbated mitochondrial swelling in FVB, but not *Fads2*^{TG} mitochondria. However, inhibition of CYP450 hydroxylase with SKF-525A attenuated swelling in *Fads2*^{TG}, but not FVB mitochondria (Figure 15F). Taken together, these results indicate that *Fads2* overexpression augments mPTP opening in response to Ca^{++}-overload at least in part by increasing metabolism of mitochondrial AA by 12/15 lipoxygenase and CYP450 hydroxylase. Products of these pathways have been previously implicated in myocardial IR injury [37-39], suggesting that *Fads2* overexpression may exacerbate IR injury by increasing mitochondrial AA content.

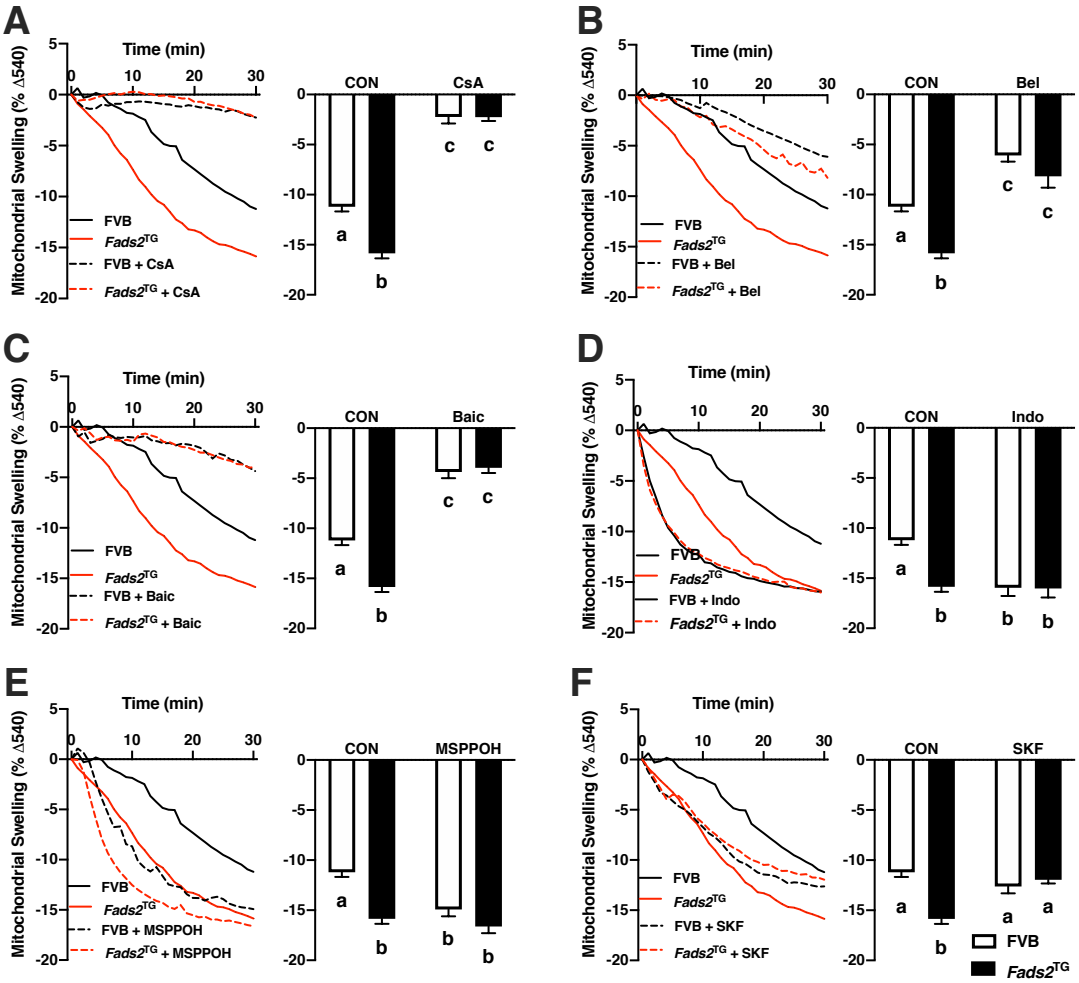

Figure 15: *Fads2* overexpression sensitizes mPTP opening to Ca^{++} overload via eicosanoid signaling. Representative line tracings of cardiac mitochondrial swelling (decrease in absorbance at 540nm) and final %-change of absorbance (bar graph) from FVB and *Fads2*^{TG} mice with **A**) mPTP inhibitor (cyclosporine A; CsA), **B**) iPLA$_2$ inhibitor (bromoenollactone; Bel), **C**) 12/15 lipoxygase inhibitor (Baicalien, Baic), **D**) cycloxygenase inhibitor (indomethacin; indo), **E**) CYP450 epoxygenase inhibitor (MSPPOH), and **F**) pan-CYP450 inhibitor (SKF); *N*= 9/group. Tukey *post-hoc* tests were used to investigate pairwise comparisons following significant ANOVA. $P < 0.05$ denoted by difference in letter.

3.5 Lower Fads2 expression decreases mitochondrial membrane AA content.

To further investigate the hypothesized links between *Fads2* expression, mitochondrial AA content, and IR injury, we next determined whether lower *Fads2* expression reduces cardiac mitochondrial AA content (Table 6). Consistent with lower systemic D6D activity, membrane

Table 6: Lower *Fads2* expression reduces AA levels in mitochondrial phospholipids. Gas chromatographic analysis of major fatty acids present on phospholipids extracted from WT (*Fads2*$^{+/+}$) and *Fads2*^{KD} myocardial mitochondria (*N*=9/group). Data are means ± SEM expressed as % of total fatty acids. A Student's *t*-test used to investigate differences between groups; **P* < 0.05 using a Student's *t*-test.

	WT	*Fads2*^{KD}
16:0, Palmitic	12.56±0.86	10.81±1.03
16:1, Palmitoleic	0.62±0.17	0.94±0.16
18:0, Stearic	20.51±0.32	21.50±0.95
18:1n9, Oleic	5.94±0.15	5.85±0.24
18:1n7, Vaccenic	2.73±0.12	2.67±0.16
18:2n6, LA	18.95±0.70	22.49±0.76*
18:3n3, ALA	0.68±0.05	1.01±0.15*
20:3n6, DGLA	0.99±0.21	0.93±0.13
20:4n6, AA	7.72±0.20	6.11±0.24*
22:5n3, DPA	1.89±0.19	1.67±0.14
22:6n3, DHA	27.53±0.54	26.01±0.85
DGLA/LA	0.053±0.011	0.041±0.005
AA/LA	0.41±0.02	0.28±0.02*
DPA/ALA	2.86±0.27	1.99±0.32*
DHA/ALA	42.16±2.58	31.03±4.72*

levels of LA and ALA were significantly greater in *Fads2*^{KD} compared to WT mitochondria, resulting in lower desaturase pathway product/precursor ratios AA/LA, DPA/ALA, and DHA/ALA. However, only AA was found to be significantly lower in *Fads2*^{KD} mitochondria compared to WT, consistent with our hypothesis.

3.6 Lower Fads2 expression reduces IR injury and improves mitochondrial Ca^{++} tolerance.

We next evaluated whether *Fads2*^{KD} mice were resistant to cardiac IR injury and mitochondrial Ca^{++}-overload compared to WT controls. Indeed, following the same 45/120-minute *ex vivo* myocardial IR protocol described above, left ventricles from *Fads2*^{KD} hearts had significantly less

(43%) infarcted tissue than WT (Figure 16A and B). Similarly, cardiac mitochondria from *Fads2*^{KD} mice maintained higher JO_2 (Figure 16C) and lower JH_2O_2 (Figure 16D) than WT across

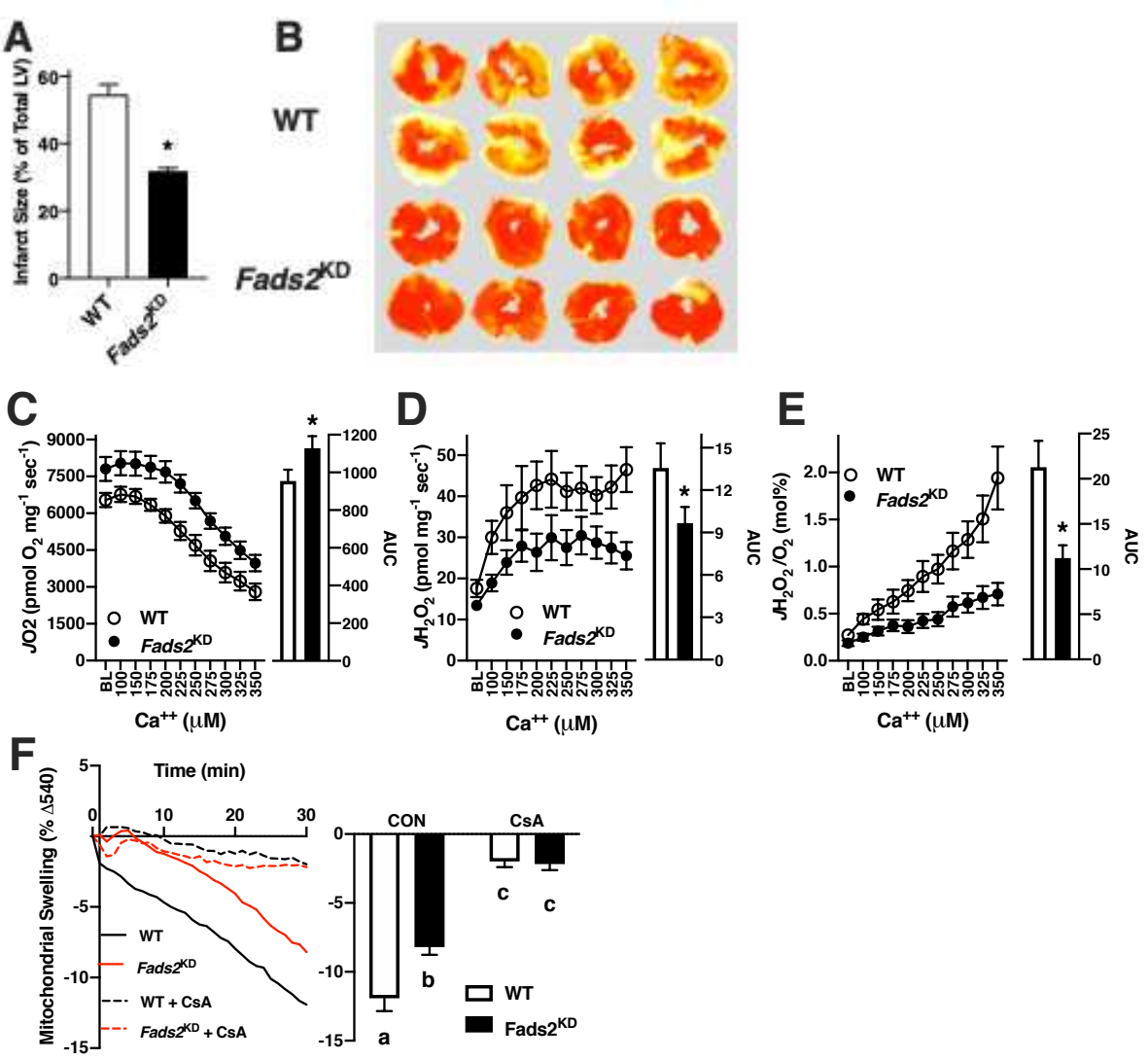

Figure 16: *Fads2* suppression reduces myocardial infarct size and improves mitochondrial tolerance to Ca^{++} overload. A) Left ventricular (LV) infarct size in *Fads2*^{KD} and WT (C57BL/6j) mice after 45/120 minutes of global *ex vivo* ischemia/reperfusion expressed as percent of total LV mass; *N*=10/group. **B**) Representative images of stained transverse left ventricular sections that generated data in panel A (infarcted tissue is yellow). Mitochondria isolated from *Fads2*^{KD} and WT (*Fads2*$^{+/+}$) mouse hearts were reconstituted with TCA cycle intermediates in the presence of ADP to support maximal oxygen consumption (JO_2; **C**) and H_2O_2 release (JH_2O_2; **D**) before sequential titrations of calcium (*N*=10/group). **E**) JH_2O_2 expressed as percent of JO_2. **F**) Representative line tracings of mitochondrial swelling (decrease in absorbance at 540 nm) and final %-change of absorbance (bar graph) with and without mPTP inhibition by cyclosporine A (CsA); *N*= 6/group. *$P < 0.05$ versus WT in panels A-E. In panel F, $P < 0.05$ denoted by difference in letter.

a wide range of Ca^{++} concentrations, resulting in significantly lower JH_2O_2/O_2 during progressive Ca^{++}-overload (Figure 16E). *Fads2*^{KD} mitochondria also swelled less compared to WT mitochondria in response to a Ca^{++} challenge (Figure 16F). This difference was abolished by the addition of CsA, indicating reduced sensitivity of *Fads2*^{KD} mitochondria to Ca^{++} induced mPTP opening. Taken together, these results further support the hypothesized links between *Fads2* expression, mitochondrial membrane AA content, and myocardial ischemic tolerance through a modulation of mitochondrial tolerance to Ca^{++}-overload.

4. Discussion

Epidemiological studies have associated *FADS2* polymorphisms and serum estimates of D6D activity with cardiovascular risk and mortality [9, 40-43] across diverse human populations [6, 44-46]. Experimental evidence from animal models support causal links between higher *Fads2* expression or D6D activity and the development of hypertensive heart disease [7], cardiac aging [8], and IR injury (Li Puma, in preparation), but the mechanisms responsible remain unresolved. In all of these studies, phenotypic changes paralleled distinct shifts in the distribution of PUFAs in cardiac mitochondrial phospholipids, with unclear pathophysiological implications. In the present study, we tested the hypothesis that *Fads2* expression modulates cardiac responses to ischemia by altering mitochondrial AA levels and functional responses to Ca^{++}-overload, based on emerging evidence that AA can be metabolized by mitochondria and contribute to the pathogenesis of myocardial IR injury [18, 24, 26]. Our results confirmed this hypothesis using *Fads2* gain- and loss-of-function approaches in mice, implicating modulation of mitochondrial AA levels as a primary mechanism by which endogenous PUFA metabolism regulates myocardial responses to pathogenic stress.

The mechanisms by which *Fads2* expression selectively impacts mitochondrial membrane AA levels were not addressed in this study, but merit some discussion. Mitochondrial membrane composition is regulated by a complex interplay of phospholipases and acyltransferases both within and outside of mitochondria [47-49], which compliments pathways of *de novo* phospholipid synthesis and acyl-chain remodeling in mitochondria and phospholipid transfer from the endoplasmic reticulum via mitochondrial contact sites [50, 51]. Previous studies in our lab have reported greater levels of AA in cardiac mitochondrial phospholipids from rodent models of aging [8] and heart failure [7], which tended to parallel patterns of PUFA distribution in serum and total myocardial phospholipids. These patterns were largely reversed by pharmacological inhibition of D6D activity *in vivo*, along with several aspects of their pathological phenotype, suggesting that changes in mitochondrial membrane composition may simply reflect systemic shifts in PUFA bioavailability. *Fads2* is primarily expressed in the liver, where D6D and downstream elongation-desaturation enzymes are conventionally thought to generate and export the majority of PUFAs for uptake and incorporation into body tissues via lipoprotein phospholipids [52, 53]. However, while similar patterns of PUFA redistribution are seen between serum and myocardial phospholipids in the *Fads2*^{TG} mouse, only AA was elevated in mitochondrial membranes, suggesting the contribution of a more mitochondria-specific mechanism. In a recent study, we found that myocardial IR injury in *Fads2*^{TG} mice was predicted specifically by the AA content of cardiolipin (Li Puma, in preparation), the signature tetra-acyl phospholipid of the mitochondrial inner membrane. Several enzymes are capable of adding polyunsaturated acyl chains to cardiolipin [54-56], but none of these have shown specificity to AA. Therefore, future studies are needed to elucidate tissue-specific localization and interaction of these enzymes with desaturation

elongation enzymes, membrane phospholipids, and mitochondrial phospholipases to define the origin and regulation of cardiac mitochondrial AA levels.

Gross and colleagues have established iPLA$_2$γ as the primary phospholipase in cardiac mitochondria, where it is robustly activated by Ca^{++} to hydrolyze AA from mitochondrial phospholipids and contributes to pathogenic signaling in heart failure and IR injury [24, 27, 39]. In the present study, IR stress induced a selective loss of AA from *Fads2*^{TG} mitochondrial membranes, which corresponded to reduced respiratory capacity and loss of outer membrane integrity. This was paralleled by impaired mitochondrial responses to progressive Ca^{++}-overload, demonstrated by a loss of OXPHOS-linked respiration, greater mitochondrial ROS release, and mPTP sensitization. mPTP opening is a primary event leading to cell death during IR [13, 14], and was nearly abolished in *Fads2*^{TG} mitochondrial by inhibition of iPLA$_2$γ with BEL. This is consistent with previous evidence linking iPLA$_2$γ to mPTP opening and myocardial infarct size [24, 39], and suggests that release of AA from mitochondrial membranes may contribute to IR injury when *Fads2* expression is elevated. This interpretation is further supported by our demonstration that suppression of *Fads2* expression decreases mitochondrial AA levels, reduces myocardial infarct size, and improves mitochondrial Ca^{++} tolerance. While hydrolysis of mitochondrial membrane lipids can have deleterious effects on mitochondrial function in general [17, 20, 57, 58], our studies targeting AA metabolism suggest a more specific role of AA mobilization and metabolism in the impairment of mitochondrial Ca^{++} tolerance, which is discussed further below.

AA released from membrane phospholipids can serve as a precursor to the generation of eicosanoids, potent lipid second messengers produced by oxygenase enzymes implicated in diverse cellular functions in the cardiovascular system [59]. Emerging evidence indicates that AA-

derived eicosanoids can be synthesized within cardiac mitochondria to participate in a variety of signaling cascades that modulate ion channel kinetics [60-62], mitochondrial function [63-65], and cell death [66-68] in response to cardiac hypoxia, ischemia, and Ca^{++}-overload [24, 26, 27]. In the current study, the greater mPTP sensitization to Ca^{++} in *Fads2*^{TG} mitochondria compared to FVB controls was abolished by inhibition of 12/15 lipoxygenase (Baicalein) and CYP 450 monooxygenase (SKF-525A), with nearly complete inhibition of mPTP opening by Baicalein in both genotypes. SKF-525A blocks CYP450 ω-hydroxylase as well as epoxygenases, while MSPPOH (which tended to increase swelling of *Fads2*^{TG} mitochondria) inhibits only epoxygenaes, implicating CYP 450 ω-hydroxylase in the pathogenic effects inhibited by SKF-525A. It has been previously shown that IR stress induces generation of LOX products (12-HETE) [69] and CYP 450 ω-hydroxylases products (20-HETE) [26] in cardiac tissue. Consistent with our findings, 12-HETE increases mitochondrial Ca^{++} concentration, leading to the loss of mitochondrial membrane polarization, ROS generation, and induction of apoptosis [64], and pretreatment with Baicalein prior to Ca^{++} overload attenuates mPTP opening in mitochondria isolated from failing human hearts [39]. Similarly, 20-HETE dissipates mitochondrial membrane potential and increases mitochondrial ROS production [67, 70, 71], and inhibition of 20-HETE production prior to IR injury attenuates myocardial infarction and cell death [37, 72]. Therefore, *Fads2* expression likely influences cardiac ischemic injury and mitochondrial Ca^{++} responses by regulating mitochondrial levels of AA available for 12/15 LOX and CYP450 hydrolase pathways.

AA-derived eicosanoids may also have cardioprotective effects during IR stress, indicated by greater mPTP opening in FVB mitochondria following inhibition of CYP450 epoxygenases (with MSPPOH) and cyclooxygenase (with indomethacin) in the present study. CYP 450 epoxygenases metabolize AA to epoxysatrienoic acids (EETs), which have been demonstrated to

be cardioprotective by activating mitochondrial K_{ATP} and BK_{Ca} channels, preserving mitochondrial membrane function during IR [63, 73-75]. Inhibition of EET production by the CYP 450 epoxygenases has been shown to increase mitochondrial swelling [39] and blunts the protective effect of EETs on myocardial infarction [76, 77]. Cyclooxygenase (COX) enzymes facilitate production of prostanoids, a large class of AA-derived eicosanoids that are most recognized for their role in inflammation [78] and regulating vascular tone [79]. The role of COX inhibition in IR injury has been focused on functional recovery post-MI, which remains controversial [80-82]. Inhibition of COX prior to ischemia has been demonstrated to exacerbates loss of cardiac function during reperfusion [83] and ameliorate cardioprotection from ischemic preconditioning [84]. These results may be due to effects on mitochondria, as the COX products PGE_2 and PGI_2 have been shown to attenuate mitochondrial ROS release [85, 86], and COX inhibition leads to mitochondrial uncoupling [87]; supporting our evidence for indomethacin increasing mPTP opening in FVB mitochondria in the present study. The attenuated effects of MSPPOH and indomethacin on *Fads2*^{TG} mitochondria implies a greater contribution of pathogenic AA-metabolites (e.g., 12/15 LOX and CYP450 hydrolase products) during Ca^{++} overload that predominate over protective effects of EETs and prostanoid, or perhaps simply a "ceiling" effect whereby *Fads2*^{TG} mitochondria previously swelled to their maximum capacity. Therefore, while there may be both beneficial and pathogenic effects of AA metabolism on mitochondrial function, the net effect of greater mitochondrial AA content and metabolism in response to Ca^{++} overload appears to be negative.

Collectively, this study demonstrates that *Fads2* expression regulates mitochondrial arachidonic acid content and functional responses to Ca^{++} overload. In particular, greater expression of *Fads2* increases mitochondrial AA content, sensitization of the mPTP, and greater

IR injury, whereas lower *Fads2* expression decreases mitochondrial AA content, increases mPTP tolerance to Ca^{++}, and protects against IR injury. Inhibition of the release (BEL) or metabolism (Baicalein/SKF-525A) of AA attenuates the greater mPTP opening in *Fads2*^{TG} mitochondria. Therefore, *Fads2* may regulate myocardial ischemia tolerance via mPTP sensitivity through arachidonic acid signaling. The present study demonstrates *Fads2* expression influences mitochondrial AA content and tolerance to Ca^{++}-overload, potentially establishing the contribution of *FADS2* SNPs in cardiovascular mortality.

REFERENCES

1. Fryar, C.D., T.C. Chen, and X. Li, *Prevalence of uncontrolled risk factors for cardiovascular disease: United States, 1999-2010.* NCHS Data Brief, 2012(103): p. 1-8.

2. Lavie, C.J. and B.J. Gersh, *Mechanical and electrical complications of acute myocardial infarction.* Mayo Clin Proc, 1990. **65**(5): p. 709-30.

3. Macic-Dzankovic, A. and B. Pojskic, *Acute heart failure after myocardial infarction.* Bosn J Basic Med Sci, 2007. **7**(1): p. 40-7.

4. Kutty, R.S., N. Jones, and N. Moorjani, *Mechanical complications of acute myocardial infarction.* Cardiol Clin, 2013. **31**(4): p. 519-31, vii-viii.

5. Braunwald, E., *Myocardial reperfusion, limitation of infarct size, reduction of left ventricular dysfunction, and improved survival. Should the paradigm be expanded?* Circulation, 1989. **79**(2): p. 441-4.

6. Ameur, A., et al., *Genetic adaptation of fatty-acid metabolism: a human-specific haplotype increasing the biosynthesis of long-chain omega-3 and omega-6 fatty acids.* Am J Hum Genet, 2012. **90**(5): p. 809-20.

7. Le, C.H., et al., *Delta-6-desaturase links polyunsaturated fatty acid metabolism with phospholipid remodeling and disease progression in heart failure.* Circ Heart Fail, 2014. **7**(1): p. 172-83.

8. Mulligan, C.M., et al., *Inhibition of delta-6 desaturase reverses cardiolipin remodeling and prevents contractile dysfunction in the aged mouse heart without altering mitochondrial respiratory function.* J Gerontol A Biol Sci Med Sci, 2014. **69**(7): p. 799-809.

9. Warensjo, E., et al., *Markers of dietary fat quality and fatty acid desaturation as predictors of total and cardiovascular mortality: a population-based prospective study.* Am J Clin Nutr, 2008. **88**(1): p. 203-9.

10. Tosi, F., et al., *Delta-5 and delta-6 desaturases: crucial enzymes in polyunsaturated fatty acid-related pathways with pleiotropic influences in health and disease.* Adv Exp Med Biol, 2014. **824**: p. 61-81.

11. Hausenloy, D.J. and D.M. Yellon, *Myocardial ischemia-reperfusion injury: a neglected therapeutic target.* J Clin Invest, 2013. **123**(1): p. 92-100.

12. Murphy, E. and C. Steenbergen, *Mechanisms underlying acute protection from cardiac ischemia-reperfusion injury.* Physiol Rev, 2008. **88**(2): p. 581-609.

13. Morciano, G., et al., *Molecular identity of the mitochondrial permeability transition pore and its role in ischemia-reperfusion injury.* J Mol Cell Cardiol, 2015. **78**: p. 142-53.

14. Ong, S.B., et al., *The mitochondrial permeability transition pore and its role in myocardial ischemia reperfusion injury.* J Mol Cell Cardiol, 2015. **78**: p. 23-34.

15. Crompton, M., *The mitochondrial permeability transition pore and its role in cell death.* Biochem J, 1999. **341 (Pt 2)**: p. 233-49.

16. Hausenloy, D.J. and D.M. Yellon, *The mitochondrial permeability transition pore: its fundamental role in mediating cell death during ischaemia and reperfusion.* J Mol Cell Cardiol, 2003. **35**(4): p. 339-41.

17. Williams, S.D. and R.A. Gottlieb, *Inhibition of mitochondrial calcium-independent phospholipase A2 (iPLA2) attenuates mitochondrial phospholipid loss and is cardioprotective.* Biochem J, 2002. **362**(Pt 1): p. 23-32.

18. Cedars, A., et al., *Calcium-independent phospholipases in the heart: mediators of cellular signaling, bioenergetics, and ischemia-induced electrophysiologic dysfunction.* J Cardiovasc Pharmacol, 2009. **53**(4): p. 277-89.

19. Jenkins, C.M., et al., *Highly selective hydrolysis of fatty acyl-CoAs by calcium-independent phospholipase A2beta. Enzyme autoacylation and acyl-CoA-mediated reversal of calmodulin inhibition of phospholipase A2 activity.* J Biol Chem, 2006. **281**(23): p. 15615-24.

20. Liu, G.Y., et al., *The phospholipase iPLA2gamma is a major mediator releasing oxidized aliphatic chains from cardiolipin, integrating mitochondrial bioenergetics and signaling.* J Biol Chem, 2017. **292**(25): p. 10672-10684.

21. Mancuso, D.J., et al., *Cardiac ischemia activates calcium-independent phospholipase A2beta, precipitating ventricular tachyarrhythmias in transgenic mice: rescue of the lethal electrophysiologic phenotype by mechanism-based inhibition.* J Biol Chem, 2003. **278**(25): p. 22231-6.

22. Wen, Y., et al., *Overexpression of 12-lipoxygenase causes cardiac fibroblast cell growth.* Circ Res, 2001. **88**(1): p. 70-6.

23. Wen, Y., et al., *Overexpression of 12-lipoxygenase and cardiac fibroblast hypertrophy.* Trends Cardiovasc Med, 2003. **13**(4): p. 129-36.

24. Moon, S.H., et al., *Cardiac Myocyte-specific Knock-out of Calcium-independent Phospholipase A2gamma (iPLA2gamma) Decreases Oxidized Fatty Acids during Ischemia/Reperfusion and Reduces Infarct Size.* J Biol Chem, 2016. **291**(37): p. 19687-700.

25. Zhang, C., et al., *The Role of Arachidonic Acid Metabolism in Myocardial Ischemia-Reperfusion Injury.* Cell Biochem Biophys, 2020. **78**(3): p. 255-265.

26. Gross, G.J., et al., *Cytochrome P450 and arachidonic acid metabolites: role in myocardial ischemia/reperfusion injury revisited.* Cardiovasc Res, 2005. **68**(1): p. 18-25.

27. Moon, S.H., et al., *Activation of mitochondrial calcium-independent phospholipase A2gamma (iPLA2gamma) by divalent cations mediating arachidonate release and production of downstream eicosanoids.* J Biol Chem, 2012. **287**(18): p. 14880-95.

28. Stroud, C.K., et al., *Disruption of FADS2 gene in mice impairs male reproduction and causes dermal and intestinal ulceration.* J Lipid Res, 2009. **50**(9): p. 1870-80.

29. Battson, M.L., et al., *Gut microbiota regulates cardiac ischemic tolerance and aortic stiffness in obesity.* Am J Physiol Heart Circ Physiol, 2019. **317**(6): p. H1210-H1220.

30. Makrecka-Kuka, M., G. Krumschnabel, and E. Gnaiger, *High-Resolution Respirometry for Simultaneous Measurement of Oxygen and Hydrogen Peroxide Fluxes in Permeabilized Cells, Tissue Homogenate and Isolated Mitochondria.* Biomolecules, 2015. **5**(3): p. 1319-38.

31. Krumschnabel, G., et al., *Simultaneous high-resolution measurement of mitochondrial respiration and hydrogen peroxide production.* Methods Mol Biol, 2015. **1264**: p. 245-61.

32. Li Puma, L.C., et al., *Experimental oxygen concentration influences rates of mitochondrial hydrogen peroxide release from cardiac and skeletal muscle preparations.* Am J Physiol Regul Integr Comp Physiol, 2020. **318**(5): p. R972-R980.

33. Fonteriz, R.I., et al., *Monitoring mitochondrial [Ca(2+)] dynamics with rhod-2, ratiometric pericam and aequorin.* Cell Calcium, 2010. **48**(1): p. 61-9.

34. Gaur, N. and Y. Rudy, *Multiscale modeling of calcium cycling in cardiac ventricular myocyte: macroscopic consequences of microscopic dyadic function.* Biophys J, 2011. **100**(12): p. 2904-12.

35. De Stefani, D., et al., *A forty-kilodalton protein of the inner membrane is the mitochondrial calcium uniporter.* Nature, 2011. **476**(7360): p. 336-40.

36. Garcia-Dorado, D., et al., *Calcium-mediated cell death during myocardial reperfusion.* Cardiovasc Res, 2012. **94**(2): p. 168-80.

37. Nithipatikom, K., et al., *Inhibition of cytochrome P450omega-hydroxylase: a novel endogenous cardioprotective pathway.* Circ Res, 2004. **95**(8): p. e65-71.

38. Kuzuya, T., et al., *Free radical generation coupled with arachidonate lipoxygenase reaction relates to reoxygenation induced myocardial cell injury.* Cardiovasc Res, 1993. **27**(6): p. 1056-60.

39. Moon, S.H., et al., *Heart failure-induced activation of phospholipase iPLA2gamma generates hydroxyeicosatetraenoic acids opening the mitochondrial permeability transition pore.* J Biol Chem, 2018. **293**(1): p. 115-129.

40. Malerba, G., et al., *SNPs of the FADS gene cluster are associated with polyunsaturated fatty acids in a cohort of patients with cardiovascular disease.* Lipids, 2008. **43**(4): p. 289-99.

41. Martinelli, N., et al., *FADS genotypes and desaturase activity estimated by the ratio of arachidonic acid to linoleic acid are associated with inflammation and coronary artery disease.* Am J Clin Nutr, 2008. **88**(4): p. 941-9.

42. Russo, C., et al., *Increased membrane ratios of metabolite to precursor fatty acid in essential hypertension.* Hypertension, 1997. **29**(4): p. 1058-63.

43. Boberg, M., B. Vessby, and L.B. Croon, *Fatty acid composition of platelets and of plasma lipid esters in relation to platelet function in patients with ischaemic heart disease.* Atherosclerosis, 1985. **58**(1-3): p. 49-63.

44. Mathias, R.A., et al., *Adaptive evolution of the FADS gene cluster within Africa.* PLoS One, 2012. **7**(9): p. e44926.

45. Merino, D.M., et al., *Polymorphisms in FADS1 and FADS2 alter desaturase activity in young Caucasian and Asian adults.* Mol Genet Metab, 2011. **103**(2): p. 171-8.

46. Sergeant, S., et al., *Differences in arachidonic acid levels and fatty acid desaturase (FADS) gene variants in African Americans and European Americans with diabetes or the metabolic syndrome.* Br J Nutr, 2012. **107**(4): p. 547-55.

47. Gonzalez-Baro, M.R. and R.A. Coleman, *Mitochondrial acyltransferases and glycerophospholipid metabolism.* Biochim Biophys Acta Mol Cell Biol Lipids, 2017. **1862**(1): p. 49-55.

48. Naoe, S., et al., *Characterization of Lipid Profiles after Dietary Intake of Polyunsaturated Fatty Acids Using Integrated Untargeted and Targeted Lipidomics.* Metabolites, 2019. **9**(10).

49. Schenkel, L.C. and M. Bakovic, *Formation and regulation of mitochondrial membranes.* Int J Cell Biol, 2014. **2014**: p. 709828.

50. Dimmer, K.S. and D. Rapaport, *Mitochondrial contact sites as platforms for phospholipid exchange.* Biochim Biophys Acta Mol Cell Biol Lipids, 2017. **1862**(1): p. 69-80.

51. Tamura, Y., H. Sesaki, and T. Endo, *Phospholipid transport via mitochondria.* Traffic, 2014. **15**(9): p. 933-45.

52. Nakamura, M.T. and T.Y. Nara, *Essential fatty acid synthesis and its regulation in mammals.* Prostaglandins Leukot Essent Fatty Acids, 2003. **68**(2): p. 145-50.

53. Nakamura, M.T. and T.Y. Nara, *Structure, function, and dietary regulation of delta6, delta5, and delta9 desaturases.* Annu Rev Nutr, 2004. **24**: p. 345-76.

54. Cao, J., et al., *A novel cardiolipin-remodeling pathway revealed by a gene encoding an endoplasmic reticulum-associated acyl-CoA:lysocardiolipin acyltransferase (ALCAT1) in mouse.* J Biol Chem, 2004. **279**(30): p. 31727-34.

55. Taylor, W.A. and G.M. Hatch, *Identification of the human mitochondrial linoleoyl-coenzyme A monolysocardiolipin acyltransferase (MLCL AT-1).* J Biol Chem, 2009. **284**(44): p. 30360-71.

56. Schlame, M. and Y. Xu, *The Function of Tafazzin, a Mitochondrial Phospholipid-Lysophospholipid Acyltransferase.* J Mol Biol, 2020. **432**(18): p. 5043-5051.

57. Penzo, D., et al., *Arachidonic acid released by phospholipase A(2) activation triggers Ca(2+)-dependent apoptosis through the mitochondrial pathway.* J Biol Chem, 2004. **279**(24): p. 25219-25.

58. Zachman, D.K., et al., *The role of calcium-independent phospholipase A2 in cardiolipin remodeling in the spontaneously hypertensive heart failure rat heart.* J Lipid Res, 2010. **51**(3): p. 525-34.

59. Jenkins, C.M., A. Cedars, and R.W. Gross, *Eicosanoid signalling pathways in the heart.* Cardiovasc Res, 2009. **82**(2): p. 240-9.

60. Lee, H.C., et al., *Effects of epoxyeicosatrienoic acids on the cardiac sodium channels in isolated rat ventricular myocytes.* J Physiol, 1999. **519 Pt 1**: p. 153-68.

61. Lu, T., et al., *Cardiac and vascular KATP channels in rats are activated by endogenous epoxyeicosatrienoic acids through different mechanisms.* J Physiol, 2006. **575**(Pt 2): p. 627-44.

62. Xiao, Y.F., L. Huang, and J.P. Morgan, *Cytochrome P450: a novel system modulating Ca2+ channels and contraction in mammalian heart cells.* J Physiol, 1998. **508 (Pt 3)**: p. 777-92.

63. El-Sikhry, H.E., et al., *Novel Roles of Epoxyeicosanoids in Regulating Cardiac Mitochondria.* PLoS One, 2016. **11**(8): p. e0160380.

64. Nazarewicz, R.R., et al., *12(S)-hydroperoxyeicosatetraenoic acid (12-HETE) increases mitochondrial nitric oxide by increasing intramitochondrial calcium.* Arch Biochem Biophys, 2007. **468**(1): p. 114-20.

65. Haworth, R.A., K.T. Potter, and D.C. Russell, *Role of arachidonic acid, lipoxygenase, and mitochondrial depolarization in reperfusion arrhythmias.* Am J Physiol Heart Circ Physiol, 2010. **299**(1): p. H165-74.

66. Yin, H., et al., *Role of mitochondria in programmed cell death mediated by arachidonic acid-derived eicosanoids.* Mitochondrion, 2013. **13**(3): p. 209-24.

67. Bao, Y., et al., *20-Hydroxyeicosatetraenoic acid induces apoptosis in neonatal rat cardiomyocytes through mitochondrial-dependent pathways.* J Cardiovasc Pharmacol, 2011. **57**(3): p. 294-301.

68. Sato, M., et al., *The roles of cytochrome p450 in ischemic heart disease.* Curr Drug Metab, 2011. **12**(6): p. 526-32.

69. Hughes, H., et al., *Gas chromatographic-mass spectrometric analysis of lipoxygenase products in post-ischemic rabbit myocardium.* Prostaglandins Leukot Essent Fatty Acids, 1991. **42**(4): p. 225-31.

70. Lakhkar, A., et al., *20-HETE-induced mitochondrial superoxide production and inflammatory phenotype in vascular smooth muscle is prevented by glucose-6-phosphate dehydrogenase inhibition.* Am J Physiol Heart Circ Physiol, 2016. **310**(9): p. H1107-17.

71. Zhao, H., et al., *20-Hydroxyeicosatetraenoic Acid Is a Key Mediator of Angiotensin II-induced Apoptosis in Cardiac Myocytes.* J Cardiovasc Pharmacol, 2015. **66**(1): p. 86-95.

72. Gross, E.R., et al., *Cytochrome P450 omega-hydroxylase inhibition reduces infarct size during reperfusion via the sarcolemmal KATP channel.* J Mol Cell Cardiol, 2004. **37**(6): p. 1245-9.

73. Gross, G.J., et al., *Mechanisms by which epoxyeicosatrienoic acids (EETs) elicit cardioprotection in rat hearts.* J Mol Cell Cardiol, 2007. **42**(3): p. 687-91.

74. Katragadda, D., et al., *Epoxyeicosatrienoic acids limit damage to mitochondrial function following stress in cardiac cells.* J Mol Cell Cardiol, 2009. **46**(6): p. 867-75.

75. Seubert, J., et al., *Enhanced postischemic functional recovery in CYP2J2 transgenic hearts involves mitochondrial ATP-sensitive K+ channels and p42/p44 MAPK pathway.* Circ Res, 2004. **95**(5): p. 506-14.

76. Gross, G.J., et al., *Roles of endothelial nitric oxide synthase (eNOS) and mitochondrial permeability transition pore (MPTP) in epoxyeicosatrienoic acid (EET)-induced cardioprotection against infarction in intact rat hearts.* J Mol Cell Cardiol, 2013. **59**: p. 20-9.

77. Seubert, J.M., et al., *Role of epoxyeicosatrienoic acids in protecting the myocardium following ischemia/reperfusion injury.* Prostaglandins Other Lipid Mediat, 2007. **82**(1-4): p. 50-9.

78. Ricciotti, E. and G.A. FitzGerald, *Prostaglandins and inflammation.* Arterioscler Thromb Vasc Biol, 2011. **31**(5): p. 986-1000.

79. Davidge, S.T., *Prostaglandin H synthase and vascular function.* Circ Res, 2001. **89**(8): p. 650-60.

80. LaPointe, M.C., et al., *Inhibition of cyclooxygenase-2 improves cardiac function after myocardial infarction in the mouse.* Am J Physiol Heart Circ Physiol, 2004. **286**(4): p. H1416-24.

81. Timmers, L., et al., *Cyclooxygenase-2 inhibition increases mortality, enhances left ventricular remodeling, and impairs systolic function after myocardial infarction in the pig.* Circulation, 2007. **115**(3): p. 326-32.

82. Kain, V., S.D. Prabhu, and G.V. Halade, *Inflammation revisited: inflammation versus resolution of inflammation following myocardial infarction.* Basic Res Cardiol, 2014. **109**(6): p. 444.

83. Mobert, J. and B.F. Becker, *Cyclooxygenase inhibition aggravates ischemia-reperfusion injury in the perfused guinea pig heart: involvement of isoprostanes.* J Am Coll Cardiol, 1998. **31**(7): p. 1687-94.

84. Shinmura, K., et al., *Cyclooxygenase-2 mediates the cardioprotective effects of the late phase of ischemic preconditioning in conscious rabbits.* Proc Natl Acad Sci U S A, 2000. **97**(18): p. 10197-202.

85. Cerioni, L., et al., *Prostaglandin E2 Signals Through E Prostanoid Receptor 2 to Inhibit Mitochondrial Superoxide Formation and the Ensuing Downstream Cytotoxic and Genotoxic Effects Induced by Arsenite.* Front Pharmacol, 2019. **10**: p. 781.

86. Shinmura, K., et al., *Prostacyclin attenuates oxidative damage of myocytes by opening mitochondrial ATP-sensitive K+ channels via the EP3 receptor.* Am J Physiol Heart Circ Physiol, 2005. **288**(5): p. H2093-101.

87. Krause, M.M., et al., *Nonsteroidal antiinflammatory drugs and a selective cyclooxygenase 2 inhibitor uncouple mitochondria in intact cells.* Arthritis Rheum, 2003. **48**(5): p. 1438-44.

CHAPTER V: PERSPECTIVES AND FUTURE DIRECTIONS

1. Perspectives

1.1 Fads2 expression, not serum AA/LA, influences CVD risk

FADS2 haplotypes associated with greater activity of its gene product delta-6 desaturase (D6D) may have provided an evolutionary advantage to early humans in environments where dietary long-chain polyunsaturated fatty acids (LC-PUFAs) were scarce. Today, higher delta-6 desaturase (D6D) activity may contribute to greater CVD risk in modern humans by favoring greater production of arachidonic acid (AA) from linoleic acid (LA), the most abundant PUFA present in the modern Western diet (CVD) [1-8]. However, D6D has been nicknamed a "Janus-faced" enzyme due to its role in both pro-inflammatory (*n*6) and anti-inflammatory (*n*3) PUFA synthesis [8]. Current dogma predicts that greater dietary intake of the *n*3 PUFA alpha-linoleic acid (ALA) should compete with the *n*6 PUFA LA for D6D, reducing AA generation and its associated effects on inflammation and disease [9-11]. However, in Chapter II, I establish that greater *Fads2* expression does not increase serum *n*3 LC-PUFAs levels compared to FVB mice fed either a balanced *n*6:*n*3 or high *n*3 diets. Moreover, lowering the dietary *n*6:*n*3 PUFA ratio decreased the serum AA/LA ratio in both genotypes, but did not attenuate the increased cardiovascular risk observed in *Fads2*^{TG} mice; revealing a disconnect between the serum AA/LA ratio and CVD risk. Therefore, while the serum AA/LA ratio may reflect the nutrigenetic interaction of *Fads2* and dietary LA in the modern diet, it alone is not the inciting cause of CVD. These conclusions emphasize the importance of considering *Fads2* expression an independent risk factor for CVD regardless of dietary PUFA intake, but argue against the serum AA/LA ratio as a mechanistic link between diet or *Fads2* genotype and CVD risk.

1.2 Cardiolipin AA content predicts myocardial ischemic tolerance

In chapter II, I demonstrated that greater *Fads2* expression reduces myocardial tolerance to ischemia-reperfusion (IR) injury only when the dietary PUFA ratio was ≥ 1. Interestingly, the high *n*3 diet did not improve myocardial infarction in FVB mice, indicating a cardioprotective interaction between *Fads2* expression and dietary ALA. However, variations in IR injury were not associated with serum or tissue phospholipid PUFA composition, but instead the AA content of the mitochondrial specific phospholipid cardiolipin. In *Fads2*^{TG} cardiolipin, the high *n*3 diet lowered AA content to that of FVB, implicating a potential mechanism for *n*3 PUFAs to improved tolerance to IR injury. Physiologically, it has been demonstrated that docosahexaenoic acid (DHA; *n*3) will displace LA in membranes, decreasing the production and incorporation of AA into various phospholipids [12-14]. While the mechanism by which *Fads2* expression influences mitochondrial AA content is currently unresolved, my studies in Chapter IV suggest that D6D-dependent AA accumulation does appear to lower tolerance to IR injury.

1.3 Mitochondrial AA content influences mitochondria tolerance to Ca^{++}-overload

In Chapter IV, I revealed that variations in mitochondrial AA content induced by gain and loss of *Fads2* expression *in vivo* did not modulate basal cardiac mitochondrial function, but instead influenced OXPHOS-linked respiration, mitochondrial ROS release, and mPTP sensitivity in response to Ca^{++}-overload. Ca^{++} activates $iPLA_2\gamma$,, which hydrolyzes AA from mitochondrial membranes, making it accessible to oxygenase enzymes for the production of eicosanoids during states of metabolic stress, such as ischemia [15, 16]. Inhibiting the release or metabolism of AA attenuated Ca^{++} induced mPTP opening in *Fads2*^{TG} mice, suggesting that greater mitochondrial AA content may exacerbate myocardial IR injury in these mice. Improvements in mitochondrial Ca^{++} tolerance and smaller infarct sizes in the *Fads2*^{KD} mice further supports the conclusion that

endogenous production of AA and its accumulation in mitochondria may contribute to the greater cardiovascular risk associated with *Fads2* genotype. Taken together, this body of work provides the first experimental evidence to support epidemiological links between *Fads2* genotype and cardiovascular risk in humans. In addition, I have demonstrated that *Fads2* expression specifically impacts cardiac mitochondrial AA levels, supporting accumulating evidence for an important role of mitochondrial AA metabolism on myocardial tolerance to IR stress.

2. Future Directions

LC-PUFA synthesis from the essential PUFAs LA and ALA primarily occurs in the liver and is then distributed to peripheral tissues [17, 18]; however, D6D mRNA levels in the heart, lungs, and brain have been demonstrated [19]. The extent to which cardiac tissue is capable of generating *de novo* AA from LA is unclear, but this remains a plausible source of AA in myocardial membranes. Interestingly, pretreatment of isolated mitochondria from cardiac tissue with the D6D inhibitor SC-26196 prior to Ca^{++}-overload abolished the difference between *Fads2*^{TG} and FVB and significantly lowered swelling in both genotypes (Figure 17A). In addition, SC-26196 mitigated the reduced tolerance to Ca^{++}-overload in *Fads2*^{TG} mitochondria (Figure 17B-E), but did not improve FVB controls. Follow up studies confirmed that SC-26196 does not function as an antioxidant in these experiments (Figure 18A and 18C). Collectively, these results suggest that *de novo* AA synthesis from LA in response to Ca^{++}-overload may occur in cardiac mitochondria, perhaps contributing to the production of eicosanoids that impact myocardial responses to pathogenic stress. To begin addressing this possibility, we probed isolated cardiac mitochondria from FVB mice for the three enzymes responsible for the synthesis of AA: D6D, elongase-5 (ELO5), and delta-5 desaturase (D5D), in tissue. Although more investigation is required to

confirm (described below), there is banding at the predicted molecular weights for all three enzymes (Figure 19A and 19B), suggesting that isolated cardiac mitochondria may have the capability to synthesize AA.

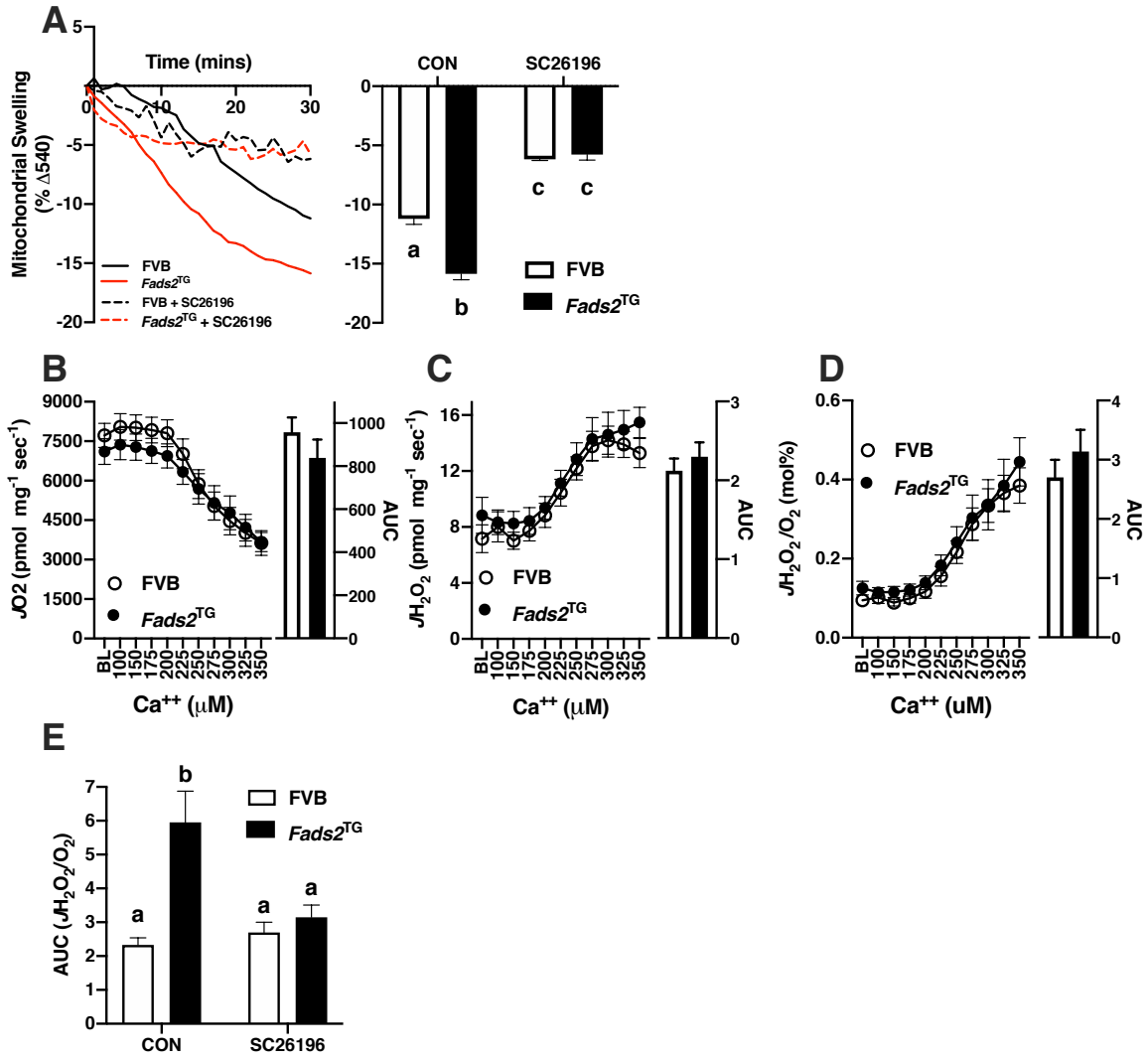

Figure 17: Acute inhibition of delta-6-desaturase with SC-26196 modulates mitochondrial tolerance to calcium overload. **A)** Representative line tracings of mitochondrial swelling (decrease in absorbance at 540nm) and final %-change of absorbance (bar graph) of FVB and *Fads2*^{TG} with SC-26196; n= 4/group. 2 x 2 ANOVA; Trt: $p < 0.05$; *Fads2*: $p < 0.05$; Int: $p < 0.05$. Mitochondria isolated from FVB and *Fads2*^{KD} mouse hearts were pretreated with SC-26196 and reconstituted with TCA cycle intermediates in presence of ADP to support maximal oxygen consumption (JO_2; **B**) and H_2O_2 release (JH_2O_2; **C**) before sequential titrations of calcium (*N*=5/group). **D**) JH_2O_2 expressed as percent of JO_2. Student's T-Test; **P* < 0.05. **E)** Area under the curve for JH_2O_2/JO_2. 2 x 2 ANOVA; *Fads2*: $p < 0.05$; Int: $p < 0.05$. Tukey *post-hoc* was used to investigate pairwise comparisons; p-value < 0.05 denoted by difference in letter.

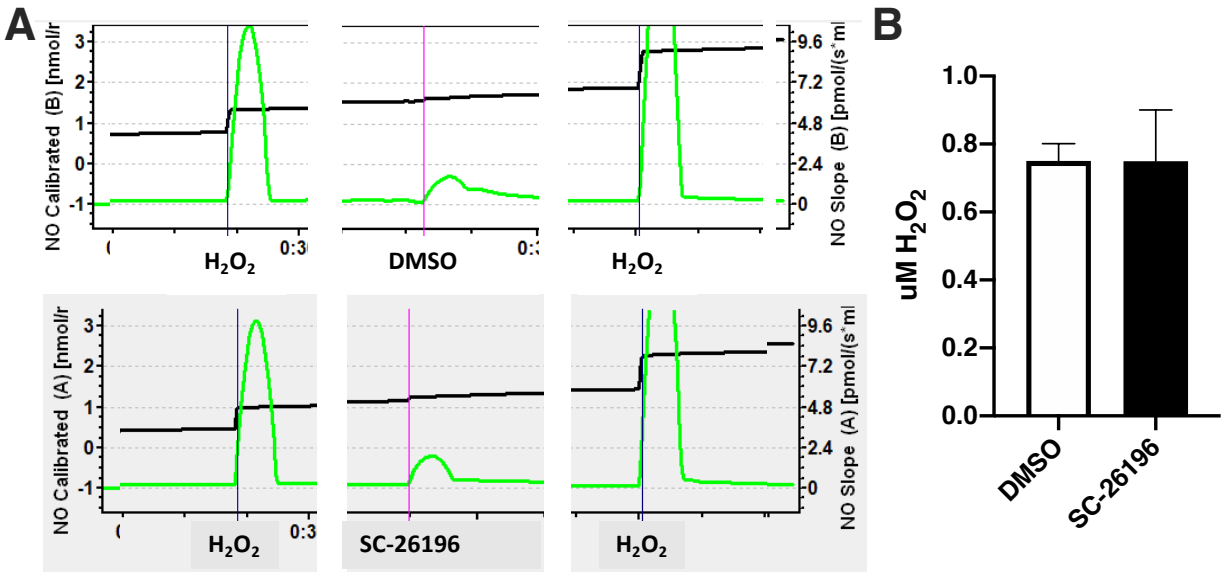

Figure 18: The D6D inhibitor SC-26196 does not act as an antioxidant. A) Oroboros oxygraph-2k tracings measuring the conversion of Amplex Red to resorufin in the presence of dimethyl-sulfoxide (DMSO) or SC-26196 in response to a 1 μM titration of H_2O_2. **B)** Measurement of resorufin fluorescence; n = 2/group.

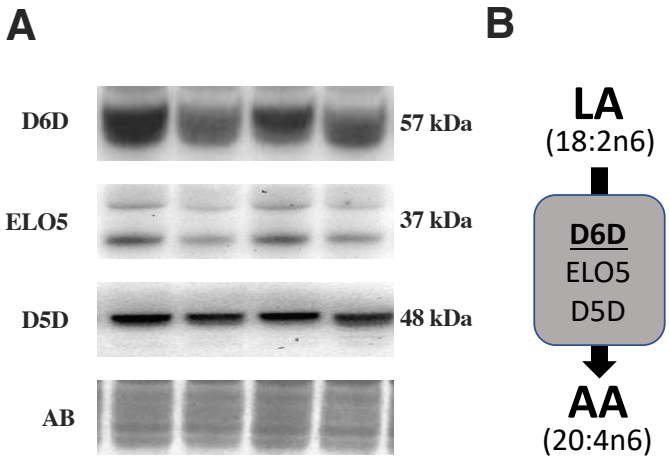

Figure 19: Banding occurs at the expected molecular weights for the main enzymes in arachidonic acid synthesis in cardiac mitochondria. A) Representative immunoblots for delta-5 desaturase (D5D), delta-6 desaturase (D6D), and fatty acid elongase-5 (ELO5) in FVB isolated mitochondria. Membranes were stained with amido black (AB) as a loading control. **B)** Desaturation-elongation pathway for *n*6 PUFAs.

To investigate the ability for cardiac mitochondria to synthesize AA *de novo* in response to a pathogenic stress (Ca^{++}-overload), several research questions should be addressed, including:

1) what is the eicosanoid profile of cardiac mitochondria exposed to Ca^{++}-overload? and 2) what is the role of D6D activity during acute stress in myocytes? For these questions to be answered, new investigatory techniques and methods will need to be developed that are beyond the scope of this dissertation. Therefore, I make the following recommendations for future research in this area: 1) Initial investigations should properly elucidate the presence of D6D, ELO5, and D5D in cardiac mitochondria and associated membranes. The current western blot data will need to be confirmed by use of negative controls and blocking peptides to determine on target specificity. Secondly, the 57 kDa band should be isolated and sequenced in order to confirm its identity as D6D. If these results are successful, then I recommend use of immunogold labeling paired with electron microscopy to determine subcellular localization of D6D and perhaps downstream pathway enzymes in cardiomyocytes. 2) To determine the eicosanoid profile of isolated cardiac mitochondria in response to pathogenic stress, mitochondrial homogenates from the *Fads2*^{TG} and *Fads2*^{KD} mouse hearts can be exposed to Ca^{++} and then prepared for liquid chromatography-MS/MS. These experiments could be complimented with inhibitors for the enzymes involved in the release and metabolism of AA as previously used in Chapter IV. 3) To measure the ability of the myocardium to synthesize AA *de novo*, cardiomyocytes and isolated mitochondria could be incubated with $^{13}C_{18}$-LA and exposed to pathologic stress (hypoxia-reoxygenation or Ca^{++}-overload) followed by evaluation with MS to determine isotope presence in AA and/or eicosanoids. 4) Depending on the success of these experiments, a cardiomyocyte specific D6D knockout mouse model should be generated as a reductionist approach to supplement the current work. These investigations would elucidate the potential for *de novo* AA synthesis in cardiac tissue. By demonstrating a novel function of *de novo* AA synthesis due to pathogenic stress, D6D may be a target for intervention in IR injury.

REFERENCES

1. Warensjo, E., et al., *Associations between estimated fatty acid desaturase activities in serum lipids and adipose tissue in humans: links to obesity and insulin resistance.* Lipids Health Dis, 2009. **8**: p. 37.

2. Warensjo, E., et al., *Factor analysis of fatty acids in serum lipids as a measure of dietary fat quality in relation to the metabolic syndrome in men.* Am J Clin Nutr, 2006. **84**(2): p. 442-8.

3. Warensjo, E., et al., *Markers of dietary fat quality and fatty acid desaturation as predictors of total and cardiovascular mortality: a population-based prospective study.* Am J Clin Nutr, 2008. **88**(1): p. 203-9.

4. Wu, J.H.Y., et al., *Omega-6 fatty acid biomarkers and incident type 2 diabetes: pooled analysis of individual-level data for 39 740 adults from 20 prospective cohort studies.* Lancet Diabetes Endocrinol, 2017. **5**(12): p. 965-974.

5. Russo, C., et al., *Increased membrane ratios of metabolite to precursor fatty acid in essential hypertension.* Hypertension, 1997. **29**(4): p. 1058-63.

6. Malerba, G., et al., *SNPs of the FADS gene cluster are associated with polyunsaturated fatty acids in a cohort of patients with cardiovascular disease.* Lipids, 2008. **43**(4): p. 289-99.

7. Martinelli, N., et al., *FADS genotypes and desaturase activity estimated by the ratio of arachidonic acid to linoleic acid are associated with inflammation and coronary artery disease.* Am J Clin Nutr, 2008. **88**(4): p. 941-9.

8. Tosi, F., et al., *Delta-5 and delta-6 desaturases: crucial enzymes in polyunsaturated fatty acid-related pathways with pleiotropic influences in health and disease.* Adv Exp Med Biol, 2014. **824**: p. 61-81.

9. Calder, P.C., *Marine omega-3 fatty acids and inflammatory processes: Effects, mechanisms and clinical relevance.* Biochim Biophys Acta, 2015. **1851**(4): p. 469-84.

10. Raederstorff, D. and U. Moser, *Influence of an increased intake of linoleic acid on the incorporation of dietary (n-3) fatty acids in phospholipids and on prostanoid synthesis in rat tissues.* Biochim Biophys Acta, 1992. **1165**(2): p. 194-200.

11. Mozaffarian, D. and J.H. Wu, *Omega-3 fatty acids and cardiovascular disease: effects on risk factors, molecular pathways, and clinical events.* J Am Coll Cardiol, 2011. **58**(20): p. 2047-67.

12. Pamplona, R., et al., *Double bond content of phospholipids and lipid peroxidation negatively correlate with maximum longevity in the heart of mammals.* Mech Ageing Dev, 2000. **112**(3): p. 169-83.

13. Pamplona, R., et al., *Mitochondrial membrane peroxidizability index is inversely related to maximum life span in mammals.* J Lipid Res, 1998. **39**(10): p. 1989-94.

14. Lee, H.J., et al., *Selective remodeling of cardiolipin fatty acids in the aged rat heart.* Lipids Health Dis, 2006. **5**: p. 2.

15. Moon, S.H., et al., *Activation of mitochondrial calcium-independent phospholipase A2gamma (iPLA2gamma) by divalent cations mediating arachidonate release and production of downstream eicosanoids.* J Biol Chem, 2012. **287**(18): p. 14880-95.

16. Cedars, A., et al., *Calcium-independent phospholipases in the heart: mediators of cellular signaling, bioenergetics, and ischemia-induced electrophysiologic dysfunction.* J Cardiovasc Pharmacol, 2009. **53**(4): p. 277-89.

17. Nakamura, M.T. and T.Y. Nara, *Essential fatty acid synthesis and its regulation in mammals.* Prostaglandins Leukot Essent Fatty Acids, 2003. **68**(2): p. 145-50.

18. Nakamura, M.T. and T.Y. Nara, *Structure, function, and dietary regulation of delta6, delta5, and delta9 desaturases.* Annu Rev Nutr, 2004. **24**: p. 345-76.

19. Cho, H.P., M.T. Nakamura, and S.D. Clarke, *Cloning, expression, and nutritional regulation of the mammalian Delta-6 desaturase.* J Biol Chem, 1999. **274**(1): p. 471-7.

APPENDIX

Supplemental Table S1: Myocardial total phospholipid fatty acid profile. Myocardial total phospholipid fatty acid ratios (expressed as % of total fatty acids) from FVB and *Fads2*^{TG} animals after 12 weeks on one of three custom diets; n=4-5/group. Data presented as mean ± SEM. Tukey *post-hoc* was used to investigate pairwise comparisons; p-value < 0.05 denoted by difference in letter.

	n6		**mix**		**n3**		**2 x 3 ANOVA**		
	FVB	*Fads2*^{TG}	FVB	*Fads2*^{TG}	FVB	*Fads2*^{TG}	Diet	*Fads2*	Int
16:0, Palmitic	12.1±0.4	12.5±0.6	11.4±0.5	12.0±0.4	11.9±0.5	12.1±0.4	0.3792	0.2824	0.9164
16:1, Palmitoleic	0.44±0.12	0.60±0.18	0.37±0.09	0.51±0.08	0.73±0.14	0.94±0.18	**0.0237**	0.1438	0.9647
18:0, Stearic	18.9±0.2	19.3±0.7	18.8±0.2	18.8±0.5	18.8±0.2	18.6±0.2	0.6273	0.8521	0.8152
18:1n9, Oleic	8.2±0.7	8.8±0.8	7.7±0.3	9.0±0.8	9.5±0.9	10.4±0.8	0.1151	0.1780	0.8766
18:1n7, Vaccenic	1.49±0.07	1.56±0.45	1.53±0.07	1.62±0.09	1.61±0.09	1.71±0.09	0.3469	0.3054	0.9878
18:2n6, LA	20.3±0.2**a**	18.5±0.5**a**	15.9±0.3**b**	16.5±1.1**b**	11.9±0.2**c**	12.7±0.4**c**	**<0.0001**	0.8299	0.1088
18:3n6, GLA	0.31±0.04	0.28±0.08	0.28±0.04	0.26±0.02	0.35±0.07	0.30±0.05	0.4333	0.6553	0.9562
18:3n3, ALA	0.07±0.01**a**	0.10±0.02**a**	1.13±0.22**b**	1.11±0.13**b**	2.54±0.18**c**	2.56±0.10**c**	**<0.001**	0.9203	0.9865
20:3n6, DGLA	0.74±0.06	0.68±0.08	0.75±0.06	0.81±0.08	0.78±0.08	0.78±0.05	0.5516	0.9869	0.7060
20:4n6, AA	10.4±0.2**a**	11.4±0.6**a**	6.0±0.5**b**	6.0±0.4**b**	4.6±0.3**c**	4.5±0.2**c**	**<0.0001**	0.2588	0.3024
20:5n3, EPA	0±0**a**	0±0**a**	0.24±0.05**b**	0.30±0.04**b**	0.77±0.01**c**	0.53±0.05**d**	**<0.0001**	**0.0252**	**0.0002**
22:4n6, AdA	6.7±1.8**a**	6.4±1.0**a**	0±0**b**	0±0**b**	0±0**b**	0±0**b**	**<0.0001**	0.8357	0.9611
22:5n3, DPA	0.74±0.05**a**	0.66±0.09**a**	3.15±0.56**b**	3.77±0.23**b**	5.32±0.38**c**	4.59±0.37**c**	**<0.0001**	0.8192	0.1103
22:6n3, DHA	18.6±1.4**a**	18.3±1.6**a**	31.8±0.5**b**	28.3±1.5**b**	30.3±1.4**b**	29.2±1.1**b**	**<0.0001**	0.1779	0.5292
GLA/LA	0.015±0.002**a**	0.015±0.004**a**	0.018±0.003**a**	0.016±0.002**a**	0.029±0.005**b**	0.023±0.004**b**	**0.0116**	0.4580	0.6999
AA/LA	0.510±0.012**a**	0.615±0.032**b**	0.373±0.038**c**	0.367±0.022**c**	0.383±0.025**c**	0.358±0.013**c**	**<0.0001**	0.2134	**0.0223**
DHA/ALA	277.1±38.7**a**	205.4±43.4**a**	31.5±8.2**b**	27±3.9**b**	12.2±1.3**b**	11.5±0.8**b**	**<0.0001**	0.2160	0.2720
AA/DHA	0.568±0.039**a**	0.635±0.062**a**	0.187±0.017**b**	0.220±0.022**b**	0.153±0.017**b**	0.156±0.011**b**	**<0.0001**	0.2135	0.6258
n6/n3	1.67±0.12**a**	1.66±0.18**a**	0.627±0.011**b**	0.723±0.077**b**	0.451±0.018**b**	0.498±0.029**b**	**<0.0001**	0.5938	0.8702
PI	217.5±11.7**a**	217.1±13.3**a**	319.5±3.8**b**	295.9±12.0**b**	317.5±11.7**b**	303.2±9.9**b**	**<0.0001**	0.2058	0.6318

Supplemental Table S2: Cardiolipin fatty acid profile. Myocardial cardiolipin fatty acid ratios (expressed as % of total fatty acids) from FVB and *Fads2*^{TG} animals after 12 weeks on one of three custom diets; n=4-6/group. Data presented as mean ± SEM. Tukey *post-hoc* was used to investigate pairwise comparisons; p-value < 0.05 denoted by difference in letter.

	n6		mix		n3		2 x 3 ANOVA		
	FVB	*Fads2*^{TG}	FVB	*Fads2*^{TG}	FVB	*Fads2*^{TG}	Diet	*Fads2*	Int
16:0, Palmitic	8.36±0.79	7.01±0.92	6.86±0.75	7.24±0.51	7.06±0.55	8.11±1.04	0.7572	0.9694	0.4181
16:1, Palmitoleic	0.491±0.041**a**	0.909±0.103**a**	0.801±0.141**a**	0.946±0.157**a**	1.260±0.161**b**	1.205±0.110**b**	**0.0052**	0.1736	0.2952
18:0, Stearic	16.06±0.74	16.58±0.71	16.12±0.25	17.41±0.50	15.53±0.59	15.92±0.62	0.3463	0.2096	0.7836
18:1n9, Oleic	8.00±0.47**a**	8.06±0.52**a**	8.52±0.73**a**	9.05±0.33**a**	11.39±0.81**b**	10.19±0.55**b**	**0.0008**	0.7022	0.3955
18:1n7, Vaccenic	2.13±0.02**a**	2.19±0.16**a**	2.82±0.31**ab**	2.71±0.20**ab**	3.01±0.29**b**	3.09±0.31**b**	**0.0089**	0.9615	0.9293
18:2n6, LA	41.93±2.54**a**	40.05±2.17**a**	38.97±1.36**a**	40.51±1.19**a**	29.91±1.34**b**	29.47±1.48**b**	**<0.0001**	0.8726	0.6937
18:3n3, ALA	0.737±0.092**a**	0.787±0.179**a**	1.739±0.171**b**	1.840±0.118**b**	4.893±0.290**d**	3.646±0.400**c**	**<0.0001**	0.1057	**0.0317**
20:3n6, DGLA	1.78±0.15**a**	1.67±0.14**a**	2.15±0.19**a**	2.29±0.26**a**	3.08±0.52**b**	3.67±0.73**b**	**0.0042**	0.5763	0.7405
20:4n6, AA	5.10±0.06**a**	7.40±0.19**b**	5.12±0.19**a**	7.47±0.19**b**	5.25±0.36**a**	5.04±0.38**a**	**0.0008**	**<0.0001**	**0.0002**
20:5n3, EPA	0.653±0.156	0.888±0.165	0.724±0.130	0.621±0.200	1.081±0.176	1.469±0.497	0.1282	0.4874	0.7113
22:5n3, DPA	12.16±1.79	8.70±0.89	8.06±1.26	7.95±1.27	9.71±1.55	10.43±1.96	0.3032	0.4935	0.4263
22:6n3, DHA	2.24±0.36**a**	2.92±0.39**a**	7.54±0.55**b**	6.99±0.87**b**	6.83±0.97**b**	6.79±0.51**b**	**<0.0001**	0.9596	0.7279
GLA/LA	0.017±0.002**a**	0.021±0.006**a**	0.045±0.004**b**	0.046±0.003**b**	0.163±0.005**d**	0.122±0.009**c**	**<0.0001**	**0.0350**	**0.0038**
AA/LA	0.123±0.008**a**	0.188±0.011**b**	0.131±0.010**a**	0.176±0.007**b**	0.175±0.009**b**	0.171±0.010**b**	0.1818	**0.0007**	**0.0152**
DHA/ALA	3.02±0.33**a**	3.19±0.79**a**	4.47±0.45**a**	3.83±0.48**a**	1.38±0.17**b**	1.97±0.24**b**	**0.0004**	0.9259	0.4734
AA/DHA	2.60±0.52**a**	2.80±0.40**a**	0.69±0.07**b**	1.19±0.18**b**	0.88±0.21**b**	0.75±0.06**b**	**<0.0001**	0.4743	0.6162
n6/n3	3.25±0.43**a**	4.48±0.21**b**	2.64±0.27**c**	3.12±0.34**c**	1.71±0.10**d**	1.76±0.19**d**	**<0.0001**	**0.0347**	0.2085
PI	159.8±8.5**a**	148.3±5.5**a**	177.7±7.0**b**	183.8±13.7**b**	182.3±3.6**b**	184.5±6.8**b**	**0.0142**	0.9003	0.6613

Supplemental Table S3: Mitochondrial phospholipid fatty acid profile (ug). Cardiac mitochondrial phospholipid fatty acid contents (μg lipid/mg mitochondria) from FVB and *Fads2*^{TG} mice before (CON) and after 45/90 min *ex vivo* cardiac ischemia/reperfusion (IR); *N*=5/group. Data presented as means ± SEM. Tukey *post-hoc* was used to investigate pairwise comparisons following significant ANOVA); $P < 0.05$ denoted by difference in letter.

	FVB		***Fads2*^{TG}**		**2-Way ANOVA**		
	CON	**IR**	**CON**	**IR**	**Genotype**	**Treatment**	**Interaction**
16:0, Palmitic	29.3±0.7	34.2±4.0	34.0±3.4	31.2±2.3	0.7604	0.7096	0.1977
16:1, Palmitoleic	0.76±0.1	0.77±0.1	1.04±0.2	1.02±0.1	0.3322	0.9999	0.9999
18:0, Stearic	45.5±1.1	48.5±5.9	52.3±4.5	47.1±3.7	0.5310	0.7975	0.3454
18:1n9, Oleic	12.5±0.4	13.6±1.5	10.6±1.0	11.0±0.8	**0.0306**	0.4807	0.7610
18:1n7, Vaccenic	3.73±0.1	4.19±0.5	3.27±0.2	3.69±0.2	**0.0375**	0.1501	0.9999
18:2n6, LA	38.7±1.9	43.3±5.8	30.9±3.0	33.2±3.4	**0.0337**	0.3829	0.7556
18:3n3, ALA	1.26±0.1	1.61±0.2	1.45±0.1	1.21±0.1	0.3777	0.5717	**0.0294**
20:3n6, DGLA	1.0±0.0	1.25±0.2	1.15±0.1	1.05±0.1	0.8688	0.5116	0.1981
20:4n6, AA	15.9±0.3**a**	17.4±1.9**a**	29.4±2.4**b**	16.0±0.1**a**	**0.0014**	**0.0018**	**0.0002**
22:5n3, DPA	2.28±0.1**a**	2.7±0.2**ab**	3.36±0.4**b**	2.66±0.1**ab**	**0.0375**	0.4607	**0.0375**
22:6n3, DHA	56.8±1.8	61.4±7.4	65.4±6.2	61.2±5.2	0.4607	0.9717	0.4400

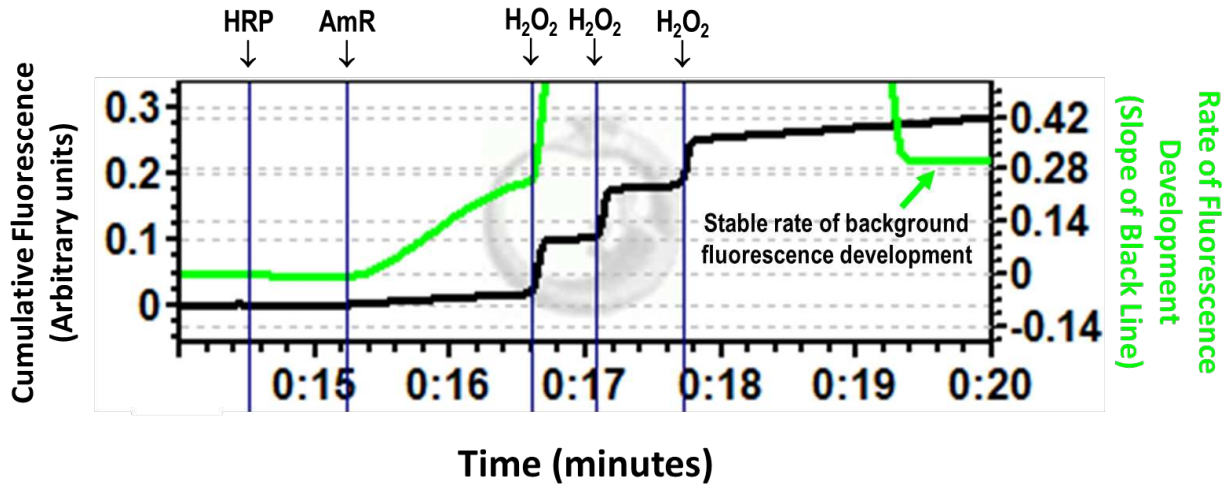

Supplemental Figure S1: H_2O_2 Calibration procedure and chemical background fluorescence. The sample DatLab tracings show cumulative chamber fluorescence (black line, left y-axis) and the rate of chamber fluorescence development (green line, right y-axis) over time during a typical H_2O_2 calibration procedure at the beginning of a fluorespirometry experiment. Initially, chamber fluorescence is stable at zero due to the absence of fluorophore, but begins to increase after the addition of HRP and AmR due to reactions with components of the MiR05 respiration buffer (1, 2). Note that the green line represents the average slope of the previous 40 two-second intervals on the black line, so fails to stabilize until after the H_2O_2 titration procedure. To calibrate fluorescence to H_2O_2 content, three rapid titrations of 0.1 µM H_2O_2 are added to the chamber to produce uniform "step" increases in chamber fluorescence (black line) that are quantified using DatLab software (Oroboros Instruments, Innsbruck, AT). The average increase in fluorescence resulting from the three 0.1 µM H_2O_2 titrations (height on left y-axis) is used to convert the fluorescence units to nmol H_2O_2. The green line can be ignored during this procedure, but a negligible contribution of background fluorescence developed during each step can be subtracted by determining the time elapsed during each interval measured and the stable rate of background fluorescence developed over time. Variations on this calibration procedure can be employed (e.g., H_2O_2 standard curve), but it is prudent to minimize the cumulative levels of resorufin fluorescence in the chamber for reasons discussed elsewhere (2) and in the main manuscript (Figure 1B).

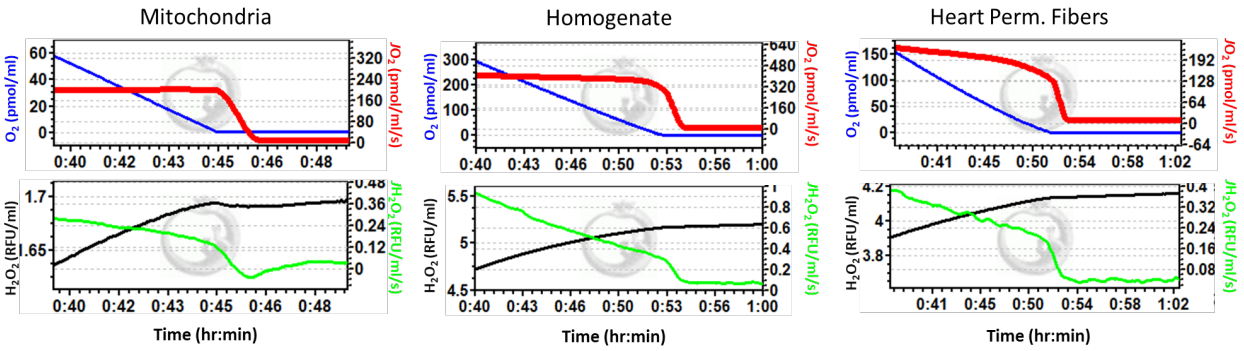

Supplemental Figure S2: Sample DatLab tracings of JO_2 and JH_2O_2 during chamber O_2 depletion. Representative DatLab tracings of the raw JO_2 (top row of panels) and JH_2O_2 (bottom panels) signals from cardiac mitochondrial preparations including chamber oxygen content (blue line, left y-axes) and the uncorrected JO_2 signal (red line, right y-axes) with corresponding recordings of cumulative chamber fluorescence (black line, left y-axis; raw fluorescence units, RFU) and rate of chamber fluorescence development (green line, right y-axis; slope of black line) from the same experiment over time as chamber O_2 is depleted*. Results show that mitochondria maintain stable JO_2 down to essentially 0 µM O_2, while homogenate and particularly permeabilized fibers begin to decline exponentially below ~20-40 µM O_2, illustrating the variations in O_2 diffusion limitation of JO_2 across these preparations. The JH_2O_2 fluorescence signal declines linearly with chamber [O_2] in all sample preparations down to near anoxic conditions, then decreases further to just above zero in anoxia, illustrating the high O_2-dependence of mtROS production and chemical background fluorescence (further illustrated in Figure S3 below).

**Note that the red and green lines are time integrals (averages) of change in the raw O_2 (blue) and fluorescence (green) signals, respectively, so do not immediately respond to the onset of anoxia.*

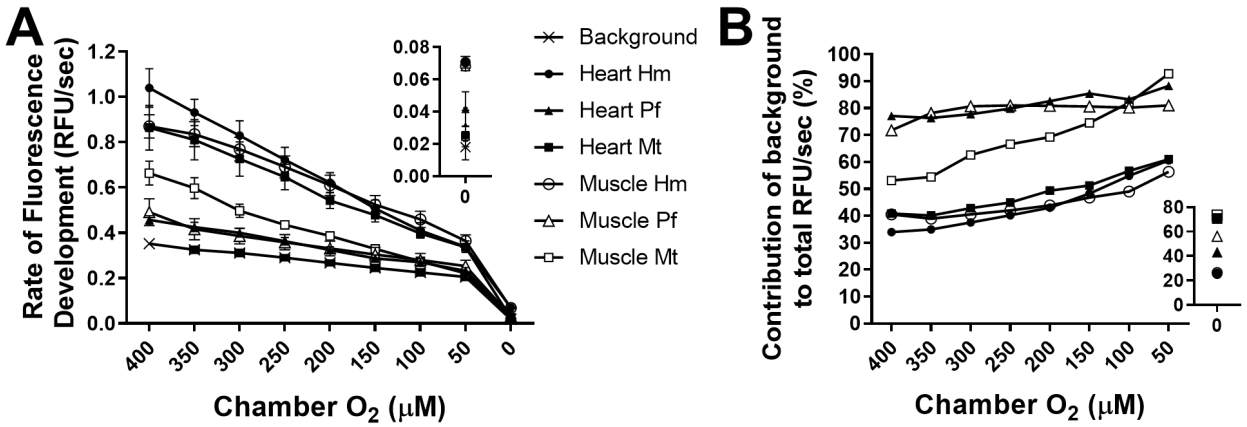

Supplemental Figure S3: Contribution of chemical background to the total rate of fluorescence development by mitochondrial preparations across different chamber O_2 concentrations. A) Total (uncorrected) rates of resorufin fluorescence developed by mitochondrial preparations and chemical background (without sample) as chamber [O_2] declines from 400 μM to anoxia. Results illustrate the linear dependence of mitochondrial JH_2O_2 and chemical background rate on chamber [O_2], and extremely low sample and background flux signals in anoxia (inset). **B)** Contribution of chemical background fluorescence to total rate of fluorescence developed by mitochondrial preparations as chamber [O_2] declines. Results illustrate that chemical background flux contributes to ~34-93% of total rate of fluorescence developed by biological samples, depending on mitochondrial preparation, tissue and chamber [O_2]. In general, the contribution of chemical background to total flux increases as chamber [O_2] declines, reflecting a greater O_2-dependence of sample (mitochondrial) JH_2O_2 than the chemical background reactions between AmR and media components. Contributions of background to fluorescence flux in anoxia (inset) were highly variable given the extremely low signal intensity, but may reflect differences in the composition of the mitochondrial preparations and/or their interaction with buffer components.

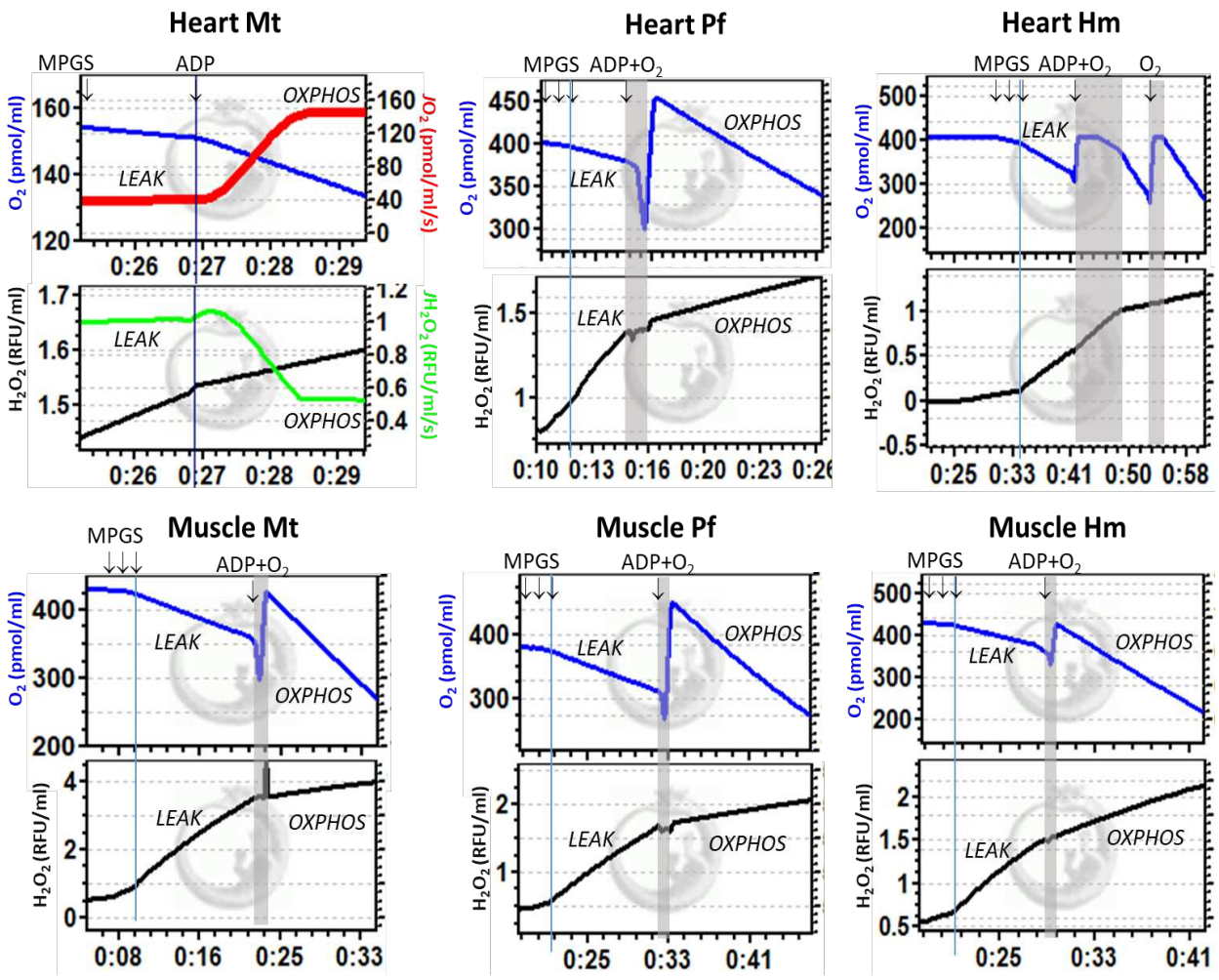

Figure S4. Representative O2 and fluorescence tracings from each of the six mitochondrial preparations. For clarity, a sample experiment in heart mitochondria (top left) illustrates the change in chamber oxygen content (blue line, left y-axes) and the uncorrected JO_2 signal (red line, right y-axes) with corresponding recordings of cumulative chamber fluorescence (black line, left y-axis; raw fluorescence units, RFU) and rate of chamber fluorescence development (green line, right y-axis) during the transition from the LEAK state supported by malate, pyruvate, glutamate and succinate (MPGS) to the OXPHOS state (induced by the addition of ADP) at room air saturated [O_2]s. Data from experiments in Figures 2 and 3 of the main manuscript are illustrated in the subsequent panel, which were collected between 350-400 µM O_2 for consistency across all mitochondrial preparations. This required reoxygenation of the chamber between the LEAK and OXPHOS states at least once during the experiment (shaded portions of the remaining panels) to obtain stable flux recordings in both respiratory states. Only chamber O_2 content and fluorescence tracing are presented from these experiments for clarity, given wide variations in the flux tracings induced by the reoxygenation procedure.